Master's thesis

Master's degree in Industrial Engineering

Analysis and redesign of a glass fiber reinforced polyamide clutch pedal for additive manufacturing

Author: Carlos Rodríguez Rodrigo
Supervisor: Andrea Bernasconi
Tutor: Domingo Morales Palma

Dept. Mechanical Engineering and Manufacturing
Higher Technical School of Engineering
University of Seville

Seville, 2018

Master's thesis
Master's degree in Industrial Engineering

Analysis and redesign of a glass fiber reinforced polyamide clutch pedal for additive manufacturing

Author:
Carlos Rodríguez Rodrigo

Supervisor:
Andrea Bernasconi
Associate Professor at Politecnico di Milano

Tutor:
Domingo Morales Palma
Assistant Professor at University of Seville

Dept. Mechanical Engineering and Manufacturing
Higher Technical School of Engineering
University of Seville

Seville, 2018

General Index

I. REPORT

Report index

Index of figures

Index of tables

1 Abstract

The engineering design process has always had limiting factors materializing ideas from its conception down to the physical world through manufacturing techniques.

Each manufacturing technique, as injection moulding, has always added constraints and limiting factors to the creativity of the engineer design during the design phase.

In the recent years, the rising of a new manufacturing technique with notorious design freedom, additive manufacturing (AM), has been in everyone's lips. Since this technique has been progressively jumping into different kind of materials, the expectations have increased into its maximum exponent.

Therefore, blind jumping into this technique is not a smart approach. This new design freedom does not cost for free. Until recent years, the achievable mechanical properties of parts made by AM have been quite poor in comparison to its similar classical fabrication approaches.

Furthermore, it would not be in another way in the science of short fiber reinforced polymer composites. The rise of this disruptive technology is promising, but the long way ahead until the process is mastered and equalled in mechanical properties to other techniques cannot be denied.

In any case, the new potential possibilities are really interesting, being AM the viable physical solution for topology optimization algorithms. The necessity of mastering the AM process, has arisen new simulations and FEM techniques in order to simulate and predict the best possible way the manufacturing process output. Some of these parameters are FEM model initial stresses and warpage, the fiber orientation, and non-isotropic material properties among others.

After the simulation and structural analysis of a current part, a clutch pedal, made of SFRP composite and manufactured for injection moulding, has gone into a redesign for AM.

This work deals with some of the previous commented parameters inherent to the AM process. These are the nozzle toolpath, the material micro-model and the printing initial stresses. Throughout new software capabilities, these features have been computed and added into structural FEA models.

A final comparison between the different models for each technology has been conducted. Some discussions about its interpretation have been finally written down, defining a set of tips for further works such as the printing of the part itself.

Ultimately, a great effort has been made not only in the technical aspects of the mechanical design for additive manufacturing, but also in its influence in the engineering design process and the new design methodologies that can arise thanks to this technology.

2 Aim of the project

The aim of the project is to perform a prospective work into the innovative way of manufacturing SFRP composites with additive manufacturing. The design freedom allowed by this technology opens feasible possibilities with topological optimization tools and new additive manufacturing simulation FEA software where the nozzle's toolpath or the internal stresses generated during printing are taken into account within the models.

This project will be used both for research purposes and for opening new possibilities in future industrial proposals where industrial components could be redesigned for additive manufacturing. This could lead to a significant weight reduction of the part while maintaining, or even increasing, its reliability.

3 Scope of the project

The scope of this project covers the analysis of a clutch pedal manufactured with the traditional methods for manufacturing short fiber reinforced polymer (SFRP) composites, performing both simulation and structural FEA.

After the understanding of the traditional techniques, this work is focused in a redesign of the part using the incoming new disruptive technologies as additive manufacturing for SFRP composites.

The new design is modelled according the intrinsic properties of the material and simulated in line with key parameters of additively manufactured processes. At the end, a final structural FEA is carried out with an upgraded model and compared with the previous analysis.

4 State of the art

4.1 Clutch pedal

4.1.1 Original design part specifications

The original part is a clutch pedal of a FIAT Punto car made of short fiber reinforced polymer (SFRP) composites, by Rhodia E.P in 1998. This material composite was the PA66-GF30, which is a Nylon 66 polyamide reinforced with 30% volume of glass fiber. Moreover, pedal was manufactured by injection moulding.

Injection moulding is the traditional manufacturing process for producing parts by injecting polymer pellets into a mould (CustomPartNet, 2007) . Since the mould fabrication is expensive, this manufacturing technology is used when thousands of parts have to be created to cover the mould manufacturing costs. In large manufacturing projects like automotive industries, this technology fits very well with economies of scale, due its economic profitability when the number of parts to be produced start to be significantly high.

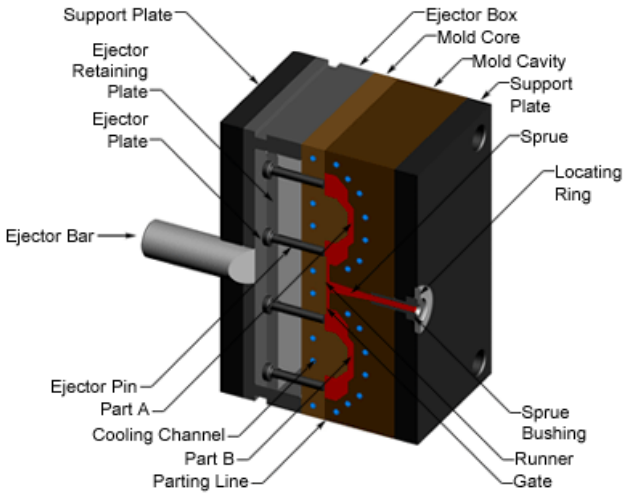

Figure 1. Injection moulding process parts (collapsed)

The parts to be used for injection moulding must be carefully designed to facilitate the process. The mould consists of two main components: the moulder and the ejector. When injection moulding techniques are desirable to be used, the design process of the part is affected by demoulding constraints itself, otherwise the part could not be possibly manufactured. The more holes the designed part has, the more complex it is and poorer tolerance the mould suffers.

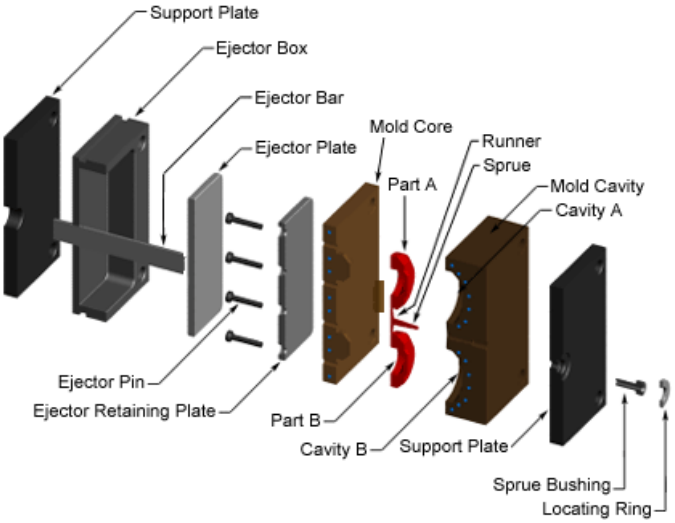

Figure 2. Injection moulding process parts (exploded)

More complex parts with perpendicular cavities to the flow direction can be made, but complex moulds are required. In this case, to create the cavities, slides are used within the mould. When the mould is opened, the slides are pulled away from the part using angled pins in the moulder half (CustomPartNet, 2007).

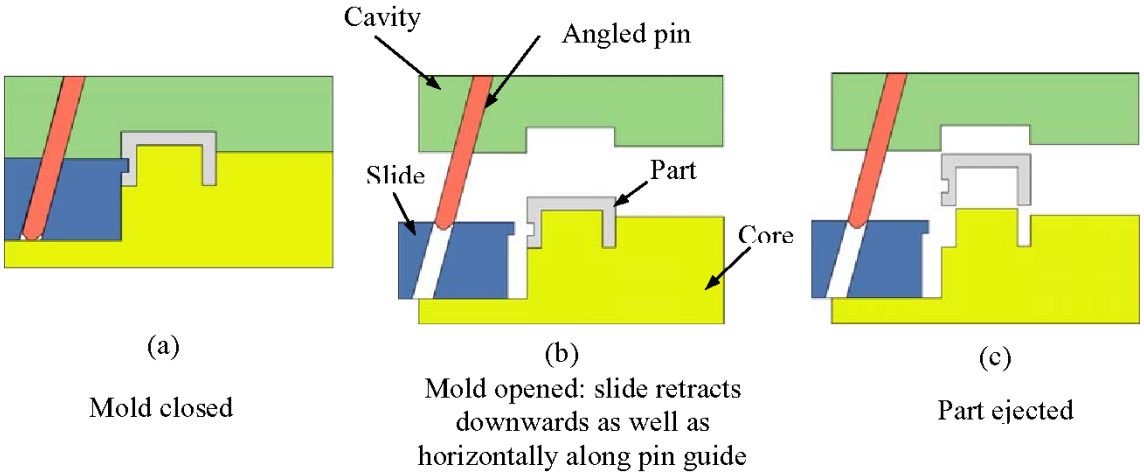

Figure 3. A complex mould with slide. Part ejection procedure

The original clutch pedal required originally a couple of this slides. The part has two perpendicular cavities to the flow direction, requiring a more complex mould which can be demoulded by the operator.

Figure 4. Clutch pedal of a FIAT punto

A table with more detailed information about the PA66-GF30 is stated below. Regarding this part, the information was retrieved from Campusplastics (CAMPUSplastics, 2018) showing that the manufacturer was RadiciGroup Performance Plastics and was commercialised under the name of RADILON A RV300.

RADILON® A RV300 | PA66-GF30 | RadiciGroup Performance Plastics

Product Texts

DESIGNATION:
Thermoplastics ISO1874-PA66,MR,14-100,GF30

BRIEF DESCRIPTION:
PA66 30% Glass fibre reinforced injection moulding grade.
For items with high stiffness and dimensional stability.

Mechanical properties	dry / cond	Unit	Test Standard
Tensile modulus	**9500 / 6500**	MPa	ISO 527-1/-2
Stress at break	**180 / 120**	MPa	ISO 527-1/-2
Strain at break	**3.5 / 6**	%	ISO 527-1/-2
Charpy impact strength, +23°C	**85 / 105**	kJ/m²	ISO 179/1eU
Charpy impact strength, -30°C	**75 / 80**	kJ/m²	ISO 179/1eU
Charpy notched impact strength, +23°C	**13 / 18**	kJ/m²	ISO 179/1eA
Charpy notched impact strength, -30°C	**11 / 11.5**	kJ/m²	ISO 179/1eA

Other properties	dry / cond	Unit	Test Standard
Water absorption	**7 / ***	%	Sim. to ISO 62
Humidity absorption	**1.7 / ***	%	Sim. to ISO 62
Density	**1350 / ***	kg/m³	ISO 1183

Figure 5. RADILON A RV300. PA66-GF30 manufactured by RadiciGroup. Source from Campusplastics

It has to be noticed how the mechanical properties change significantly depending on the working conditions (atmospheres with moisture). This must be taken into account during the design phase, where the working environment will certainly determine the final mechanical properties of the resultant part and its expected behaviour.

The Nylon 66 is frequently used in applications for high mechanical strength and stiffness under heat or chemical conditions which require good material stability (HellermannTyton, 2011).
On the other hand, glass fiber as a reinforce material is commonly used for applications which require a medium or high mechanical properties when humidity is accurately controlled and reduced. In this case, glass fibers can add the interesting property of thermal insulation. Furthermore, by trapping air within the fibers, the thermal conductivity reaches an order of 0.05 W/(mK) (Incropera, 2012).

The combination of both can release a reinforced polymer like the PA66 GF30. It has higher mechanical properties than the raw polyamide, making the materials proper for high static loaded operations over long periods and for higher temperatures working conditions, due to the thermal properties of the glass fibers. The ratio of a low density of 1.34 g/cm3 over high Elastic modulus makes the fiberglass a good lightweight material. Additionally, the PA66-GF30 has good weldable and bondable capabilities (Ensinger, 2018), reducing assembly issues when joining parts all together.

All these properties make the PA66-GF30 a good candidate for mechanical engineering, automotive, aircraft and aerospace applications.

The clutch pedal has three different parts: the two ends and the inner bracket.
In the free end, there is the pedal itself, where the loads are eventually applied by the car driver. These loads appear distributed around the pedal surface when the user clutches, and are transmitted to the other end throughout the inner structural element. In the opposite end, where the loads are transmitted, it is clawed and holed with a bush and pinned to the mechanisms of the gear box and the transmission system.

4.1.2 Automotive clutch mechanism

As we know, in vehicles, the mechanism that transmits the power generated by the engine to the wheels or the accessory equipment of the vehicle is the power train (Integrated Publishing, 2007). Cars need to move and operate in different range of speeds, and vehicle powertrain components make this possible. The clutch is part of the power train, and is used to connect and disconnect the engine.

The mechanism that allows the user to connect and disconnect the engine to his control is called clutch mechanism. Three types of clutch mechanisms can be found: with levers, with steel cables or a hydraulic system.

The clutch linkage mechanism uses levers and rods to transfer motion from the clutch pedal to the clutch fork (Integrated Publishing, 2007) (the final lever of the mechanism which transfer the motion to the pressure plate, activating its connection to the engine). When the pedal is pressed, a pushrod pulls on the bell crank, which opposite end is connected to the release rod. This one transfers bell crank movement to the clutch fork.

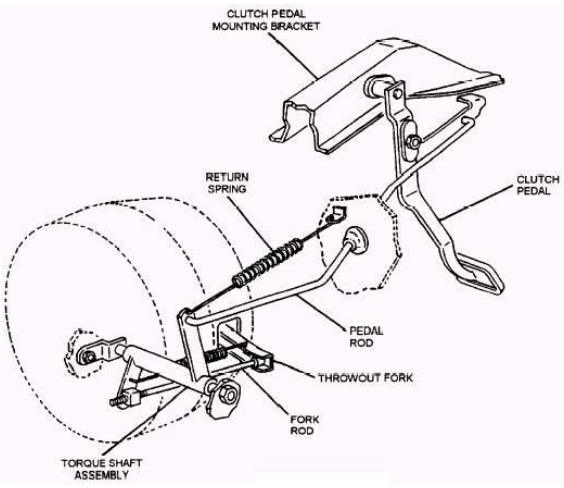

Figure 6. Clutch linkage mechanism

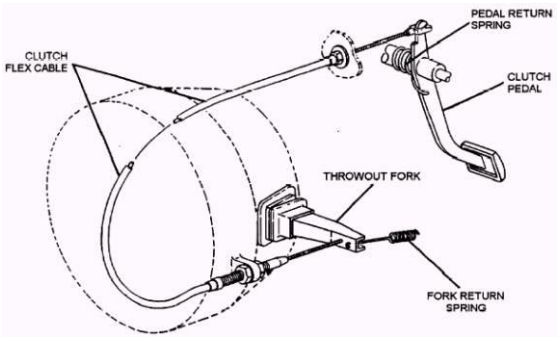

Figure 7. Clutch cable mechanism

The other type of mechanism, the clutch cable mechanism uses a steel cable to transfer the movement from the pedal to the clutch fork (Integrated Publishing, 2007). The cable housing is stationary, allowing the cable to slide inside the housing when the pedal is pressed. The slide of the cable activates the clutch rod.

The last type, uses a hydraulic clutch as the system to amplify the pedal movement which activates the clutch fork (CustomPartNet, 2007). This type is the most spread nowadays. The clutch pedal shoves on a master cylinder which drives a piston in a slave cylinder which pushing the clutch fork.

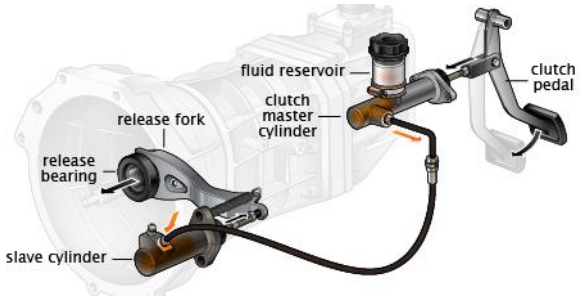

Figure 8. Hydraulic clutch

4.1.3 Traditional design materials

Car clutch pedals have been made traditionally with polymers reinforced with glass fibers (*Figure 9.a*) or with welded metal bars (*Figure 9.b*). For large productions, the solution with reinforced polymers will be cost effective at long term because they are manufactured using injection moulding. In cases when the car clutch pedal is not produced for large scales but for low volume productions, welded bars could be a more accurate choice, as well as the final part is stronger than the one made of reinforced polymers.

Figure 9. Clutch pedals made by injection moulding (a) and by welding (b)

4.2 Short fiber reinforced polymers composites

4.2.1 Introduction to composite materials

The composite materials are the materials made from two or more constituent materials which often significantly differ for physical or chemical properties and that, when combined, produce a structure with characteristics different from those of the individual components (Bernasconi, Composite materials I, 2018).

The individual components remain separate and distinct within the finished structure.

In general, fibers are the principal load-carrying members, while the surrounding matrix keeps them in the desired location and orientation. In this way, it acts as a load transfer medium between them, and protects them from environmental damages due to elevated temperatures, humidity and abrasion.

That is why, composite materials have a really good ratio stiffness over density.
The main difference between an alloy and a composite material is that you can distinguish the phases clearly.

Composite materials have very good mechanical properties and they are very strong compared to weight. This specific property make the composite materials a good solution for lightweight designs.

On the contrary, they are fragile with linear behaviour up to failure, with no yielding. This leads into absence of residual strength after you reach the maximum strength.

Different material combinations become into different stiffness/weight ratios.

4.2.2 Anisotropy and heterogeneity

At certain scale, all the materials are heterogeneous and present anisotropic behaviour. Fortunately, at a sufficiently large scale, some materials can be considered as homogeneous and isotropic.

A material is heterogeneous when its properties depend on the position, on the contrary to the homogeneous materials, in which the material properties are independent on the position.

When it is said that a material presents anisotropic behaviour, is because its properties are dependent on direction. In a different way, when the material is isotropic, has the same mechanical properties in all directions.

The FE method make use of continuous and homogeneous materials. It can be easily removed the anisotropy but no the heterogeneity hypothesis. As introduced before, composite materials are not homogeneous at certain scale; even metals are not homogeneous.

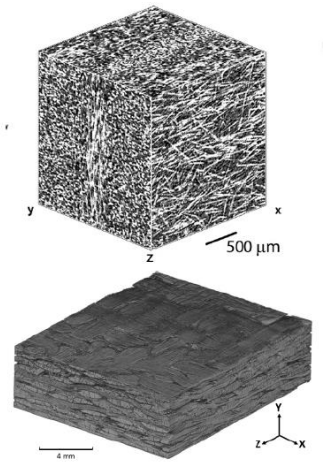

Figure 10. Representative Volume Elements (RVE)

This minimum scale in which materials do not behave has homogeneous, this minimum size, it is considered the smallest volume a material can be considered under homogeneity assumptions. This is called the Representative Volume Element (RVE).

With this procedures, FE models are handier when non-homogeneous materials have to be faced. It has to be remembered that any conclusion smaller than the RVE is not consistent for the assumptions of homogeneous materials.

4.2.3 Composite materials classification

The upper hierarchy in the classification of composite materials appears with three main families: Particle reinforced, fiber reinforced and structured.

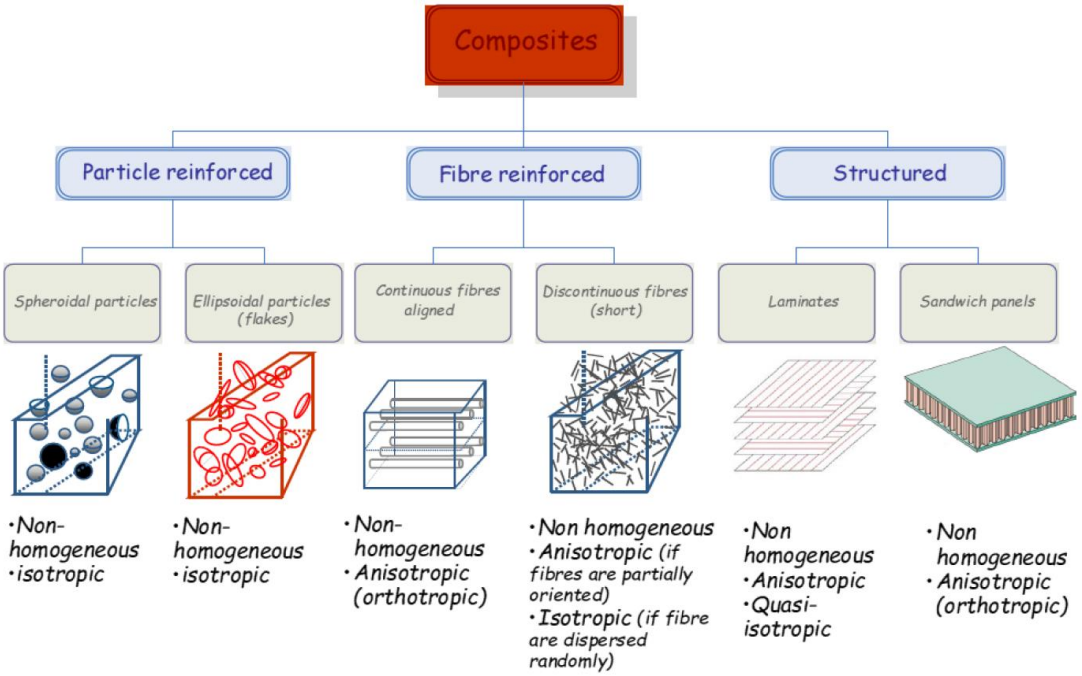

Figure 11. Diagram of the classification of composite materials

Particle reinforced composites contains materials in which discontinuous reinforced phase is surrounded by the matrix. The particles may be either relatively big or very small and dispersed. For this composite type, the particle's shape may be either spheroidal or ellipsoidal. In both cases the particle phase merge with a result inseparable of the two phases.
With this characteristics, the matrix performances are better and the transition temperature and creep resistance is improved. This kind of composites is common when speaking of metal matrix

composites. Apart, these materials are considered non-homogeneous and isotropic (Bassi, 2016).

The structured composites are the type of materials which consists on a combination of different parts, each of them with its particular characteristics. They are the laminates and the sandwich panels. Both of them are considered non-homogeneous and anisotropic, but laminates may be also quasi-isotropic depending the lamina pattern superposition.

The last family, is the family of the **fiber reinforced composite materials**, in which a phase of fibers constitutes the reinforcement. Depending the length and ratio of the fiber dimension, the properties of the material varies significantly. There are two types: the long fiber reinforced composites, with a significant long reinforcement, and the short fiber reinforced composites in which the reinforcement are dispersed fibers of finite dimensions, delivering very complex configurations (Bassi, 2016).

4.2.4 Introduction to SFRP composites

One variety of the fibre reinforced composite materials are the short fiber reinforced polymers (SFRP) composites. In this type of composite, the fibers are not continuous but they are 0.2-0.3 mm long. Their orientation depends on the flow direction during the injection moulding process. This, influence their mechanical performance in a way that their properties behaviour become anisotropic and heterogeneous (Fu S-Y, 2009).

In SFRP composites are differentiated phases: the fibers and the matrix.

The fibers are chopped and are discontinuous inside the matrix. Sometimes, the direction can be random (it would lead in quasi-isotropic properties) while more often there is a main fiber direction.

With fibers inclusion into the matrix, the strain failure is decreased but the maximum stress and elastic modulus increased, therefore the composite becomes stiffer but brittle.

Final properties are trade-off between stiffness/strength and ductility.

The **combination** of a **high ratio between Young's modulus and density with** an **improved design structure** (to reduce maximum stresses appeared along the structure and maximize its stiffness), **makes the SFRP composites a good material solution for lightweight applications**.

4.2.5 Polyamide 6 reinforced with glass fibers

Even if raw polymers like the polyamide 6 are one of the most significant materials used in many industries, for instance in electronic, automotive, industrial or medicine, its mechanical properties like the Young's modulus are very low to bear loads during its applications.

The mechanical properties of the PA6 are a Young's modulus between the 3000 and 1000 MPa and a Stress at yield between 80 and 45 MPa. Additionally, the PA6 has good resistance to creep, excellent abrasion, chemical and heat resistance and low coefficient friction (Pentagon Plastics Ltd., 2014).

On the contrary, fibers with fiber-form allows to increase the maximum tensile strength and stiffness of the material but there are some disadvantages: fibers alone cannot support longitudinal compressive loads and their transverse mechanical properties are inferior to the

longitudinal properties. That is why fibers alone are not suitable for structural purposes, and must be added to matrices (Gibson, 2011).

The mechanical properties of glass fibers are a high tensile strength between 2800 and 4500 MPa, a high Young's modulus between 72000 and 80000 MPa with a low density. Furthermore, glass fibers have low humidity absorption and are good electrical insulators (AZO Materials, 2001).

That are the reasons why glass fiber reinforced polymers cover a relevant position in the market and have a wide variety of applications that ranges from short to long discontinues fibers with polymeric matrices

However, polymeric materials are negatively influenced by moisture and temperature affecting their behaviour. They tend to absorb humidity from the atmosphere and this strongly influences its performance, decreasing its strength and stiffness.

4.2.6 Rule of mixture

In unidirectional, continuous fibre reinforced materials mechanical properties depend on fibre and matrix properties, combined on the basis of fibre volume fraction.
Rules of mixtures are valid for predicting some elastic constant and tensile strength in unidirectional continuous fibers, but it does not for SFRP composites becoming this formula not compliant.

$$E_1 = E_f V_f + E_m E_m$$

Where

$$V_f = \left[1 + \frac{\rho_f}{\rho_m}\left(\frac{1}{W_f} - 1\right)\right]^{-1}, \qquad V_m = 1 - V_f$$

And where *V* is the phase volume content percentage and *W* is the phase weight content percentage. In addition, the sub-index *f* is referred to fibers and *m* to matrix. Additionally, E_1 is the young modulus along the longitudinal 1-axis.

The main factors influencing the material performance of SFRP are the **fiber volume fraction**, the **fibre length** and the **fibre orientation**.

4.2.7 Stress distribution in the fibre and aspect ratio

Coming from analytical models like the Shear Lag Model from a representative volume element (RVE), the stress equation is defined as:

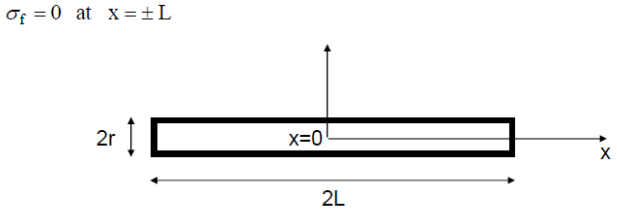

Figure 12. Fiber of the Representative Volume Element (RVE)

$$\sigma_f = E_f \varepsilon_1 \left[1 - cosh\left(\frac{nx}{r}\right) \text{sech}(ns)\right], \quad n = \sqrt{\frac{2E_m}{E_f(1+v_m)\ln\left(\frac{1}{f}\right)}}, \quad s = \frac{L}{r}$$

Where *s* is the **fibre aspect ratio**. If the aspect ratio increases, the fiber will tend to be slender. Besides, the reinforcing efficiency decreases as the fibre length is reduced.

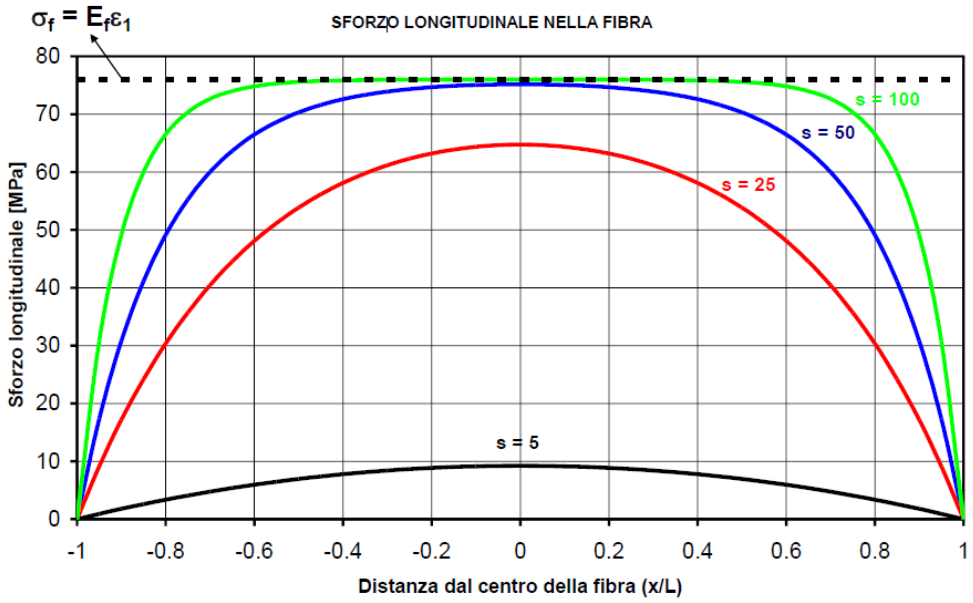

Figure 13. Longitudinal stress along the fiber

Additionally, the stress transfer aspect ratio (s_t), exhibit by fibers in which the peak central stress (x=0) closely approach the maximum possible (at which its strain is equal to the value being imposed on the composite).

So, for this maximum value of stress, the range for the stress transfer aspect ratio (s_t) will be:

$$S_t \geq \frac{3}{n}$$

Being *n* 0.1 for polymeric matrix composites and 0.4 for metal matrix composites.
Therefore, the range for the stress transfer aspect ratio will be:

$$Metals \quad 7 < s_t < 30 \quad Polymers$$

If the aspect ratio and the stress equation is included in the rule of mixtures, the theoretical result will be closer to the experimental value, but still it will not take into account the full FLD and FOD, making the equation not completely valid.

4.2.8 Fiber length distribution (FLD)

During the compounding and injection moulding processes, the fibers suffers a gradually and progressively shorten of their length.

The mechanical properties of SFRP composites are dependent on the FLD (Fu S-Y, 2009) which is subjected to the fiber content and process conditions. A higher viscosity of the melting will produce additional interaction between fibers and therefore its damage and shortening.

Using experimental measurements it can quantified the number of fibre's length from a specimen carefully prepared.

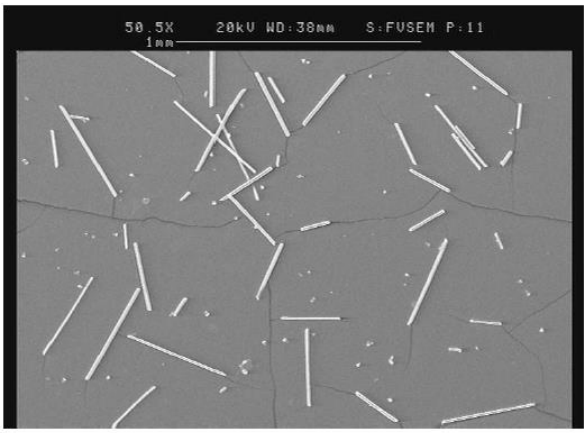

Figure 14. Example of the photomicrograph of a SFRP composite specimen (Bernasconi, Short fibre composites, 2018)

Once this have been done, it is possible to proceed with statistical analysis. It is assume a fiber length (*l*) which can vary from zero to l_{max} for case of a particular SFRP composite. Then, the fiber length l_{max} can be divided into *n* intervals and each fiber length will be equal to *Δl*.

Therefore, the relationship between these parameters is the following:

$$n = \frac{l_{max}}{\Delta l}$$

If *Δl* is increased, *n* will decrease.
At this point is usual to define a set of lengths containing families of fibre's length which ranges from *l* and *l* +*Δl*.

If *N* is the total number of lengths which have been measured already, it is possible to evaluate the number N_i of fibers which belong to a particular interval *i = (l, l + Δl)* and its relative fraction fibers frequency *h(l)* within the *i*-th interval. Therefore, it can be obtained:

$$h(l) = \frac{N_i}{N}$$

Where *l* is the total length at the beginning of the *i*-th interval. Consequently, the combination of expressions defined before gives the evaluation of the probability density function (FLD):

$$f(l) = \frac{N_i}{N\Delta l}$$

This equation describes well the FLD and can be plotted for obtaining a histogram showing the probability density which a fiber could have for a certain length.

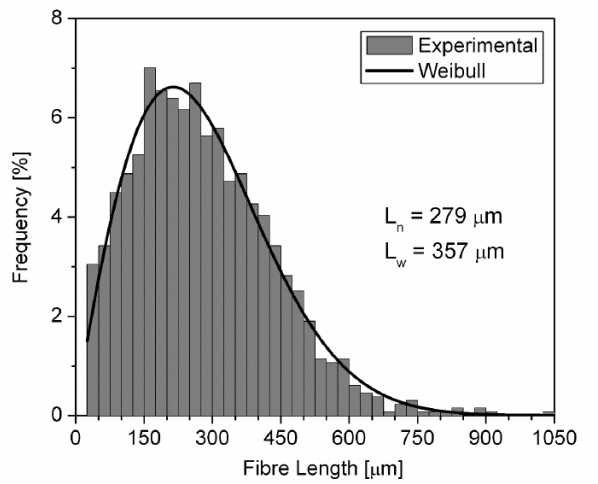

Figure 15. Example of the histogram of a fiber length distribution (FLD) (Bernasconi, Short fibre composites, 2018)

Once this is done, some statistical trends can be modelled and studied through different possible functions

The suggested by Fu and Lauke (Fu S-Y, 2009) is shown ahead.

$$f(l) = abl^{b-1}e^{-al}$$

Where *a* and *b* are constants that have to be determined through a best-fitting process.

4.2.9 Fibre orientation and weld lines

The flow of the polymer filling the cavity induces a complex phenomenon resulting in a fibre orientation pattern known as skin-core-skin.

If the polymer is very viscous appears a shear flow which leads residual stresses. The walls are colder than the polymers, so it gets the elongation of the flow. In addition, the material starts solidifying near the surfaces an evolving along the direction of the flow.

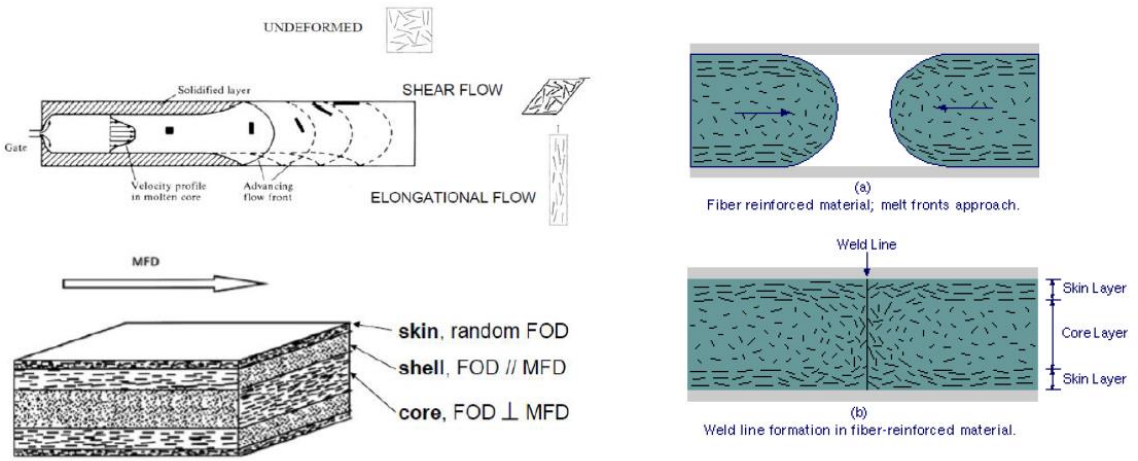

Figure 16. Fiber orientation evolution towards the flow direction. Weld lines creation and skin-core-skin pattern

Due the shear flow appearing near the wall, the orientation is parallel to the flow, creating a skin. On the contrary, in the core the orientation is almost perpendicular to the flow direction.

Therefore, surfaces with fibers randomly oriented and not aligned with the longitudinal stress, makes the material weaker.

Multiple gates or need for the flow to pass around inserts, cause the formation of weld lines.

The typical fibre orientation patter in a regular square mould is shown in the following image:

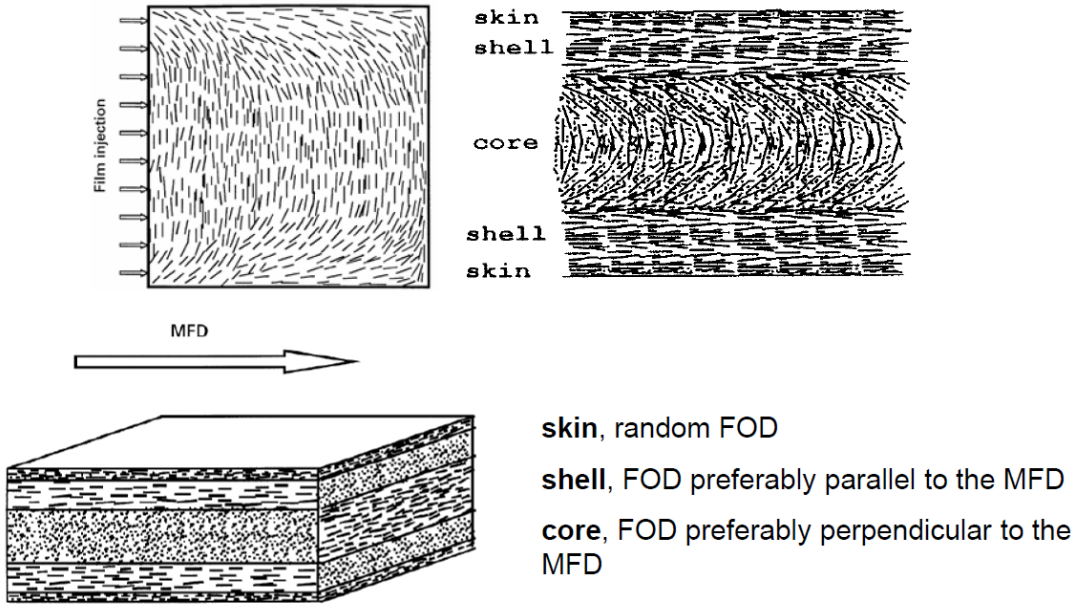

Figure 17. Fiber orientation distribution in the cross section of the MFD

4.2.10 Measurement of fiber orientation distribution (FOD)

As was previously discussed, fiber orientation affects significantly the mechanical properties of the SFRP composite. In addition, the fiber orientation can be strongly influenced by processing condition and mould geometry (Fu S-Y, 2009).

Fiber orientation can be measured using an image analyser system.
For small specimens, fibers will be aligned preferentially along the flow direction, but as the specimen thickness increases, fiber orientation also changes.

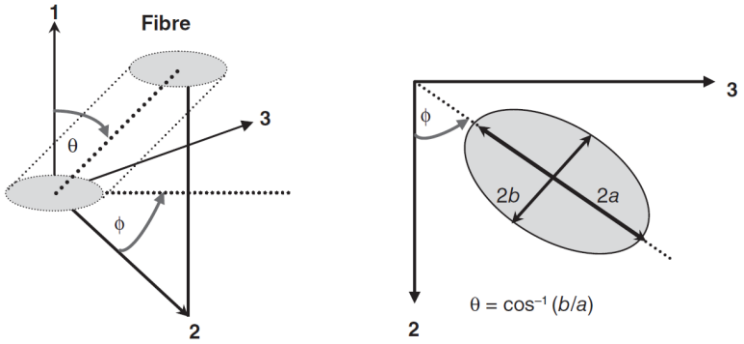

Figure 18. Definition and determination of the fiber orientation θ angles and ϕ (Hine, 1996)

From the *Figure 18* and its reference system, two Euler angles (θ, ϕ) define the 3D orientation of a fibre at the spatial position. The θ is defined as the angle that the fibre makes with the injection direction and can be obtained as $\theta = \cos^{-1}(b/a)$.
The ϕ is the angle that the fibre makes with the 2-axis when projected to the plane 2-3 and is determined from the orientation of the semi-major axis of the ellipse to the 2-axis (*Figure 18*).

The disadvantage of the approached explained above is that uses destructive techniques for determining fiber orientation.

4.2.11 Definition of fiber orientation distribution (FOD)

To describe the fibre orientation distribution (FOD) in SFRP composite, a spatial curvilinear coordinate system is adopted (Fu S-Y, 2009).

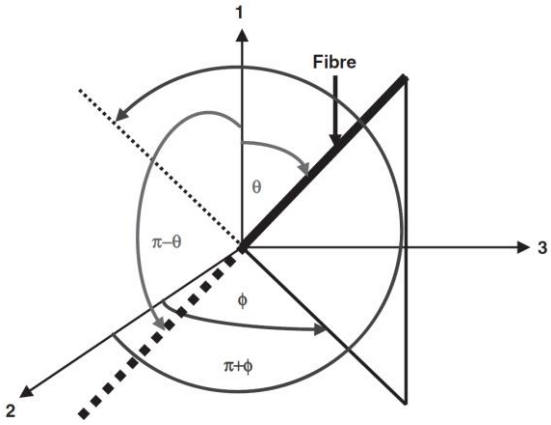

Figure 19. Definition of the fibre orientation angles: θ, π-θ ,ϕ and π+ϕ

The angle θ is projected from one end of the fiber to the 1-axis, the π-θ is the angle at the other end of the fiber wit the 1-axis, ϕ and π+ϕ are the two angles of the projection of the two fiber ends onto the 2-3 plane with the 2-axis.
The function which describes the fibre orientation distribution *g(θ)* is defined as follows:

$$g(\theta) = \frac{\sin\theta^{2p-1}\cos\theta^{2q-1}}{\int_{\theta_{min}}^{\theta_{max}} \sin\theta^{2p-1}\cos\theta^{2q-1}d\theta} \quad \text{for} \quad 0 \le \theta_{min} \le \theta \le \theta_{max} \le \pi/2$$

Where *p* and *q* are shape parameters that can be employed to determine the shape of the distribution curve, and $p \geq 1/2$ and $q \geq 1/2$.
$g(\theta)d\theta$ is the probability which the fibre orientation is between θ and $d\theta$.

The cumulative distribution function of fibre orientation (θ) is $G(\theta)$, the cumulative percentage of fibres whose orientations varies from θ_{min} to θ:

$$G(\theta) = \int_{\theta_{min}}^{\theta} g(\theta)\,d\theta = \frac{\int_{\theta_{min}}^{\theta} \sin\theta^{2p-1}\cos\theta^{2q-1}d\theta}{\int_{\theta_{min}}^{\theta_{max}} \sin\theta^{2p-1}\cos\theta^{2q-1}d\theta}$$

The most probable fibre orientation angle at which the fibre probability density is the highest (θ_{mod}) its defined as:

$$\theta_{mod} = \arctan\left\{\left[(2p-1)/(2q-1)\right]^{1/2}\right\}$$

So, for a combination of the values *p* and *q*, the fibre orientation curve are:

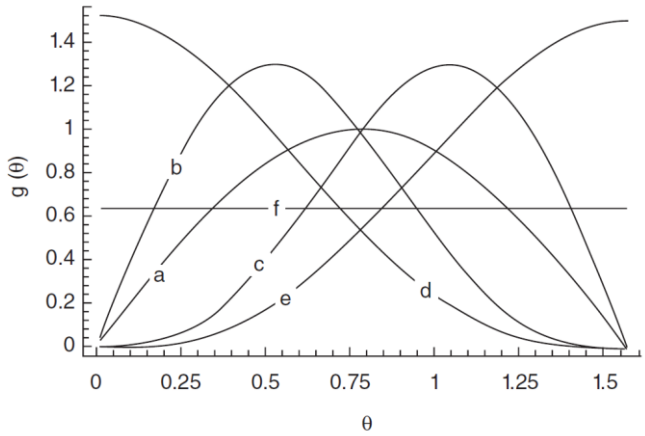

Figure 20. Fiber orientation curves for p and q

The curves shown in *Figure 20* are the combination of: (a) p=q=1; (b) p=1, q=2; (c) p=2, q=1; (d) p=1/2, q=2; (e) p=2, q=1/2; (f) p=q=1/2 (random distribution).

Afterwards, similar to $g(\theta)$ it can be defined an orientation probability density function $g(\phi)$ for the fiber orientation angle ϕ.

$$g(\phi) = \frac{|\sin\phi|^{2s-1}|\cos\phi|^{2t-1}}{\int_{\phi_{min}}^{\phi_{max}} |\sin\phi|^{2s-1}|\cos\phi|^{2t-1}\,d\phi} \quad \text{for} \quad 0 \leq \phi_{min} \leq \phi \leq \phi_{max} \leq 2\pi$$

The probably function for a pair of orientation angles (θ, ϕ), also known as the orientation distribution function $g(\theta, \phi)$, is defined such that the probability of the fibers lying in the infinitesimal ranges of θ to $\theta + d\theta$ and ϕ to $\phi + d\phi$ is given by $g(\theta, \phi)d\psi$, where $d\psi$ is the infinitesimal solid angle (Fu S-Y, 2009).

$$g(\theta,\phi)d\psi, \qquad d\psi = sin\theta d\theta d\phi$$

Since

$$g(\theta,\phi)d\psi = g(\theta)g(\phi)d\theta d\phi$$

Finally, the orientation distribution function $g(\theta,\phi)$ is obtained, which satisfies its periodic condition and its normalization condition.

$$g(\theta,\phi) = g(\theta)g(\phi)/sin\theta$$

4.3 Additive manufacturing

4.3.1 Science and technology

Additive manufacturing or also popularly called 3D printing, is the manufacturing technology in which the part is build up layer by layer directly from digital 3D model data, obtaining a final product without any intermediate tooling (Gibson I, 2014).

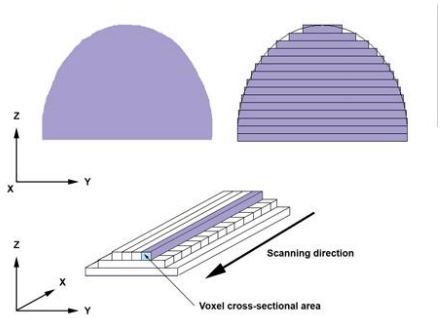

Figure 21. The layering process in additive manufacturing

Traditionally, additive manufacturing (AM ahead) has been used for what was called rapid prototyping (RP ahead) (Chua C K, 2010). This is because AM allow to churn out a high number of parts with a relatively easiness. At the same time, RP consists in rapidly creating physical prototypes of a design before its final release or commercialization (Gibson I, 2014). In the 1980s, at the early ages of the technology (Hoffman, 2018), new possibilities of building up highly complex geometries with the elimination of specific tooling raised (Haden E. Quinlan, 2017), but still the poor mechanical properties in the final part, have been AM a traditional candidate for rapid prototyping.

When AM was still a brand new technology, stereolithography processes were used with photopolymers sensible to ultraviolet light lasers (Gibson I, 2014). Still in the 1980s, fused deposition modelling started to be used with extruded polymers.

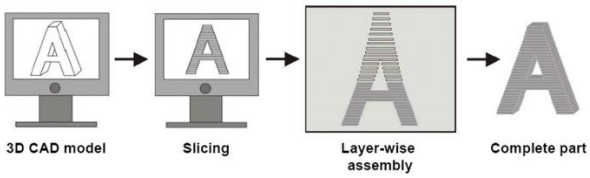

Figure 22. Conventional steps from CAD model to a complete part

Since the 2000s, when the term additive manufacturing gained wide popularity to refer to the technology more than 3D printing (Hoffman, 2018), the term subtractive manufacturing (or subtractive technologies) appeared as a heteronym for the traditional manufacturing processes where material is removed from raw material using techniques as machining.

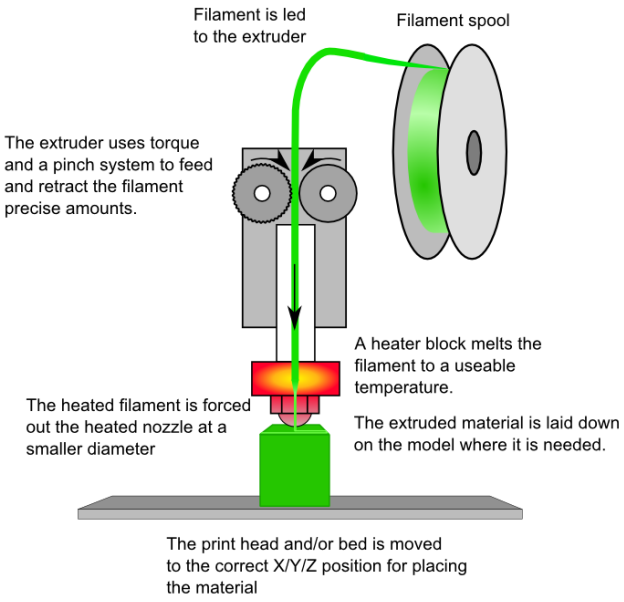

Figure 23. Fused Filament Fabrication (FFF) process in AM

In the 1990s, AM with metals emerged together with the technologies of selective laser sintering (SLS) and selective laser melting (SLM). At that time, subtractive technologies where completely developed and the achievable part tolerances and strengths with traditional processes had no competitors in the market (Gibson I, 2014). It has been like that during a couple of decades until the 2010s, where the developing of metal AM had a significant push in the aerospace and turbine industries (Roland Berger, 2016).

Since 2013, AM for metals has become the talk of the town and different companies realized the ground breaking potential of this new production technology and the actual mature state, which is ready to be launched for large productions.

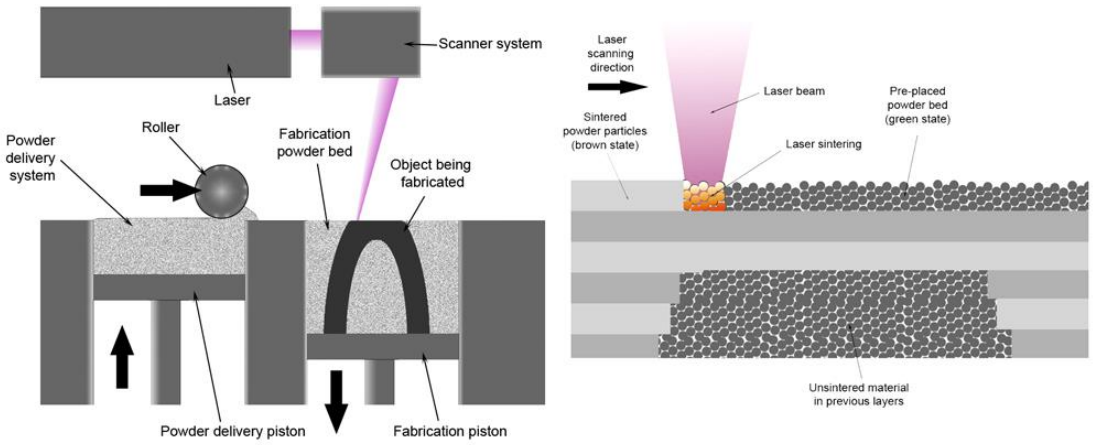

Figure 24. Selective Laser Melting (SLM) process in AM

This is not happening only for metals, also since the 2010s other materials have aroused in AM appearing as a vanguard technology born in research laboratories. Even more, it is starting to gain territory in sectors where parts have been traditionally manufactured with other technologies and materials.

For example, in the fashion industry, clothes are being designed and additively manufactured for experimental purposes (Baggaley, 2018).

In 2012, 3D Bio-printing technology has been developed with biotechnology to print living cells and organs with inkjet printing techniques (BBC, 2012) to regenerate and repair organs and body parts that have been damaged.

4.3.2 Materials and applications

4.3.2.1 Textile and fabrics

AM cost efficiency and flexibility can offer products for the textile production of 3D objects using flexible filaments such as thermoplastic elastomers and PLA. Properties as good adhesion and 3D printed stable structures are key for a reliable fabric manufacturing (Korger M, 2011).

Figure 25. 3D printed trainers

In the textile industry, custom fit shoes are being 3D printed for athletes (Resins Online, 2013), and other initiatives are appearing like customized 3D printed t-shirts (Locker, 2016), where it's taken advantage for the elasticity of the printed material from another perspective.

4.3.2.2 Food

Food can be 3D printed in an automated additive manner. Extruding the food in layers and taking profit from its freedom to print semi-prepared food, can end up with food dishes made of different shapes.

AM of food is a reality and is being developed by squeezing out food like chocolate, pasta and pizza (Wong, 2014).

4.3.2.3 Polymers and plastics

As introduced before, the initial application of AM was for Rapid Prototyping using thermoplastics (Gibson I, 2014). In this case, polymers are the cheapest and most developed materials available for AM and technologies. Besides, there are also commercial 3D printers available to be sold for household uses (SPI Lasers, 2018).

Figure 26. 3D printed parts made of plastic

The most common thermoplastics used in AM are: polylactic acid (PLA), acrylonitile butadiene styrene (ABS) and Polycarbonate.

Compared to other materials, polymers tend to have low mechanical properties such as strength and stiffness and low thermal and chemical properties (Bates, 2018). For this reason, they are used for unload applications. Despite this, polymers are the most spread material used in AM.

Some of its applications when 3D printed are Rapid Prototyping, industrial applications and aerospace, medical, automotive industries, manufacturing parts to be used for unload purposes.

In architecture, AM of plastics has found a useful application for creating physical models, being a way to create a first prototype of the building.

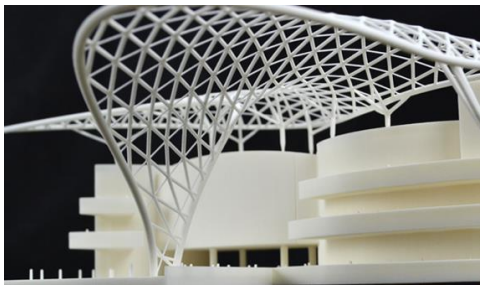

Figure 27. 3D printed building prototype made of plastic

4.3.2.4 Metals

Since the 2010s, metal additive manufacturing has jumped into the enhancement resolution process. In this regard, any companies have started to invest large amount of money to improve this technology at the same time they are announcing the era of a new manifesting paradigm.

The moment the mechanical properties of final parts made by AM meet the design requirements, new possibilities are available. Applications like aerospace, automotive, medical, mould tooling and conformal cooling channels (Renishaw, 2016) for metal AM can start growing into markets where traditional subtractive manufacturing techniques had no competitors until the recent years.

No longer as a prototyping technology, cases like the redesign of a helicopter engine by GE Aviation (Zelinski, 2017), using new design techniques for additive manufacturing, achieve a significant reduction of the number of the engine parts from 900 to 16. This shows the impact this technology has, not only in the conception redefining how the parts must be designed and manufactured, but the impact in the supply chain, reducing its complexity.

Another example of what can be achieved is what Renishaw is developing for healthcare solutions (Renishaw, 2016). The new possibilities that metal AM offers for complex geometries fits with the individual customization that medical devices need in their manufacturing for craniomaxillofacial implants and guides.

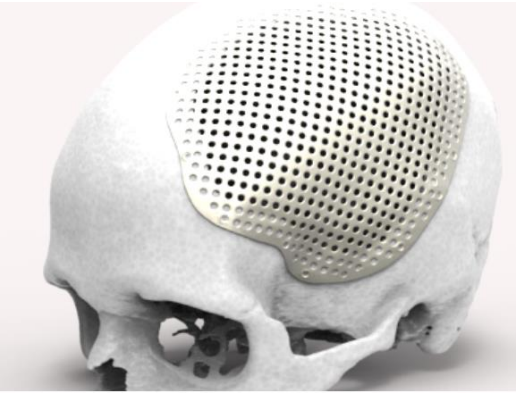

Figure 28. 3D printed craniomaxillofacial implant made of surgical metal

4.3.2.5 Composite materials

An important point is the incoming use of composite materials with continuous fibers in additive manufacturing systems is arising. The rise of AM technologies is giving a change to alternative materials which requires a certain level of evolution and maturation of the technology in the aerospace and automotive industries.

An example developed in the market is what Markforged did in 2013, introducing the first commercial small 3D printer that was capable of building polymer structures with continuous carbon fiber reinforcement in the x/y plane (Gardiner, 2016).

In the same way, in the science of short fiber reinforced polymers composites, commercial 3D printers capable of 3D print reinforced polymers are growing. Moreover, they are even able to produce the world's first 3D printed composite auto body in 44 hours and then increasing print size to 6m by 2.4m by 1.8m and printing speeds up to 45-68 kg/h (Gardiner, 2016).

Even if this information proves that the manufacturing technology capabilities are possible, the achievable product reliability and the mechanical properties of the final printed part are poor. This can be noticed from different research publications regarding this topic. In the next section, different sources will bring up the matter.

4.3.3 AM for SFRP composites

4.3.3.1 Research

After performing a research about AM for SFRP composites, different authors discussing the pros and cons about the simulation of AM for SFRP composites and the experimental tests done in different researches have arisen.

P. Parandoush and D. Lin from Kansas State University in the US, made a review on additive manufacturing of polymer fiber composites (Parandoush P, 2017).
In their research, they use technologies as fused deposition modelling (FDM) and stereolithography (SL).

With FDM technologies, they state that most of the efforts done until now have been focused in the development of filaments with short fiber additives. The inclusion of fibers in filament reduces tape swelling at the printing head during deposition and increases the stiffness. Moreover, the utilization of ABS and PP have been used to overcome drawback at low aspect ratio of fiber in SF filled parts. They highlight that processing temperature affects the surface morphology and therefore its mechanical properties. Apart from that, there is a clear superiority in the achievable mechanical properties of continuous fiber composites versus SFRP composites.

The usage of stereolithography techniques using photopolymers with high weight ratio of short fibers can yield comparable results. Although, their efficiency is limited to fiber fracture during mixing, random orientation and uneven length.

The paper of P.Parandoush and D. Lin makes reference to two probability functions for modelling the fiber length and fiber orientation distribution to predict elastic properties (Fu S-Y, 2009). Besides, the Halpin-Tsai theory for unidirectional short fiber composites is mentioned too (Fu S-Y, 2009).

Traditionally these authors approached their theories for conventional injection moulding manufacturing systems. Even if these equations can be used for 3D printed parts, length and orientation of the fibers used in the process should match the assumptions. FDM, SLS and extrusion with SFR can be modelled with these analytical methods having in mind that high void content is present in AM.

The authors conclude their article commenting the current approaches for structural and manufacturing simulations.
The moment a FEM is likely to be carried out, the void content would need to be incorporated in the FE model. Additionally, the approaches for mechanical modelling of fiber composites are homogenization. Also, the need for simulation of the 3D printing process is certain. Unit cells depend upon the microstructure of the composite SFC with random orientations.

T.Hofstatter together with some of his colleagues from the Technical University of Denmark discus about some applications of fiber-reinforced polymers in Additive Manufacturing (Hofstätter T, 2017).

They state that vat polymerization and material extrusion techniques increase adhesion between matrix and fibers in composites printed with AM technologies. In comparison with traditional injection moulding technologies for SFRP composites, with AM, a reduction of production costs as well as the environmental impact of prototyping and proof-of-concept manufacturing can be achieved.

T.Hofstatter discuss about the results of some printed specimens.
Air intrusions are likely to occur while using freely extruded filaments. Although, it was noticed the clustering of fibers within the filament. This clusters contain fiber groups with a high grade of orientation, appearing a general tendency of fiber orientation.
The fiber orientation characterizes the general flow of the polymer through the nozzle as well as the deformation after the nozzle exit. The defection of some critical parameters was found: the control of the velocity and pressure of the extrusion nozzle is key (Hofstätter T, 2017).

The authors conclude that the use FRP in AM helped to improve lifetime and reduce crack propagation. Moreover, the inclusion of Short Carbon fibers showed an increasing effect on Young's modulus but, decreasing strength and tensile strength. Consequently, the material must be used in low-strength regimes.

Regarding cons detected, there is a need of improvement in the fiber -matrix interfaces to reduce failures and standard deviation of the mechanical properties.

Other authors like M. Ivey and Garret W. from the University of Alberta (Canada) have tried to characterize SFRP composite using low-cost 3D printers and comparing PLA samples against PLA/CF (Ivey M, 2017).

They observed a significant quantity of large void in PLA/CF printed samples when compared to the PLA. The extruder nozzle clogging may be a significant factor in the void appearing when printing PLA reinforced with carbon fibers.

They noticed a notable fiber orientation with the filament extrusion direction (assumption of orthotropic material or transversally isotropic is valid). A good fiber distribution and dispersion was also detected.
This fact makes valid the assumption of homogeneous material at a macroscopically level.

Both characteristics may allow mechanical properties of 3D printed components to be tailored by controlling the orientation of print layers. Nevertheless, major gaps appeared at the boundary between the shell and infill and dimensional accuracy was poor at the edges.

During the test, additively manufactured specimens produced lower tensile properties than equivalent injection moulded parts.
In the same way, 3D printed components exhibit a lower elastic modulus than injected moulded components due to the orientation of plastic fibers within the sample structure, voids present, and incomplete bonds between layers in the 3D printed structure (Ivey M, 2017).

Other sources from authors at Florida University State University, College of engineering in the US, reviewed contemporary and modern techniques for advanced materials manufacturing (Frketic J, 2017).

They made some investigations about extrusion of SFRP composites since this technique is the most common for this type. Composites made with material extrusion along the print direction had the highest modulus, thus providing the ability to tailor stiffness in specific directions.

There is a corresponding lack of stiffness in the direction transverse of printing for material extrusion composites; probably due boundaries between layers yield voids and discontinuities.

The strength of printed fiber reinforced composites does not have such clear delimitations as the elasticity, but material extrusion dies have the highest strength of the different methodologies, it may due to the higher loading percentages of chopped fiber within these printed composites.
Poor interfacial properties between the matrix and reinforcement material and fiber pull-out are common (which leads to low load transfer to the fiber component of the composite).

The ability to redirect the reinforcing material during the printing process is currently gaining traction due to its ability to customize part strength.
AM has the ability to align fibers multiple ways as well as control fiber volume throughout the part (not possible for traditional manufacturing techniques). On the contrary, interfacial properties must be better understood. This is something in which further works will have to perform deeper investigations (Frketic J, 2017).

Another paper from authors B. Brenken, E.Barocio and A. Favaloro from the Composites Manufactuirng and Simulation Center in Indiana, reviewed the FFF for fiber reinforced polymeric materials (Brenken B, 2018).

They start the discussion about the comparison between discontinuous fiber-reinforced printed polymers and aircraft aluminium alloys. The authors state the comparison cannot be fairly made yet, firstly because of the fiber damage during the printing process and printing defects related with related void formation, decreasing enormously the mechanical properties of the polymeric parts manufactured with FFF.

The second argument exposed is about the reported properties transverse to the deposition direction for thermoplastic fiber-reinforced materials are especially low; identifying the transverse directions as one key limitation of printed materials (Brenken B, 2018).

Although, FFF method shows promising potential for the application to composite tooling. Significant time and cost saving are possible in comparison to traditional tool manufacturing, especially for prototype and low series tooling.

Most studies in the field of flow and fiber orientation assume an uncoupled, isotropic Newtonian flow, while the material should be modelled as a viscous fiber suspension flow.
No publication has considered the effect of the fibers on the resulting bond formed between adjacent beads yet. How the viscosities transverse to the printing direction change with the addition of fibers has to be investigated (Zhong W, 2001).

There are only a limited amount of relevant works published in the identified research areas. Usually studies investigate significantly simplified versions of the FFF process where not all involved phenomena are taken into account (Goh G D, 2018) (Ning F, 2015).

FFF process itself is still empirically calibrated. A need for further models is necessary.

4.3.3.2 Summary and conclusions

Even if the amount of specific bibliography published nowadays is not overwhelming, the significant relevance of the studies, aim the same conclusions about this new way of manufacturing short fiber reinforced polymers composites.

The different authors cited above seem to point into the same direction having similar comments and conclusion in their respective investigations. A summary of the main concepts has been gathered in the following lines:

Research conclusions about printing SFRP composites in AM
1). **Fiber damage** during printing process reduce significantly **mechanical properties** of the printed part. 2). The **control** of the **velocity and pressure of the extrusion nozzle** is key if void appearing and interfacial failure is wanted to be diminish. 3). The **extruder nozzle clogging** may be a significant factor in the **void appearing**. 4). Printing defects like **voids creation** decrease drastically the **mechanical properties** of the additively manufactured part. 5). High void presence in AM printing technologies. **Voids presence needs to be incorporated in the FE model**. 6). **Longitudinal properties of SFRP composites** made by AM **equal** properties in a part manufactured by **injection moulding**. 7). **Transverse properties of SFRP composites** made by AM are **especially low** in comparison to its similar in injection moulding. 8). **Poor interfacial properties** between the matrix and reinforcement material. 9). **Fibers** tends to be **aligned** to the **filament extrusion direction** (anisotropic, orthotropic and transversally isotropic properties are valid). 10). **Good fiber distribution and dispersion** along the **printing direction** (homogenization is a valid assumption). 11). Points 9) and 10) allows a **certain control** over the mechanical properties and **tailor the stiffness in specific directions**. 12). **Processing temperature** affects the **surface morphology** and therefore its **mechanical properties**. 13). AM allows a significant **reduction of production costs**, **time** and **environmental impact** during manufacturing.

Table 1. Research conclusions about printing SFRP composites in AM

In terms of cause and effect relationships, the information above can be rewritten as follows:

Cause and effect relationships of key parameters in 3D printed SFRP composites
Improper control of velocity and *pressure of extrusion nozzle* would be the **cause** for the **effects** of *void creation* and *poor Interfacial properties*. At the same time, *fiber damage during mixing*, *void creation*, *poor transverse properties, poor interfacial properties* and *uncontrolled processing temperature* would be the **cause** for the **effect** of *reduction in the mechanical properties* of the composite.

Table 2. Cause and effect relationships of key parameters in 3D printed SFRP composites

4.4 Topology optimization

As was said before, additive manufacturing brings complexity for free during the design phases but, is that complexity necessary?

In order to take full advantage of AM, the object has to be redesigned following optimal functional design methodologies.

An optimal functional design brings: Weight reduction, reduction of number of components to be assembled, surface topology enhancing and changes in the final shape. All these facts can increase the product's quality.

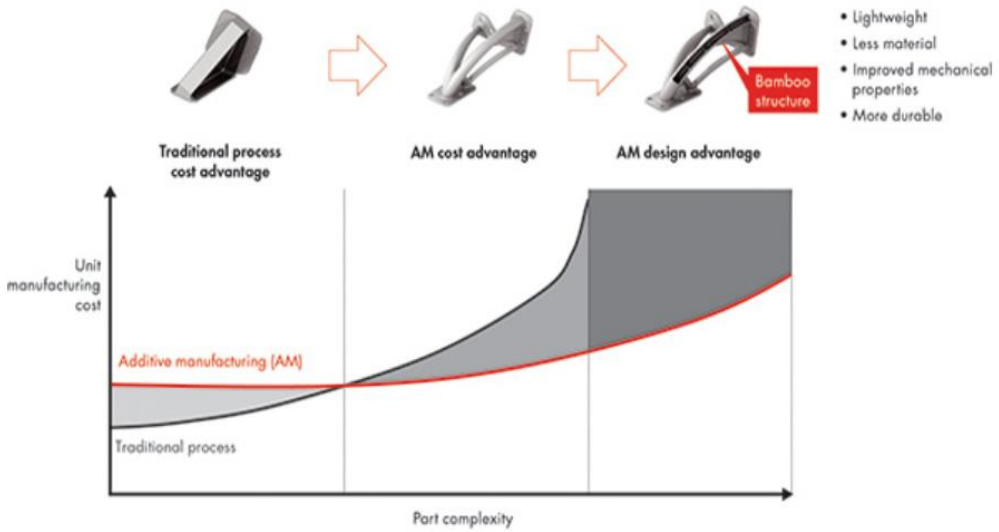

Figure 29. Advantages of AM in terms of cost and design when the complexity of the part increases. Source: Bain

Topology optimization is a mathematical approach that optimizes material layout within a given design space, for a given set of loads and boundary conditions such that resulting layout meets a prescribed set of performance targets or design specifications (Colosimo, 2017).

On the contrary as parametric design does, the non-parametric design through FEA can analyse a new shape in terms of different element connectivity, not always having the same shape.
With topology optimization it is possible to perform an optimization task to start an initial design and optimize it (material removed where is not necessary). Therefore, changes in the connectivity appears (holes between elements) (Bernasconi, FE based optimum design, 2018).

Given an initial material distribution, topology optimization produces a new landscape by scaling the relative material densities of the elements in the design domain. Stiffness is assumed to depend on density.

Starting from a mesh of solid elements, each iteration modify the density of elements and there, appears a relationship between this density and its strength.

It can be made softer elements where they are not needed. Where the stress are very low, the material can be removed without affecting the general behaviour of the structure.

These parts in where the number of elements are low, they become softer and therefore the stresses will be even lower (element less charged are like springs in parallel, the stress per head will be distributed). The engineer has to stabilize the threshold for the density and for the kind of interpolation is performed.

At the end of the optimization process, elements with large relative material densities are retained, while those elements whose relative material densities have become sufficiently small are assumed to be voids.

For the purpose of this project, is going to use Tosca, the non-parametric structural optimization tool module in ABAQUS/CAE. Tosca allows three classes of structural optimizations: topology, shape and sizing (Dassault Systemes, 2018).

4.4.1 Optimization Statement

The optimization statement is the minimization of an objective function (*f(x)*) subjected to equality (*h(x)*) and inequality (*g(x)*) constraints, the three of them as a function of the design variables (*x*).

$$Minimize\ f(x), subjected\ to\ g(x) \leq 0\ and\ h(x) = 0$$

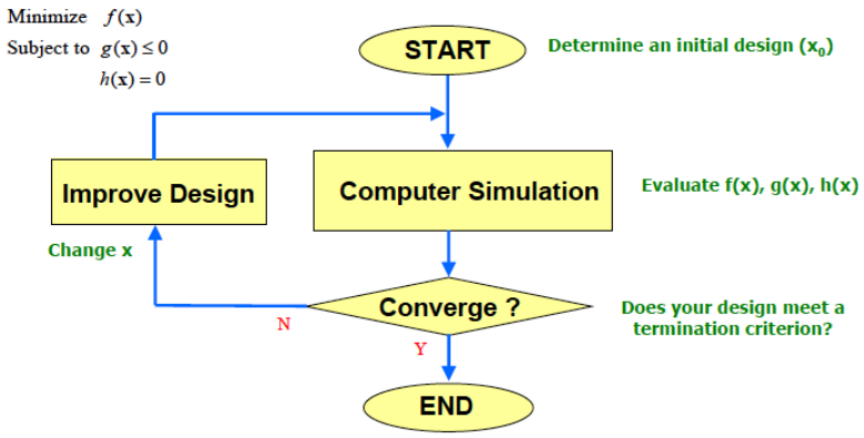

Figure 30. The optimization procedure algorithm (MIT, 2017)

4.4.2 Algorithms for topology optimization in Tosca

The module Tosca is based in two kind of algorithms for its optimization problems:

a) Condition-based optimization

It is an iterative redesign rule that changes the design to achieve an optimality condition. Allows only to find the stiffest possible structure for an amount of material removed.

b) General (sensitivity-based) optimization

This is the algorithm used in the optimization problem of this work.

A general sensitivity-based topology optimization allows for applying a range of constraints and objective functions to the model (Bernasconi, FE based optimum design, 2018).
For each optimization problem, it has to be defined a set of parameters.

4.4.2.1 Loads and boundary conditions

The set of loads and boundary conditions have to be defined into the problem geometry.

4.4.2.2 Design variables

They are the parameters chosen to describe the design of a system. They are controlled by the designer. They can be the geometry of the cross-section of a beam.

4.4.2.3 Objective functions

The objective function must be expressed as a function of the design variables.

Objective functions can be created from any previously defined design responses. The target for the objective function can be to minimize the weighted sum of the design responses or to maximize the sum of the specified design responses.

4.4.2.4 Constraints

The constraints must be expressed as a function of the design variables.

Several constraints options are allowed in sensitivity-based optimization problem. The constraints are always inequalities in sensitivity-based optimization problems. They can be a stress or a displacement value for example.

4.4.2.5 Design domain

The region of the model which will be included in the optimization problem. For structural optimization they are usually the elements of the structure itself.

4.4.3 Statement of a topology optimization problem

For the case of a beam structure clamped at one end (Bernasconi, FE based optimum design, 2018), if it is desired to minimize the tip displacement of the beam, it can be defined the following variables:

Objective function: Minimize the displacement at the free end
Constraint: Reduce mass by a given amount
Design domain: All elements in the beam structure.
Design variables: Relative density of each element in the design domain.

Therefore, it is desired to find:

$$\rho'(x,y): u_{out}(\rho') = min_{\rho} min_{out}(\rho)$$

Subjected to:

$$\sum_{e=1}^{n} v_e \rho_e \leq V \quad , \quad 0 \leq \rho_e \leq 1$$

And where:

v_e is the element volume, p_e is the element relative density, n is the number of elements in the optimization domain and V is the volume corresponding to the imposed mass reduction.

For static problems, the default interpolation technique used is the Solid Isotropic Material with Penalization Method (SIMP).

For this method, the stiffness matrix is scaled as:

$$K_{SIMP(\rho)} = \sum_{e=1}^{N} [\rho_{min} + (1 - \rho_{min})\rho_e^P] K_e$$

And where:

K_e is the element stiffness matrix at the global level, the p_{min} is a small relative density, p_e is the element relative density, P is a penalty term and N is the number of elements in the domain.

4.4.4 Criteria for convergence

The criteria for convergence is evaluated after the 4th design cycle and are the following ones:

The **objective function delta criterion**, which it stops the optimization if the percent change in the objective function over two cycles is less than a prescribed value.
The other is the **element density delta criterion**, where the optimization stops if the percent change in the sum of element densities over two design cycles is less than a prescribed value.

4.5 The design process paradigm

4.5.1 The engineering design process

Since late 1950s, companies have tried to define a methodical process consisting of a series of steps that engineers can use to create functional objects and products. The process usually starts with a first conceptual step pushed ahead by the designer creativity and ends with a final product which functionalities complies with the expected ones

Different authors have tried to formulate definitions and organize the engineering design process in different ways.

In the late 1980s, Pahl, G and Beitz, W defined the design methodology as a concrete course of action for the design of technical systems that derives its knowledge from cognitive psychology and from the practical experience of the designer in different domains (Pahl G, 2007).

They made special emphasis in the iterative nature of the approach, which must not be considered completely rigid.

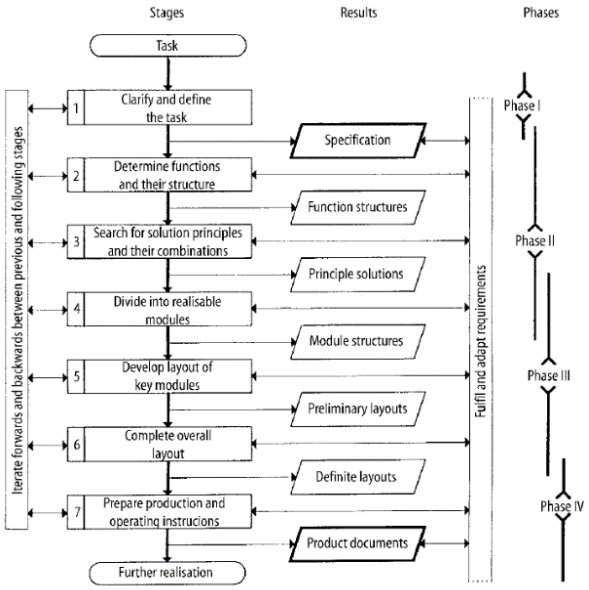

Figure 31. The engineering design process proposed by Pahl, G and Beitz, W.

In 1992, David G. Ullman stated that there are six phases of the mechanical design process: Product discovery, project planning, product definition, conceptual design, product development and product support (Ullman, 2015). The design process focuses the effort on early phases (Product definition. Conceptual design and Product development), which applies to design of systems, subsystems and components.

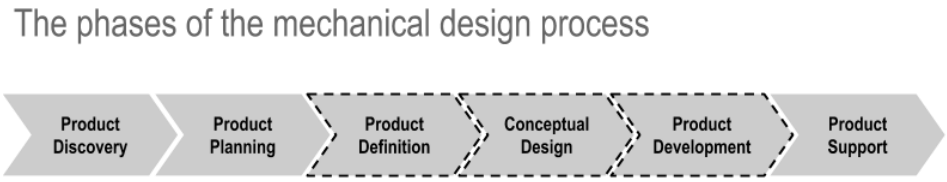

Figure 32. The phases of the mechanical design process

This approach leads directly to an easy integration of the design process into companies' departments, assigning to each one (Marketing, R&D, Production, etc) the different steps of the design process suggested by the author.

Multiple authors (Dym, 2008) (Braha D, 1997) point out the fact that the design process is a purely iterative process in which the last step is just a check out of the initial design specifications. If

these specifications are not yet compliant the cycle continues, if it does, the design cycle ends. The inner steps are defined in major or minor number depending the source.

Other authors, define the design process from the perspective of the field of industrial design. Tomas Maldonado (Maldonado, 1993), the acclaimed Argentinian Industrial designer, defined the design like a creative activity which consist in determining the formal properties of the objects to be industrially produced. Maldonado, referred to these formal properties not only as the object's exterior characteristics, but as the customer point of view.

4.5.2 Design for manufacturability (DFM)

This classical design process approach fit conveniently the traditional manufacturing techniques based on material subtraction. They are widely used, and commence with a raw material which is methodically subtracted by machining concatenated operations, with its completion obtaining the final product. This method has been developed strong constraints to the way how the part has to be manufactured, being the number of subtractive operations a key factor to be minimized, in order to reduce manufacturing cost, time and material waste.

Manufacturability can be affected by other factors like the type and the form of raw material, dimensional tolerances and finishing processes.

The design processes stated above have been following traditionally the need to manufacture the resulting part of the design cycle. This is known as design for manufacturing or design for manufacturability (DFM).

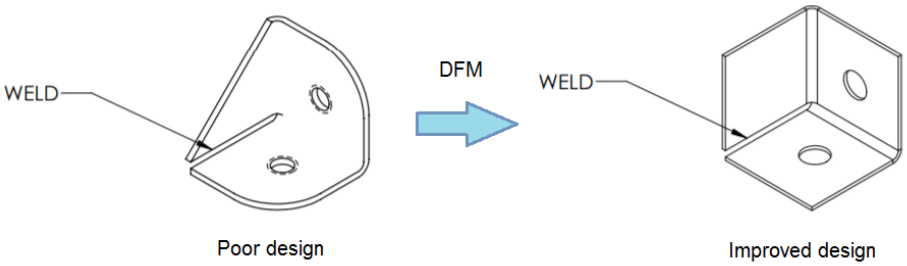

Figure 33. An example of a design improved using Design for Manufacturability

DFM could be defined as the establishing the shape of components to allow efficient, high-quality manufacture (Pahl G, 2007), not altering its functionality. For each manufacturing process, different guidelines can be followed to obtain results in consistent components and little waste. The manufacturing process chosen for the component should include tooling and fixturing, being treated with the developing of the component (Pahl G, 2007) (Bralla, 1998). The omission of these ones usually release components that are difficult or impossible to make. Therefore, **the manufacturability of a component is an active constraint during its conception**. For DFM, **cost become as a function of design and therefore design must minimize the function of cost,** being able to be considered as an **optimization problem**.

4.5.3 Design for additive manufacturability (DFAM)

In the same way, there are guidelines to reduce manufacturing costs for subtractive methods as CNC, Furthermore, there are methods for the rising additive manufacturing technologies. Therefore, **design considerations such as cost and reliability can be optimized to the capabilities of additive manufacturing** (Tang Y., 2015).

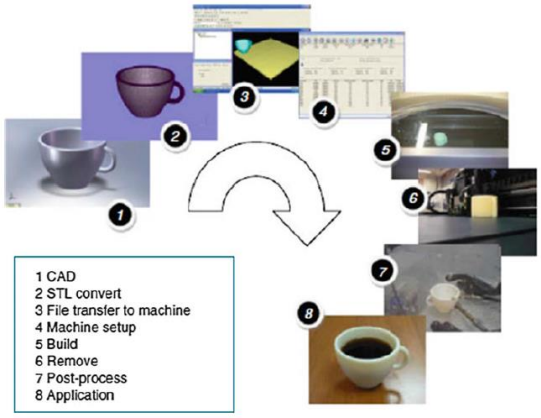

Figure 34. The generic AM process (Images)

With AM, a number of steps emerge to form a generic AM process which goes from the part conceptualization to its final application. I. Gibson (Gibson I, 2014) proposes that all AM parts must start from a CAD model, which has to be converted to STL file format to be accepted by the AM machine. The transfer of the STL to the machine could require additional manipulation depending special characteristics of the machine, part position or building orientation. The AM machine will require then a proper set up previous the building process. Therefore, the automated process can start on the building of the part. After the part completion, this must be removed carefully from the machine. One last thing would be, if necessary, post-processing processes like support removal which are essential for keeping intact the part integrity while manufacturing, but useless for its final functionality. Finally, the part is ready for its application.

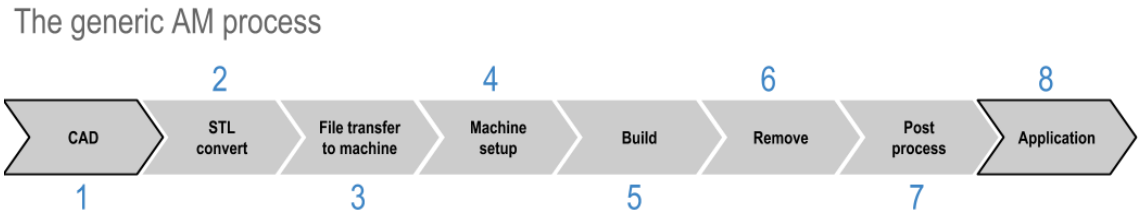

Figure 35. The generic AM process (Diagram)

This methodology is considered apart from the classical DFM because of its additive nature (the material is progressively added instead is subtracted from raw material) and the enormous design freedom provided by AM. This technology has been described as revolutionizing by many authors (D'Aveni, 2015) (Quinlan H E, 2017) (ESA, 2018) (Langefeld, 2013), and the main reasons for these acclaimed citations are its reduction in process steps, high design freedom and the parts complexity achievable (Gibson I, 2014)

Some of the common DFAM methods are:

4.5.3.1 DFAM with topology optimization

Topology optimization is a non-parametric structural optimization method in which connectivity of the design domain changes. Given an initial material distribution within the part, topology optimization rescales the relative material density of the elements in the design domain, producing a new scenario. This is done with mathematical algorithms, producing an iterative loop until the solution is compliant.

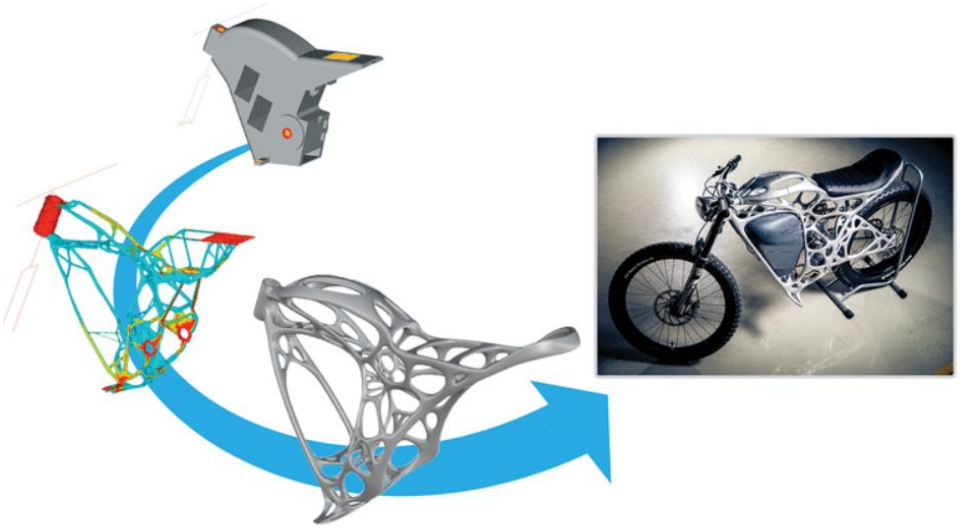

Figure 36. Practical application of a redesign chassis using topology optimization and AM (Atair, 2016)

The resulting part has a brand-new shape, with significant complexity, impossible to achieve with traditional manufacturing techniques. This technique was explained in the *Chapter 4.4* due its relevance in this project.

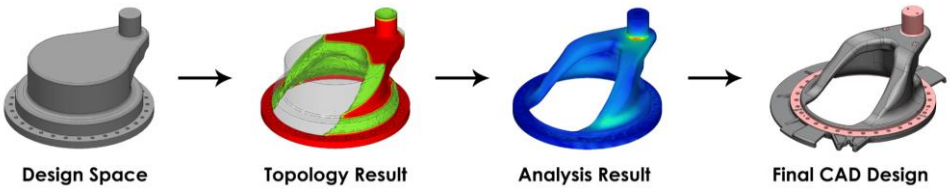

Figure 37. Example of engineering optimization techniques (Luxon Engineering, 2018)

This technique can be introduced in a series of steps within the design process as described in a study by Roland Berger (Roland Berger, 2016) based on a finite element method, topology optimization is proposed in a geometry that needs to be implemented.

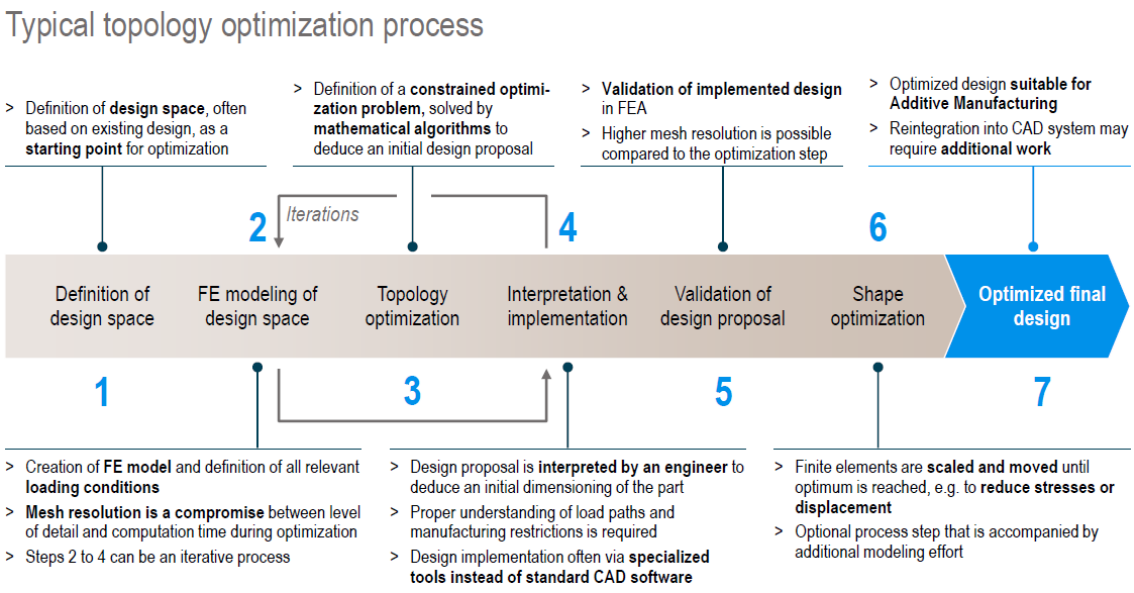

Figure 38. Typical topology optimization process. Source: Roland Berger

What if it is wanted to integrate both process methodologies? (The generic AM process and the typical topology optimization process) The following combination will be obtained:

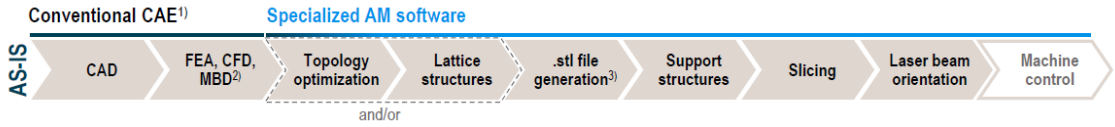

Figure 39. Conventional CAE with Specialized AM software. Source: Roland Berger

This would release the traditional AM engineering process integrated with new techniques for AM design approach, which incorporate design restrictions at the beginning, which could not be the best way to reach the best possible solution.

The solution proposed by Roland Berger in their study (Roland Berger, 2016) tries to take full advantage of strong points and capabilities of AM like the huge design freedom available. This, combined with high computational capabilities, releases into an iterative process where an extra amount of effort is invested in the product development stages. The investment of a large number of simulations can have its turn-over in the following process steps, obtaining a final product fully optimized with guaranteed reliability or in this case, with reduced changes to obtain a part that needs to be redesign or modified.

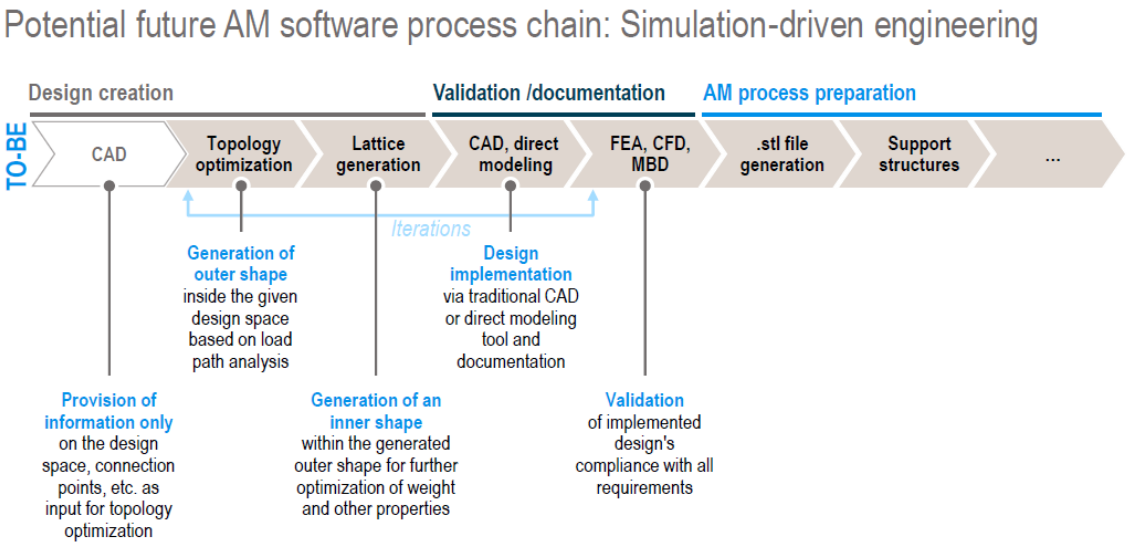

Figure 40. Future AM software process chain. Source: Roland Berger

A summary of the integration of techniques for AM design into the mechanical design process can be shown in an easy way at the diagram (Roland Berger, 2016).

4.5.3.2 Design for lattice structures

Thanks to the complexity achievable with additive manufacturing technologies, different parts can be manufactured with multi-scale structures or lattice structures. These structures are made for micro or macro-scales following a pattern of lattice structures. In mechanical applications, the resultant part is a modification of the original one in which the outer surfaces of the ribs remain

still while the inner volume of the structural elements is filled with a certain pattern of lattice structure, which has the interesting property of increasing stiffness for a lighter weight. This redesign release into lighter parts with shapes impossible to be manufactured by traditional subtractive manufacturing techniques (Tang Y., 2017).

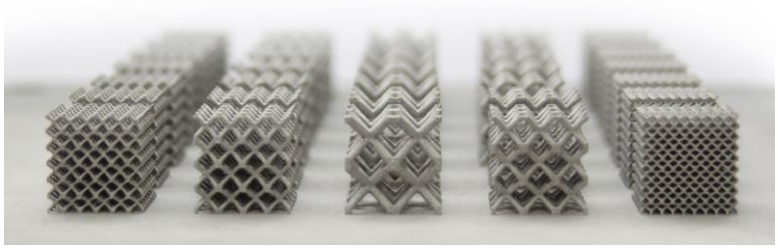

Figure 41. Metal lattice structures specimens for additive manufacturing

Cutting edge technology software aims the designer to obtain optimal paths and shape for the given loads and boundary conditions of the part, obtaining this way different results depending the characteristics of the lattice structure desirable (Materialise, 2017).

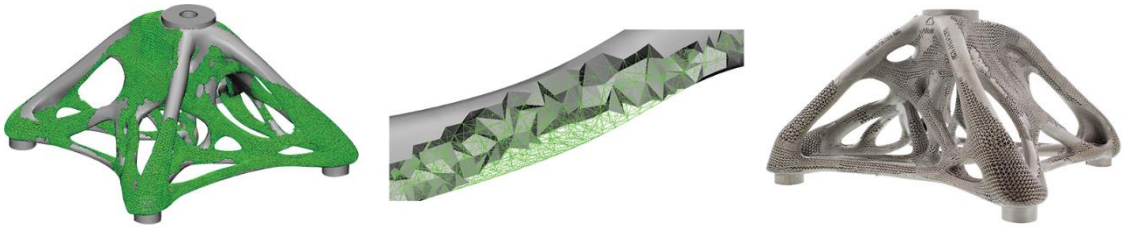

Figure 42. Practical application of a redesign using lattice structures (Materialise, 2017)

4.5.3.3 Additive manufacturing for mass customization

Other potential advantages that AM offer is the significant reduction of operations from its digital modelization (CAD) to its manufacturing. The reduction in the number of operations decrease significantly the cost and leading time of customizing products (LaSelle, 2018). In future scenarios where additive technologies are enhanced, the intermediate phases between the demand (customer) and the manufacture would be reduced so drastically (and therefore the leading times) that the customer could become its own designer (LaSelle, 2018) (Paoletti, 2017).
This radical change in the supply chain (D'Aveni, 2015) would revolutionize the market into an ultra-customized one in where the customer decides the final shape and properties of its product.

Additive manufacturing could allow this scenario to come true since the price of the production process is the same for either 1 or 10000 additively manufactured parts. Therefore, you can mass customize parts with AM and it would not affect your production costs when using 3d printing (Zeijderveld, 2018).

In the Siemens' magazine (Siemens, 2018) the evolution of productions systems since 1850 and how the trend of the market has guided the evolution of manufacturing technologies it is explained here. The current trends of the market of mass customization is increasingly pulling the business models into individual production systems. The benefits of significant lead time decrease and design freedom of additive manufacturing point out the rise of this technology as the one which will dominate the business models in the coming years. The ultra-customized market will tend into individual production single-customer systems.

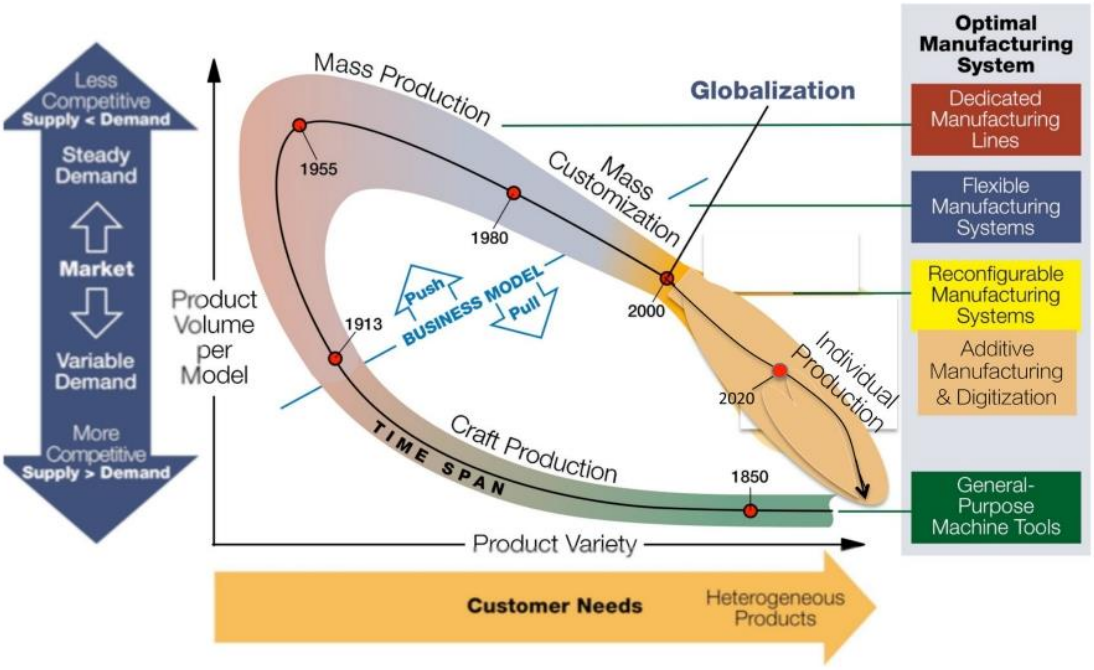

Figure 43. The evolution of production systems (Siemens, 2018)

All these new design techniques explained above, open new possibilities, removing and adding at the same time different design constraints, that the designer must have in mind, redefining this way how engineering parts are designed.

5 Analysis of the part manufactured by IM

5.1 Clutch pedal model

5.1.1 CAD model

On the basis of the aforementioned information, we can distinguish three regions in the pedal part. The first one is the curved plate where the user presses the pedal itself when clutches. The pressure force is transferred throughout the second region, the structural region to the last region, the connection to the clutch linkage mechanism where the movement of the pedal is transferred in order to activate the clutch.

Preliminary analysis of the part performed by visual inspection, suggests that the part is strongly influenced by the demoulding constrains to its manufacturability. This leads to a cross-truss shape along the structural element. This shape could be beneficial for increasing the stiffness of the clutch pedal. Another relevant point is that the original design has many sharp edges and intersections along the bracket with no smoothing or fillet addition. This is actually a bad design decision, since sharp edges will lead to stress concentration. The structure is full of non-smoothed intersections, therefore many weak points arise along the structure, being possible failure points.

It is known that for the original part, an equivalent punctual load of 200N applied in the centre of the pedal surface expects a normal displacement of 3 mm. This will be our reference for the analysis results of the current part. It is also known that the original part, failed during normal operation in on the intersections of the cross-truss shapes. Therefore, the analysis performed in the pedal must be a Linear Elastic Analysis. This reproduces forces and displacements expected during normal use of the pedal

To perform a Linear Elastic Analysis where the part is under static forces, force applications and boundaries conditions must be defined. This transition from the original part to the virtual model must be done in a way where the model behaves as it does under normal circumstances. As introduced in previous paragraphs it can be defined as follows:

- **Load application**: An equivalent punctual force of 200N applied normally to the curved clutch surface.
- **Boundary conditions**: The region where the clutch pedal is joined with the linkage mechanism is going to be substituted by clamping boundary conditions, limiting this way any possible displacement or rotation.

The equivalent model will act as a cantilever bracket, with a complex curved shape.
Notice that there is a factor that undoubtedly will make the analysis of this part much more interesting: the torsional evolution along the bracket's shape, becoming a three-dimensional problem instead a simplified two-dimensional-one. Certainly, the complex shape of the structure will release a non-so obvious behaviour of the part, appearing stress peaks along the bracket in different regions.

Once this is known, from the complete CAD model the region for the analysis will be extracted (the bracket) and some geometry will be modified or removed. The pedal surface is removed and the end with the clamping modified. In the clamping side a smother surface has been added where the boundary conditions will be applied to reduce possible stress concentration at the clamping.

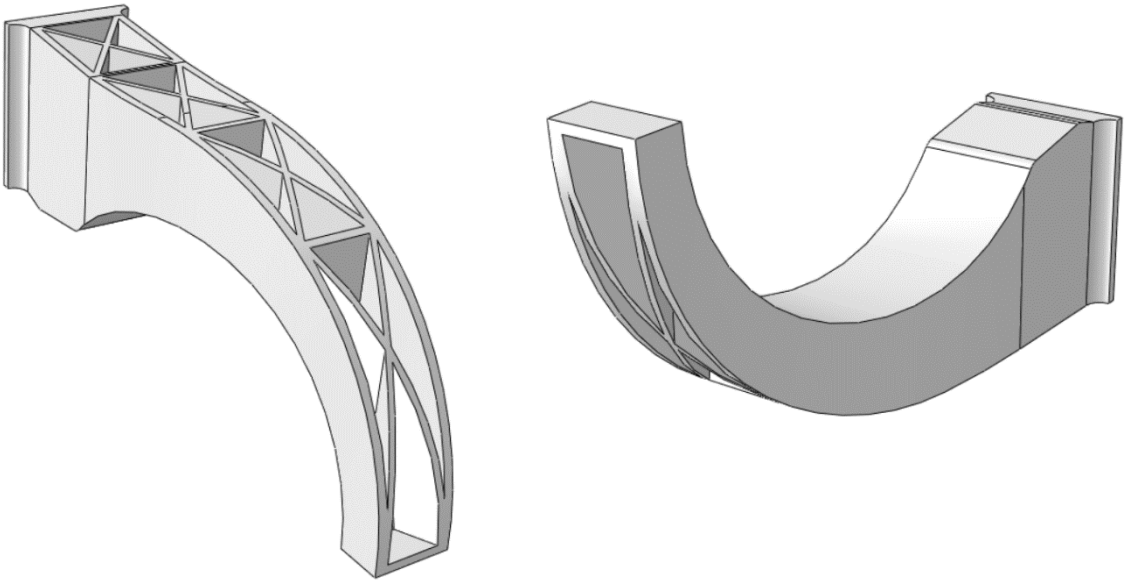

Figure 44. Injection moulding part CAD model

5.1.2 Material model: Isotropy or Anisotropy?

The geometrical modelization of the clutch pedal has been discussed, but there are other factors regarding the intrinsic properties of the material and its behaviour, which will require an entire section to be discussed about.
Parts made of steel or other metal alloy can behave properly under hypothesis of isotropy and homogenization. This is because the intrinsic properties of metals, which behaves properly under these conditions when materials are modelled with this hypothesis.
However, there are other materials in which this hypothesis does not work properly due its nature. Short fiber reinforced polymers composites, as seen in (*Chapter 4.2*) behave better under anisotropic conditions and with a fiber orientation distribution tensor, becoming the material heterogeneous.

Once it is clear, the hypothesis and the conditions when the SFRP composites behaves better according experimental tests, the next question is: How can we model this kind of materials?

Traditional CAE modules of the software packages ABAQUS; ANSYS or Nastram can model materials with isotropic properties or composite materials with continuous fibers according the behaviour of its laminates, but they don't take into account fiber orientation for short fiber reinforced polymer composites.

The solution is the combination of results from different software to create a full model which considers the anisotropy of the material and its fiber orientation. MoldFlow fiber orientation tensor plus structural ABAQUS CAE with isotropy properties integrated both into DIGIMAT can deliver a proper final model. In this fused resulting model, in which fiber orientation will determinate the behaviour of the part can be run with ABAQUS again and deliver a final simulation.

5.2 Structural FEA with isotropic material properties

5.2.1 Linear elastic FEA definition

A Linear Elastic analysis will be performed with the software package ABAQUS/CAE. In this first simulation, an analysis with isotropic and homogeneous material properties is carried out.

5.2.1.1 Property module:

The material elastic law is isotropic elastic with a Young's Modulus of 10000 MPa and a Poisson's ratio of 0.4.

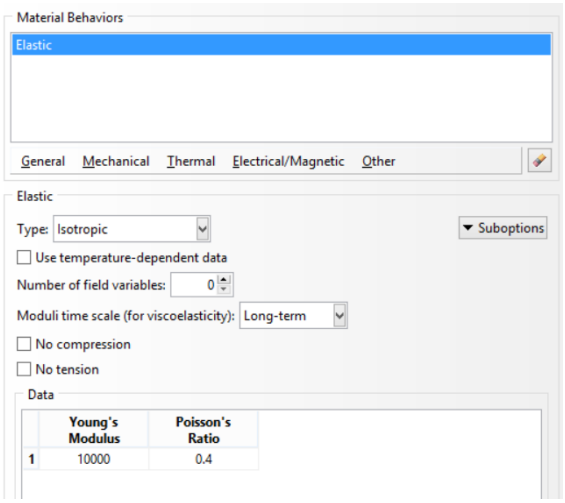

Figure 45. Material behaviour window

The part section has been defined as a Solid and Homogeneous including the material behaviour commented above.

5.2.1.2 Step module

The analysis type is defined in this window. This is done creating a step with a static and linear perturbation procedure.
The nature of the analysis will be therefore an implicit analysis in where ABAQUS will have to calculate the stiffness matrix of the model to solve a linear elastic problem.

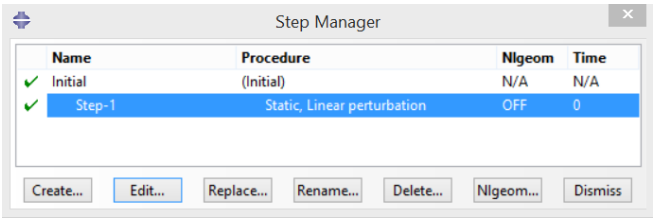

Figure 46. Step manager window

5.2.1.3 Interaction module

A reference point is placed where the equivalent load is placed in the space. This reference point is attached to the pedal surface as if both would be part of the same body. If the RP is displaced, the pedal surface will do it in the same direction and magnitude.

The coupling type selected is kinematic, and all the degrees of freedom has been constrained. With this configuration the desired effect can be achieved.

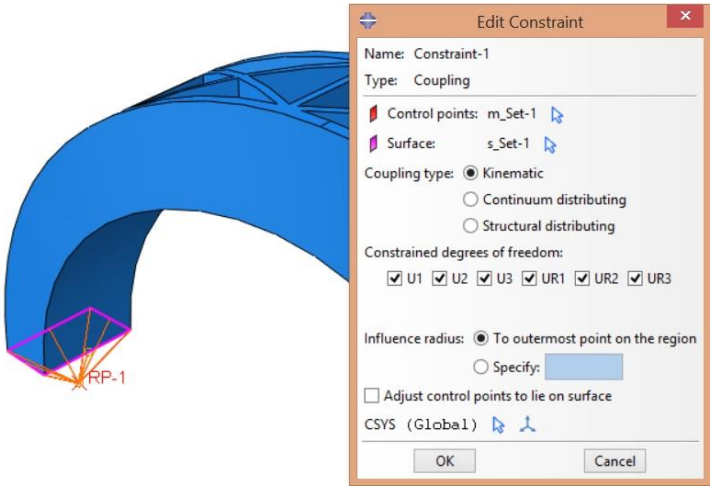

Figure 47.Constraints definition in the IM model

5.2.1.4 Load and Boundary conditions:

The equivalent load of 200N is applied in the reference point created at the bottom of the pedal. At this place, the load has an inclination of 45º as in the horizontal and vertical axis. The type of load selected has been of course a concentrated force.

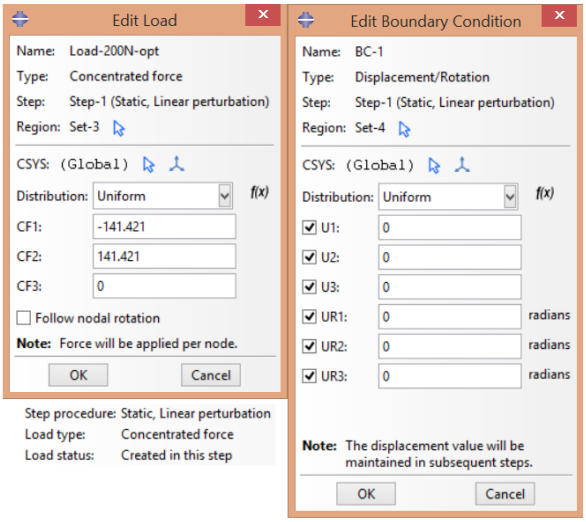

Figure 48. Load and boundary conditions for the IM model (I)

The boundary conditions have been defined constraining the displacement and rotation of the lateral surface where the clamping is placed. The displacement in each axis and its rotation has been not allowed.

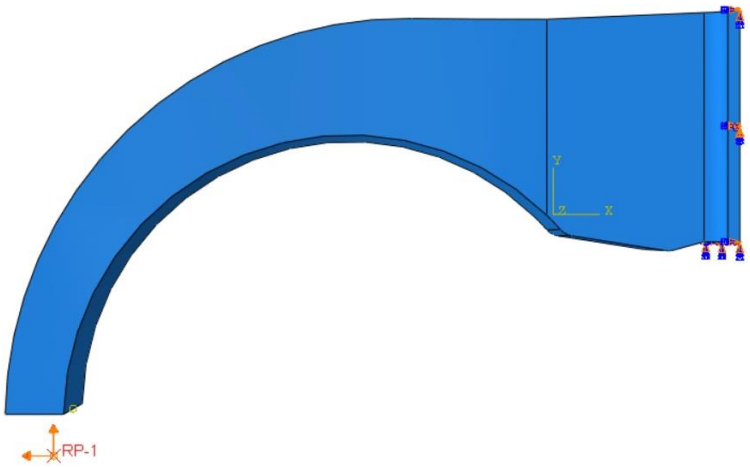

Figure 49. Load and boundary conditions for the IM model (II)

5.2.1.5 Mesh definition

The mesh definition is probably the step which requires more attention the moment of its creation. This will affect significantly the output of the analysis, and depending a proper mesh setup, the results could not be compliant nor adequately shown.

The finer the mesh, the finer the results will be presented, and the evolution in the displacement field and specially the stress fields will be better captured in the analysis output.

The mesh definition consists in the definition of the global seeds, the element type and its internal controls.

The approximate global size for the mesh has been chosen 2 mm. This will provide a mesh fine enough to obtain good results with no unnecessary computational effort.
The curvature control and the minimum size control has been set by default.

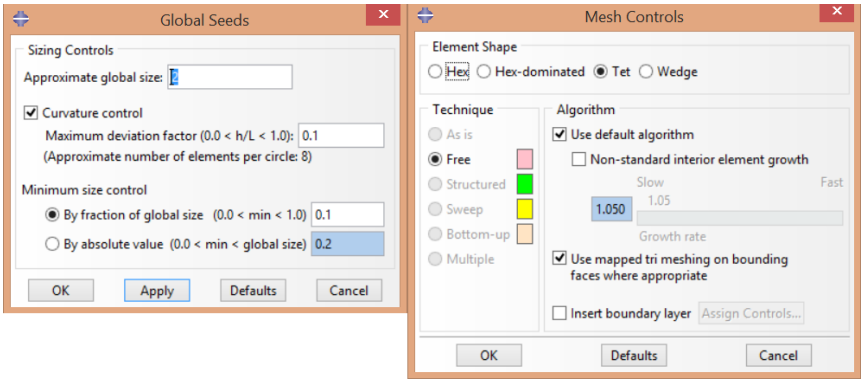

Figure 50. Global seeds and mesh controls for the IM model

Within the mesh controls, the element shape chosen was tetrahedral, with the technique 'free', and the algorithm options set by default.

In the other hand, the element type had the following features:
It was chosen among the standard element library. The element family was a 3D Stress.
The element type chosen was the C3D10, a 10-node quadratic tetrahedron. This element has a general purpose tetrahedral element with 4 integration points (Dhondt, 2014). The shape functions available are 'hex', 'hex-dominated', 'tet' or 'wedge'. Moreover, this element behaves very well and is good general purpose element.

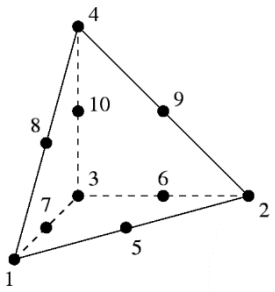

Figure 51. A 10-node quadratic tetrahedron element, the C3D10

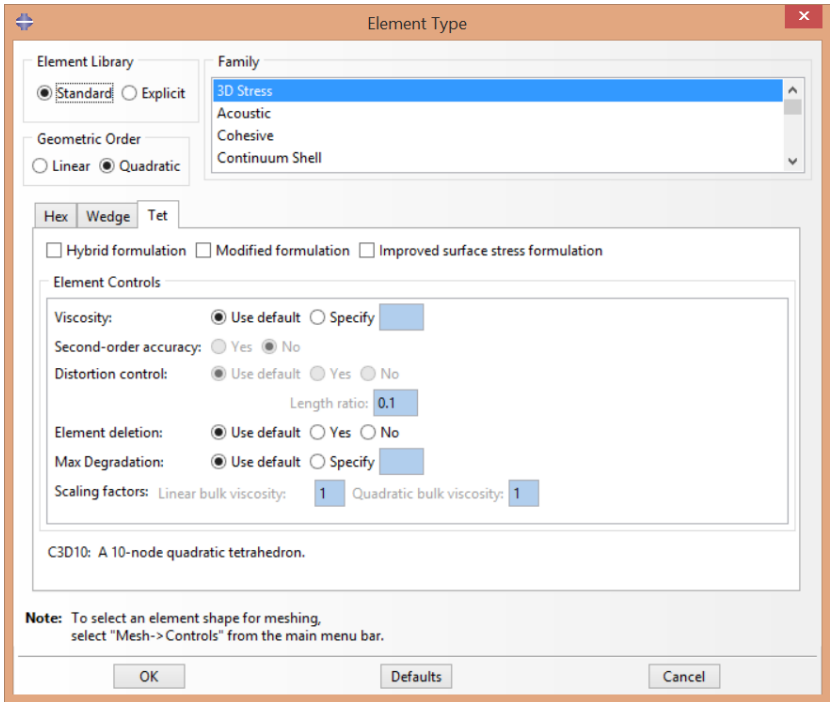

Figure 52. Element type definition in the IM model

The resulting mesh can be shown in the next image:

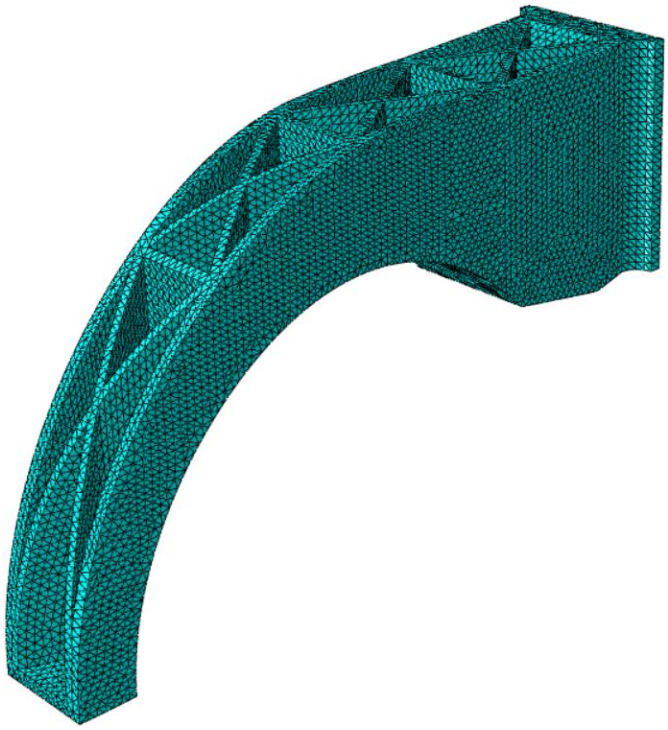

Figure 53. Structural mesh of the IM model

At this stage, the FE Linear Elastic Analysis is set up with the part geometry, the material properties, the load definition and application, the definition of boundary conditions, the definition of problem to be carried out, the element type and its configuration and the mesh creation. Afterwards, the analysis will be ready to be run. Once the analysis is completed successfully, the results will be shown, and pertinent discussions of the results will be made.

5.2.2 Analysis results

5.2.2.1 Displacement

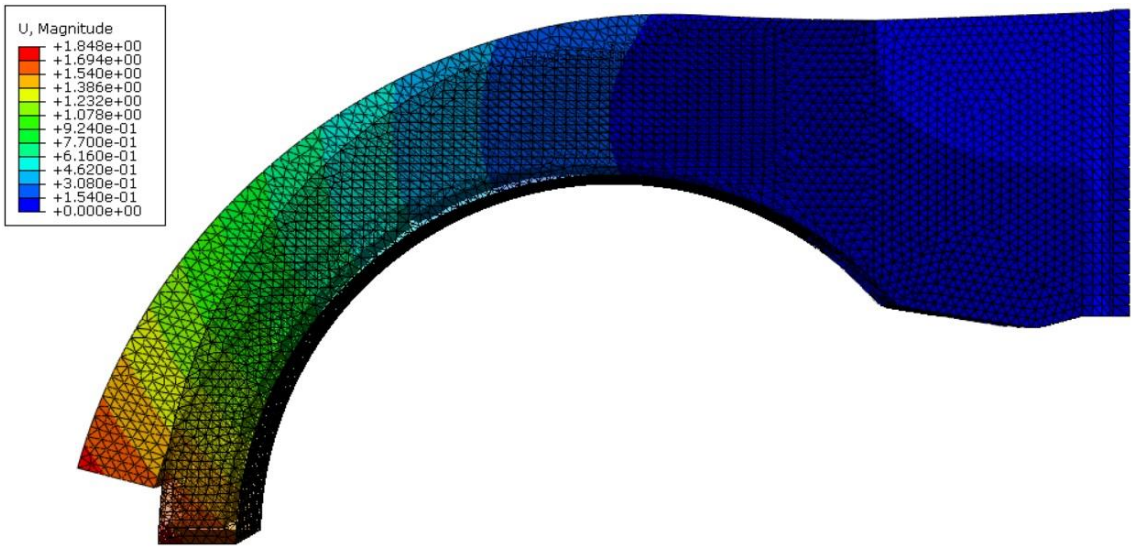

Figure 54. Displacement magnitude of the IM iso model analysis. Lateral view

The final displacement results from the analysis was a resultant displacement in the tip of the bracket pedal of 1.848 mm. So, for isotropic material properties, the expected deformation of the clutch pedal is this figure.

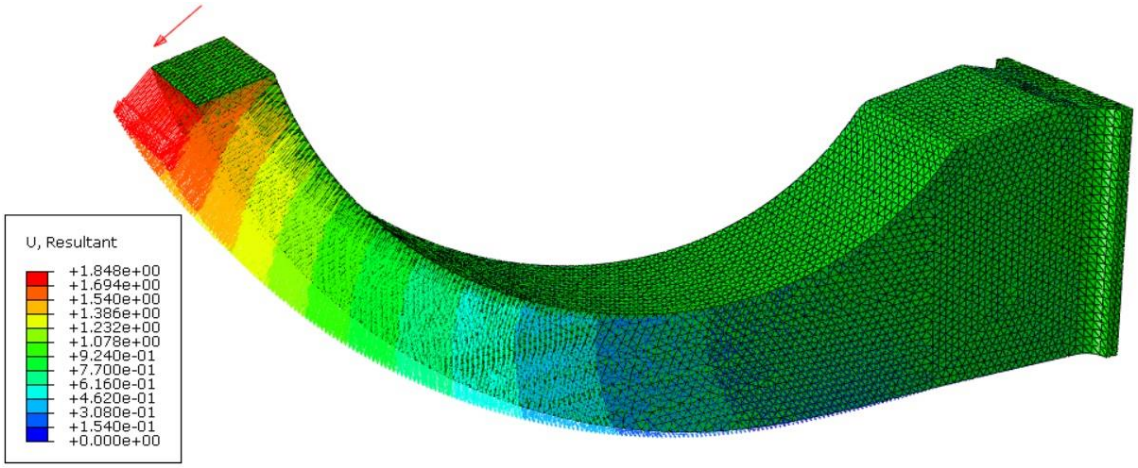

Figure 55. . Displacement vector of the IM iso model analysis. General view

5.2.2.2 Von Mises Stress

The criteria of Van Mises has been used to the stress analysis along the structure.

Some plot options has been changed to show the results in a determined way. The deformation scale factor has been set to approximately 11 times the real behaviour.
The computation of the scalars before averaging the 100% have been changed in order to take more accurate results in the elements shown.

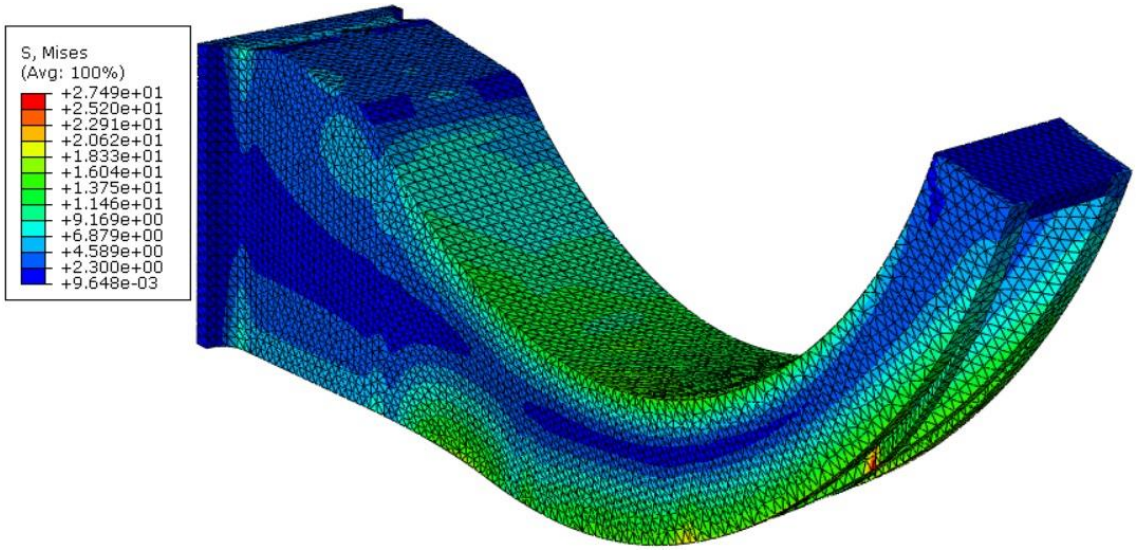

Figure 56. Von Mises stress of the IM iso model analysis. General view

The maximum stress appears in the cross intersection of the fourth row of crosses, and it raises up to 27.49 MPa. As it was said before, the sharp edges in each intersection causes a stress concentration, and in this case rise until the maximum value for a force of 200N. This force do not cause pedal mechanical failure, but if the force increases linearly to values over 800N, the part could break, and if it does, it will be in the intersection region.

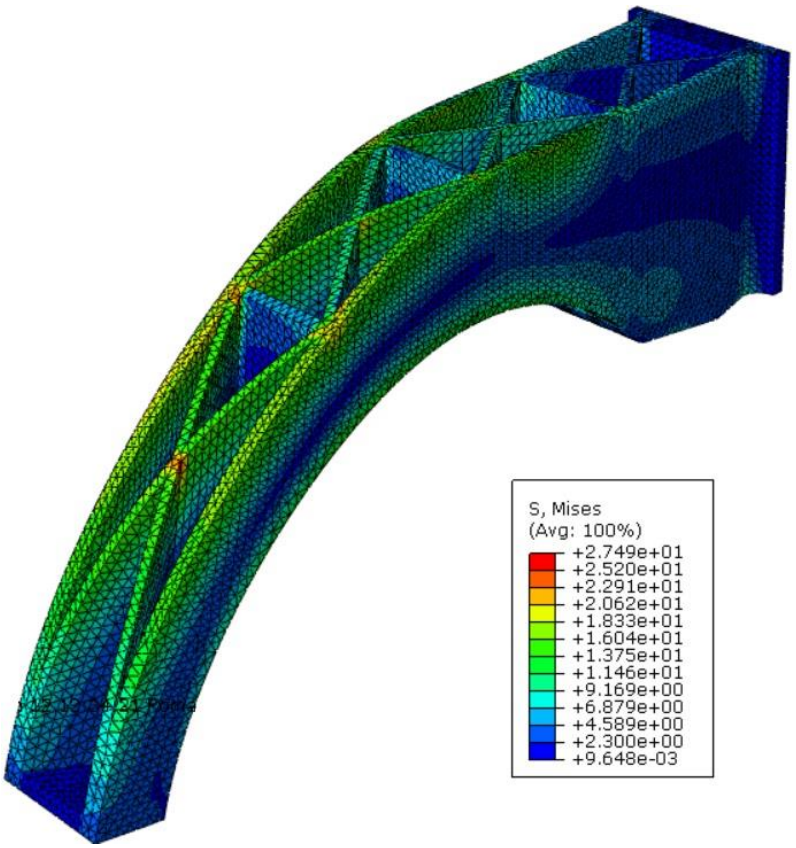

Figure 57.Von Mises stress of the IM iso model analysis. Isometric view

To sum up, for isotropic material properties, the maximum Von Mises stress will show these values.

5.2.2.3 Results extraction

A table has been created where the date which will be extracted to be used in the following steps is written. For Autodesk Moldflow the CAD model and the ABAQUS mesh file are going to be necessary. Additional information can be shown below.

ABAQUS results data processing			
Results extracted from ABAQUS	**File format**	**Does it need manual modification?**	**Data file goes as an input for**
ABAQUS Mesh file	*.inp	YES	Autodesk Moldflow
CAD model	*.xml	NO	Autodesk Moldflow

Table 3. ABAQUS results data processing

5.2.3 ABAQUS mesh file modification

The mesh file extracted from ABAQUS, generates structured sets of information. This sets include the list of elements, nodes, material properties, constraints and the step definition. **Autodesk Moldflow will need only information related to the mesh, there are nodes and elements.** Therefore, the remaining set of data must be eliminated from the file before introducing it to Autodesk Moldflow. This modification can be done manually as follows:

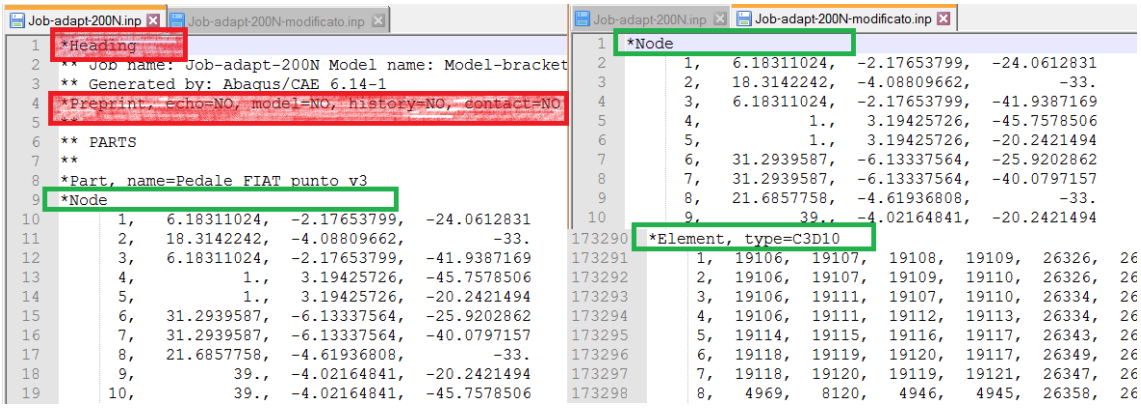

Figure 58. ABAQUS file modification for the flow simulation

The new modified file was named *'Job-adapt-200N-modificatio.inp'*.

5.3 Injection moulding flow simulation

In order to obtain the fiber orientation vector, the process of injection moulding must be simulated. The software Autodesk Moldflow allows to simulate with great accuracy and a high number of possibilities this manufacturing process (Autodesk, 2018).

5.3.1 Moldflow mesh definition

Thee information within the CAD model of the bracket for injection moulding is initially requested from MoldFlow as an input

Once the CAD model is uploaded into Moldflow, the first step is to create the Mesh part. **In Moldflow mesh elements must be smaller than ABAQUS mesh elements**. This way, fusion mesh errors will be avoided and fiber orientation will be properly captured in the model.

The global size chosen for the element was 0.8 mm. This size element was smaller than the one used for ABAQUS 2 mm, so the procedure set up correctly.

After some hours running the mesh calculation, the result was the following:

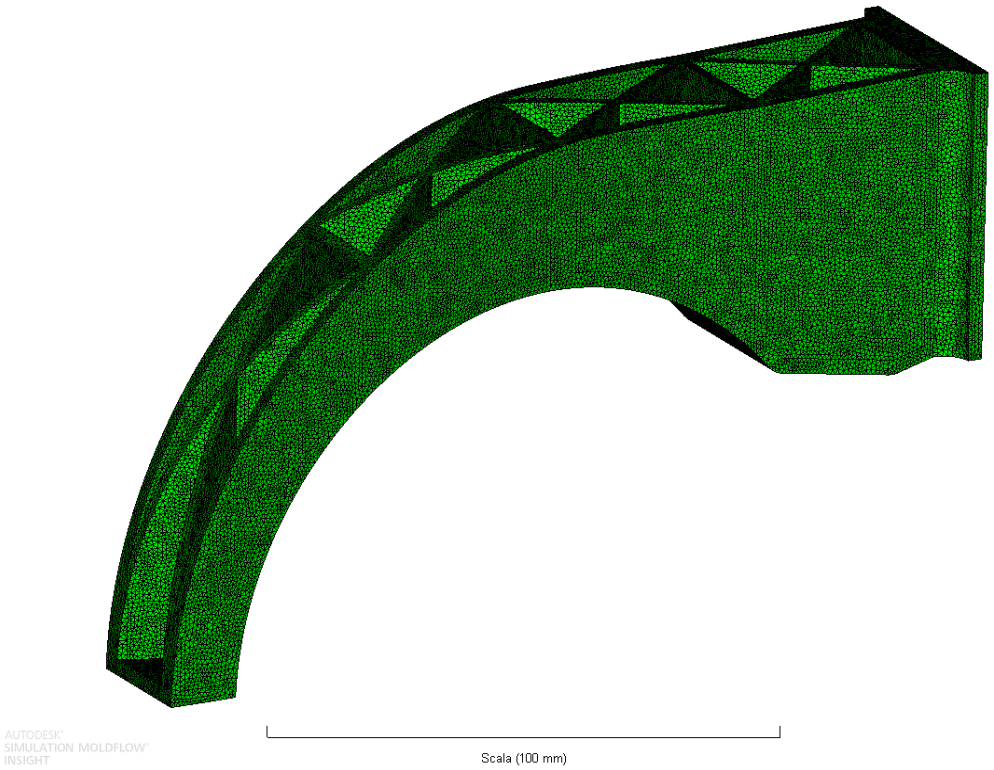

Figure 59.Flow simulation mesh of the IM model

The second step was to define some manufacturing process parameters. Note that for these simulations, the sprue and the runner were not included, which should be included if there is an interest in manufacturing the part. Here are only simulation and analysis purposes, therefore the inclusion of the gate or injection point is enough.

5.3.2 Injection point

The injection point is probably the most important parameter to be defined for injection moulding simulations. This is because the material flow will enter filling up the part along the mould cavity, and the injection point is its starting point. Due anisotropy material properties, the material flow will determine the final mechanical properties of the part. If a chosen injection point makes get aligned the fibers in the longitudinal direction for example, but it is expected that the part is going to be subjected to perpendicular stresses, the resulting part will have weak mechanical properties because of a poor design.

Thus**, if the expected load directions are known, the injection point definition is a key factor to make stronger and durable parts** manufactured with injection moulding.

The bracket is expected to bend and slightly get twisted from the end where the load is applied. Therefore, three possible positions for the injection point that will deliver a better part where proposed. The IP is placed in the right (*Figure 60.b*), in the left (*Figure 60.a*) or down the part (*Figure 60.c*).

5.3.3 Material selection

Moldflow has a database with a range of materials and manufacturers. Internally, these materials have the necessary parameter that the software will require to perform the simulation. The material used is the Radilon A RV300 - PA66-GF30 from RadiciGroup Performance Plastics.

5.3.4 Other process parameters

Injection moulding temperature has to be defined as well. A value of 230 ºC was set.

5.3.5 Simulation results and interpretation

After everything was set up, the simulation was run. Once it was completed, many interesting results could be shown. The most important was the Fiber Orientation Density (FOD) tensor, in which the orientation of the fibers depending its position along the part can be appreciated. This tensor goes from 1 to 0, meaning 1 a full fiber aligned with the flow direction, and meaning 0 a fiber perpendicular to the flow direction. Furthermore, the results are coloured for easier understanding, associating red colours when the tensor gets closer to 1 and turning to colder colours like purples and blues when the tensor value drops to 0.

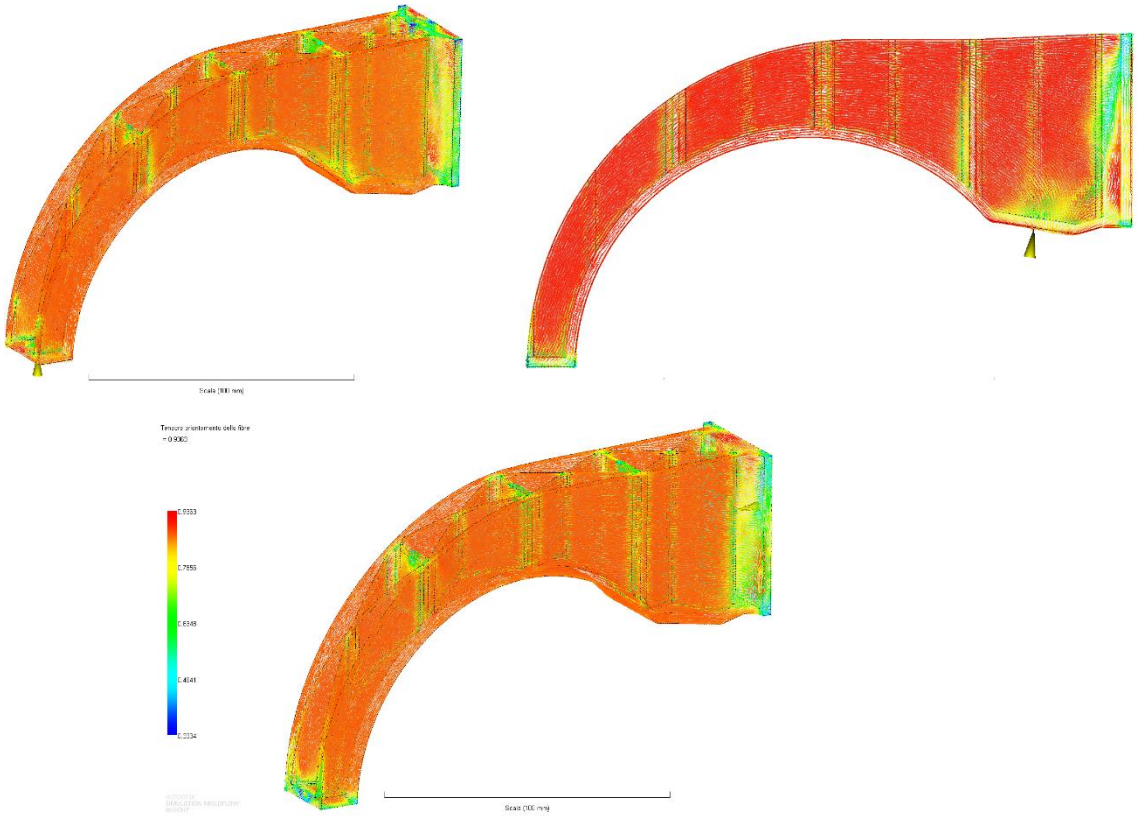

Figure 60. Fiber Orientation Density (FOD) tensor for different injection points: left (a), right (b) and down (c)

Another interesting result to show, is the representation of welding lines appearing along the bracket. They appear when different sections of the main flow converge into one, creating this interface which weaken the part. They have to be taken into account, because the part will have more chances to fail from these areas. The number and position of welded lines can be an interesting factor to choose between different Injection points.
As shown in the figure below, due the complex shape of the part, many welding lines appear in different regions. If a welded line run into a sharp edge, the criticality of that zone is even higher. The designer must bear in mind these parameters if a reliable part wants to be created.

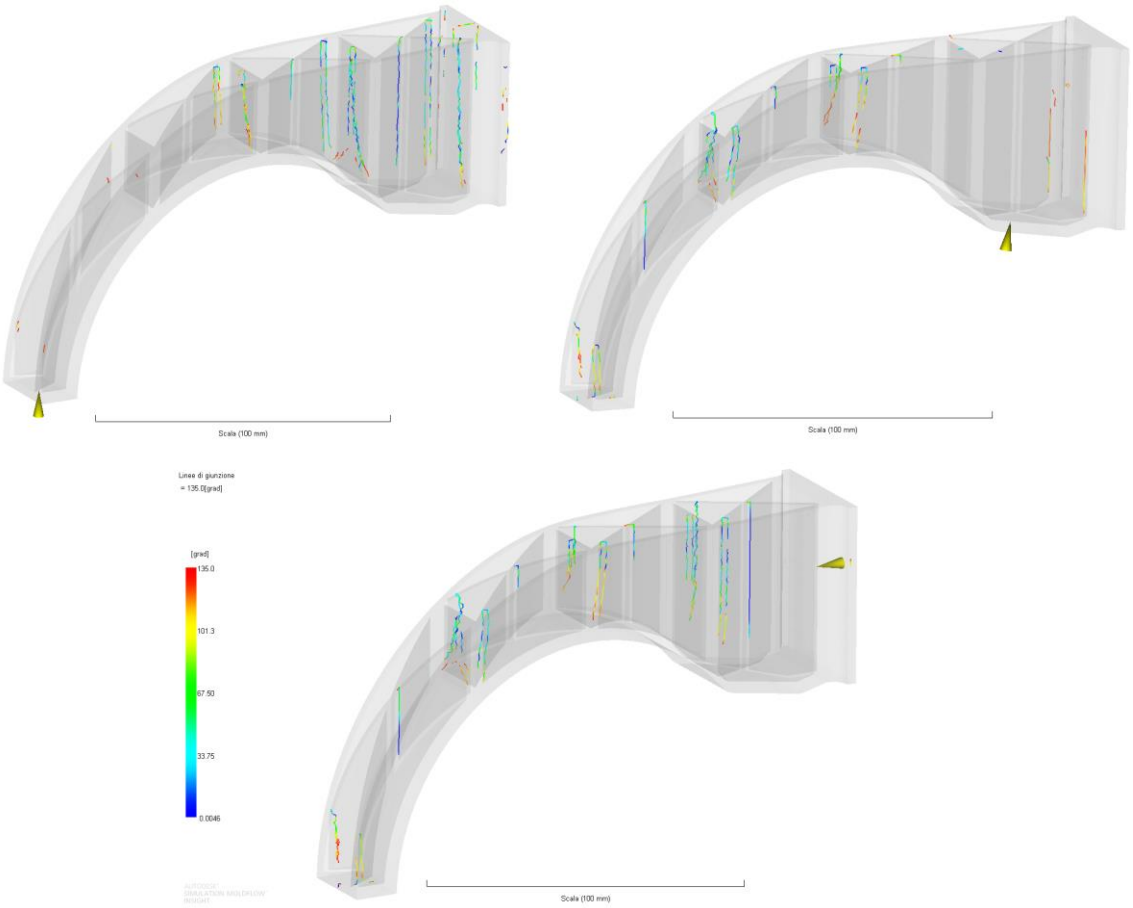

Figure 61. Welding lines created for different injection points

Therefore, the chosen alternative will be the injection point in the right. This way, less welding lines appear in the clamping nearby. The region around the clamping will probably be one of the most critical. Avoiding welding lines around this place, will reduce the chances of material failure in the area. Note that even if the fiber orientation tensor evolve in a similar way along the mid part of the structure, it significantly change for each alternate, where boundary and load conditions are applied. Fibers tend to be orthogonal to the material flow in these areas; thus, weaken the bracket. Fibers should be aligned as homogeneously as possible to avoid high strength drop; this is another reason to choose the alternative with the injection point selected in the right; the fiber orientation there looks less messy and tends to follow a common path.

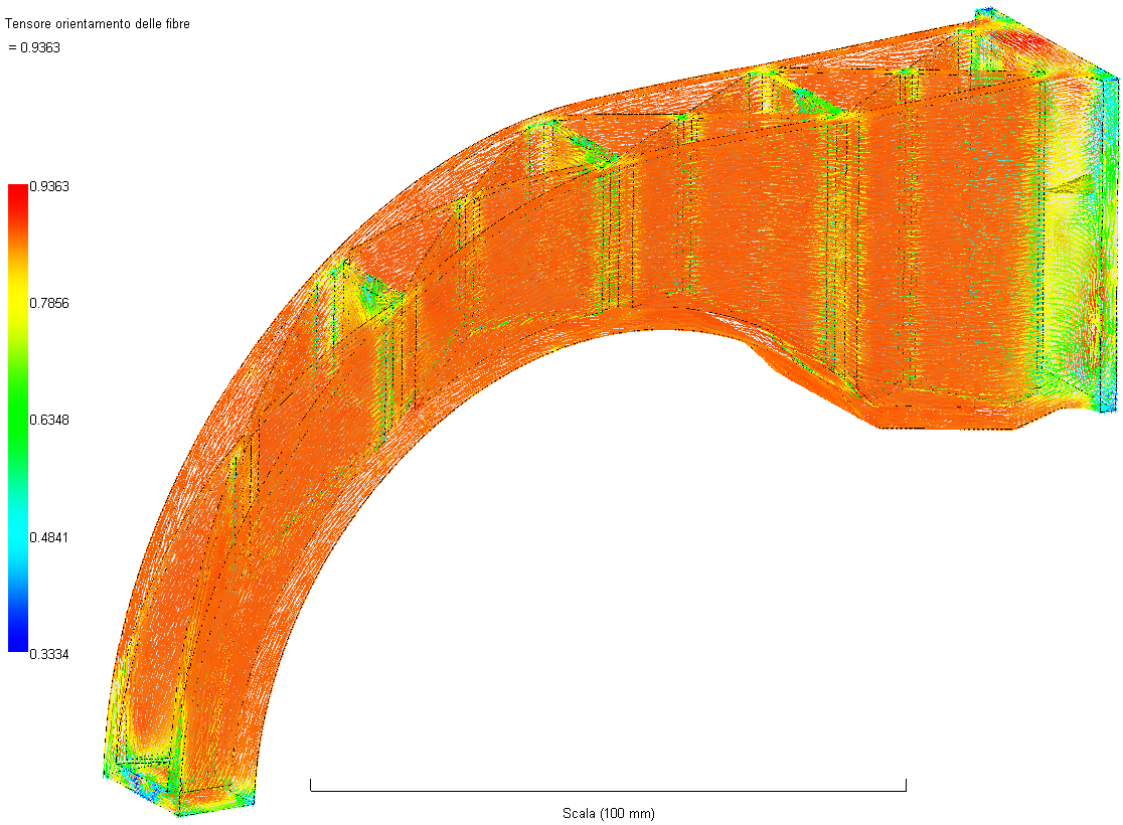

Figure 62. The chosen FOD tensor with the injection point placed at the clamping

From the final model and its results, some information has to be extracted to be used as an input for the next step.
The most relevant data are the mesh used in Moldflow and the Fiber Orientation Distribution (FOD) tensor which can be extracted into a file.
Moldflow allow the extraction of this information in a determined format. The Mesh data will be a '*.inp' file. The FOD tensor can be extracted as a '*.xml'. Both files will be the input data in the next step for the execution of the final model.
Digimat-MAP will require these files, but a manual modification of one of them must be done first to guarantee the computational stability while running the next step.
All this information is summarized in the next table:

5.3.6 Results extraction

Moldflow results data processing			
Results extracted from Moldflow	**File format**	**Does it need manual modification?**	**Data file goes as an input for**
Moldflow Mesh file	*.inp	YES	Digimat-MAP
FOD tensor file	*.xml	NO	Digimat-MAP

Table 4. Moldflow results data processing

5.3.7 Moldflow mesh file modification

The file mesh extracted from Moldflow, generates structured sets of information. This sets includes the list of elements, nodes, material properties, the position of the injection point, the

constraints and the units used. **Digimat-MAP only reads files with information related to nodes and elements**, therefore the remaining set of data must be eliminated from the file before introducing it to Digimat-MAP. This modification must be done manually as follows:

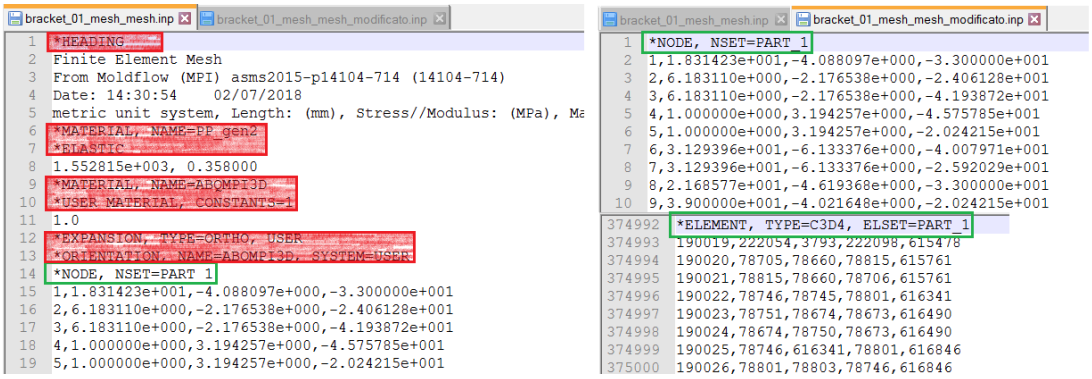

Figure 63. Simulation flow file output modification

The new modified file, will be now ready.

5.4 Merging FOD tensor with the mesh file

The next step is to use the Moldflow Mesh and its FOD tensor as a reference to integrate in the Mesh used previously in ABAQUS, the FOD tensor. For doing that, is used the Digimat-MAP modulus.

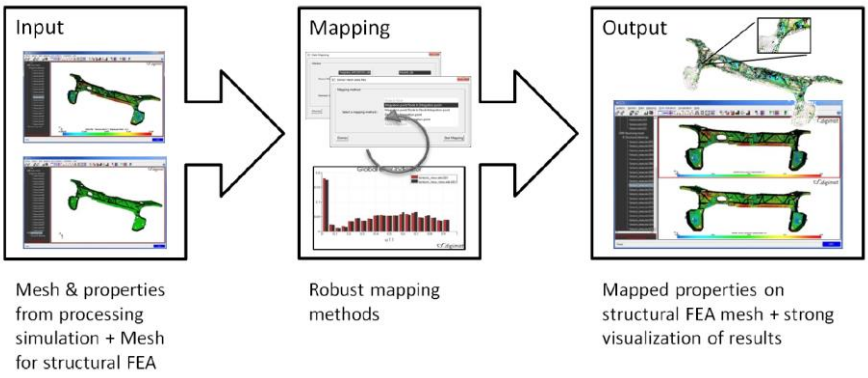

Figure 64. Digimat-MAP diagram process (Ex-Stream, Digimat-MAP VII, 2018)

Digimat-MAP is a 3D mapping software used to transfer different kind of Mesh properties between injection moulding simulations and structural FEA (Ex-Stream, Digimat-MAP VII, 2018). These properties are fiber orientations, residual stresses, temperatures, weld lines, porosity or volume fractions.
A mapping tool is a useful aid to transfer appropriately mesh property to capture changes in the material microstructure composition.

In the first instance, the mesh from Moldflow must be uploaded as a 'Donor mesh' and the ABAQUS mesh will be used as an input for the 'Receiving mesh' window.

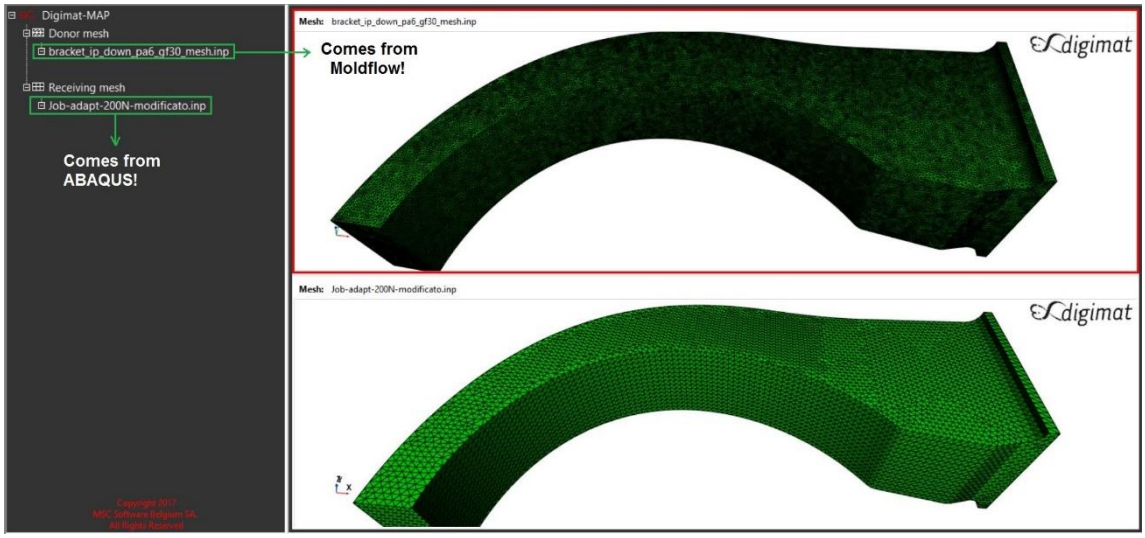

Figure 65. Mapping meshes of the IM models (I)

The next step is to upload the FOD tensor. This will be integrated in the Moldflow mesh, therefore will appear charged inside the 'Donor mesh'.

At that point, the problem is set to run the mapping process. Due both meshes match its systems of reference and have exactly the same geometry, neither further options nor parameters have to be changed.

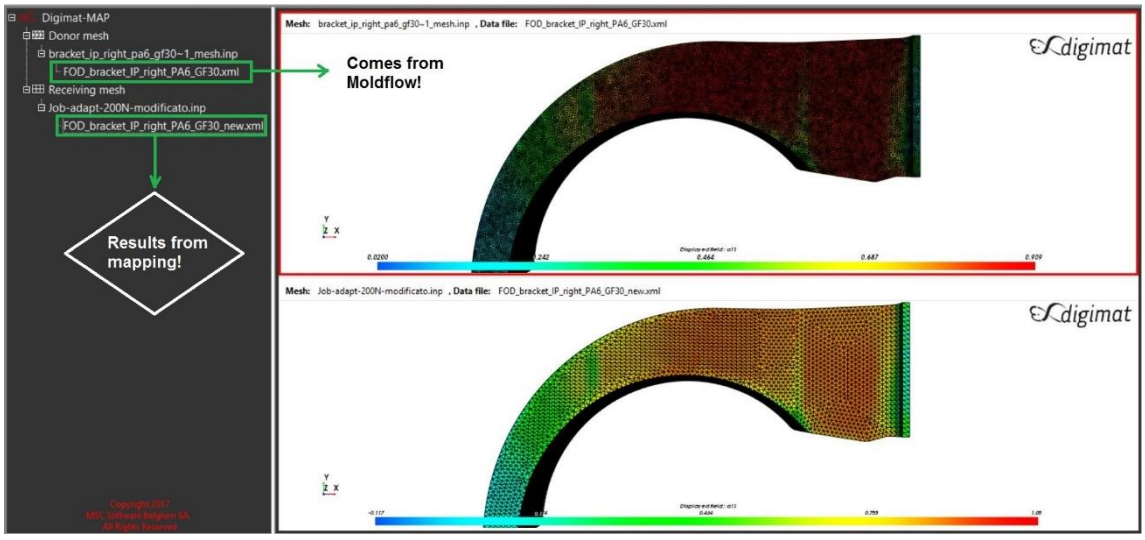

Figure 66. Mapping meshes of the IM models (II)

After some computational time effort, results will emerge resulting in the 'Receiving mesh' merged with the FOD tensor. It can be appreciated because of the different mesh refinements, the fiber distribution density appears with different intensity in both models. Thanks to the tip followed when defining the Moldflow mesh, now the data merged correctly in the 'Receiving mesh' with no errors.

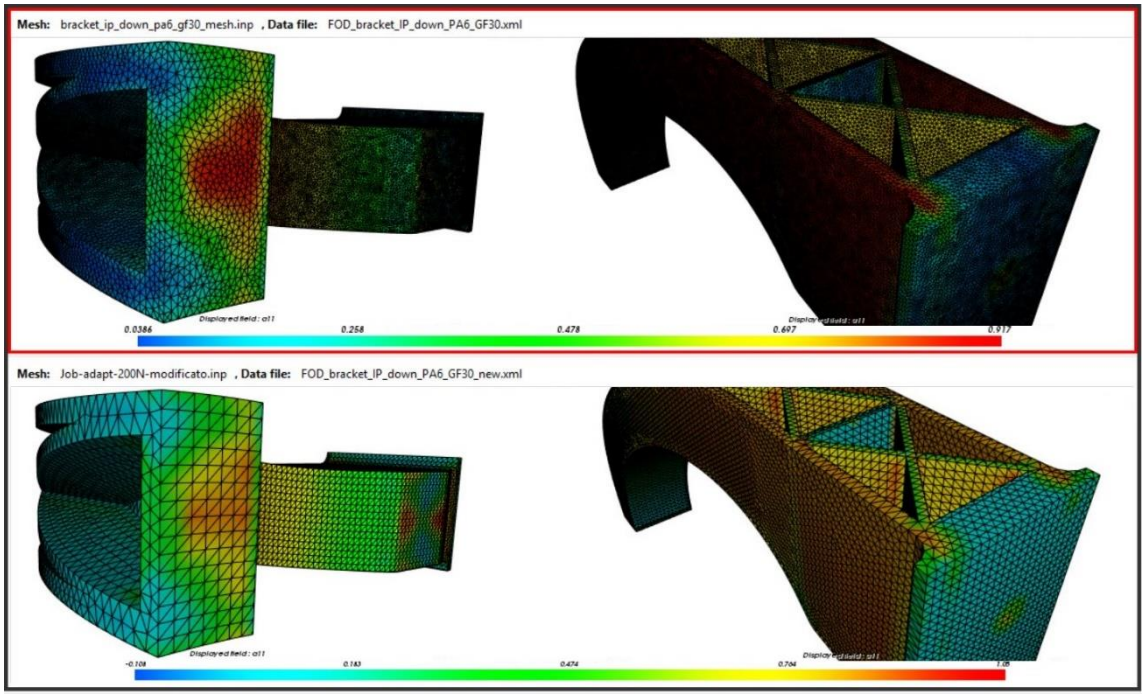

Figure 67. Mapping results for the IM model

From the results given by Digimat-MAP, the fiber orientation of the 'Receiving mesh, can be saved in '*.xml' or '*.dof'' formats. The second one is of our interest, because it will be required in the next Digimat modulus.

5.4.1 Results extraction

Digimat-MAP results data processing			
Results extracted from Digimat-MAP	**File format**	**Does it need manual modification?**	**Data file goes as an input for**
FOD tensor file	*.dof	NO	Digimat-RP

Table 5. Digimat-MAP results data processing

At this point, our final model is in an intermediate state where FOD tensor has been integrated into the structural mesh. There is one more thing remaining: The modelization of the material.

5.5 Material model for injection moulding

Material models can be defined with Digimat-MF. This application is used to model the linear and non-linear material behaviour of reinforced plastics for injection moulding and additive manufacturing parts and compute thermo-mechanical problems (Ex-Stream, Digimat-MF IV, 2018).

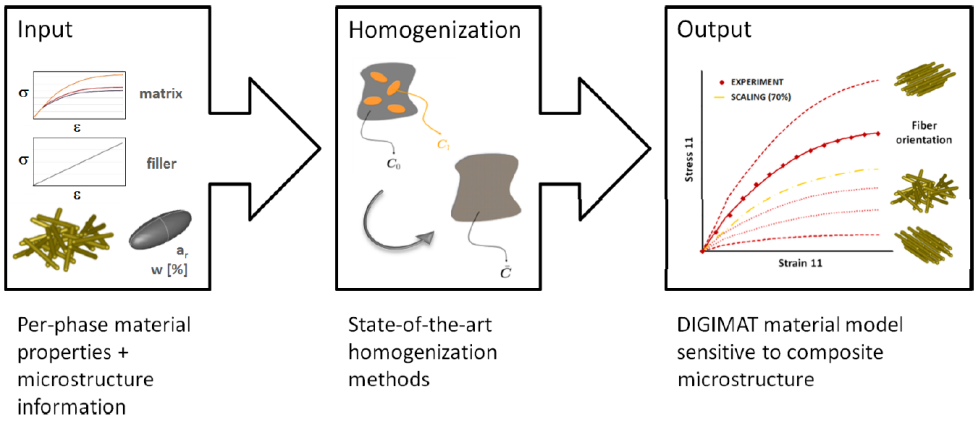

Figure 68. The homogenization process performed in Digimat-MF (Ex-Stream, Digimat-MF IV, 2018)

Digimat-MF is the homogenization module of Digimat.
Digimat can use this material model with the fiber orientation to predict the micro-mechanical behaviour if the material.

Starting with glass and matrix isotropic material properties, using semi-analytical mean-field homogenization approaches, a model for a homogenised anisotropic material is created.

The model has been named as IM_PA6_GF30 which is constituted by Glass as fibers and PA6 as the matrix.

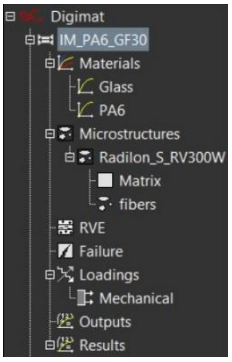

Figure 69. The IM_PA6_GF30 model

The first thing to be defined in the model is related to general parameters, like the units system, the type of analysis the model will be run for, and the mean field homogenization scheme. The analysis carried out will be mechanical.

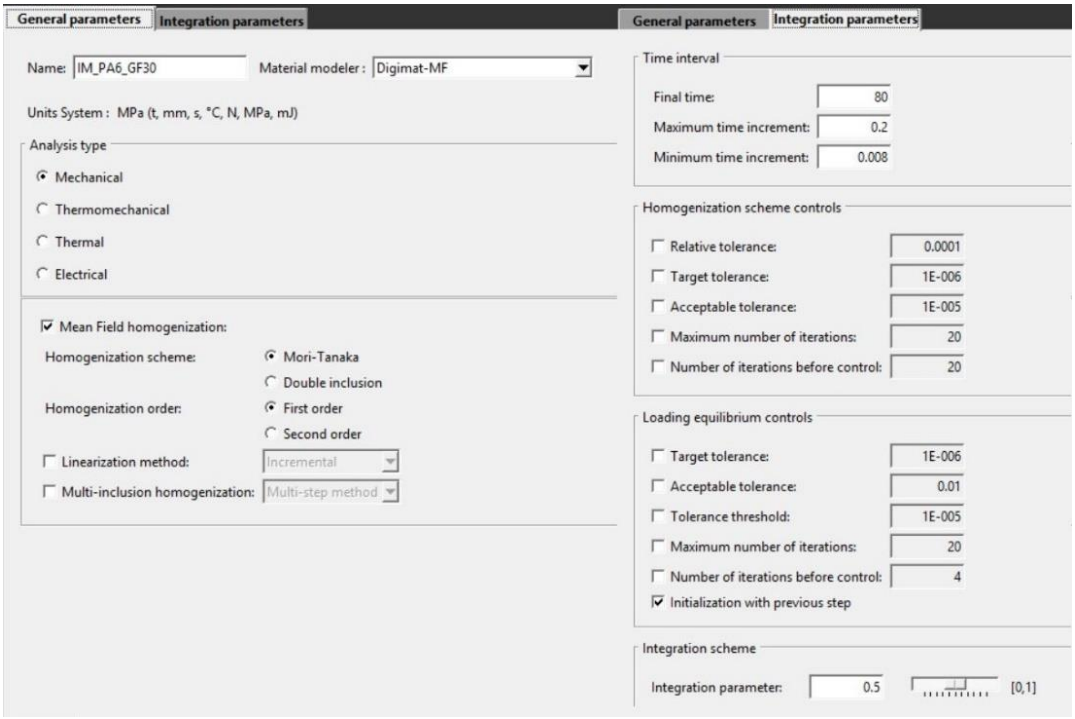

Figure 70. General and integration parameters of the IM_PA6_GF30

Also, the integration parameters must be defined in the early model characterization. Most of the parameters to control the homogenization, loading equilibrium and integration scheme have been left as default. The time interval minimum and maximum increment has been set to 0.008 and 0.2 respectively.

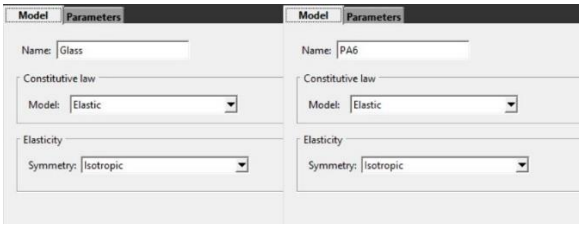

Figure 71. Glass and PA6 models of the IM_PA6_GF30

After this, each material property must be defined individually. This definition, both for the glass and for the Nylon 6, the material model is elastic and its elasticity symmetry is considered isotropic. As individual raw materials, this modelization could be considered well approached.

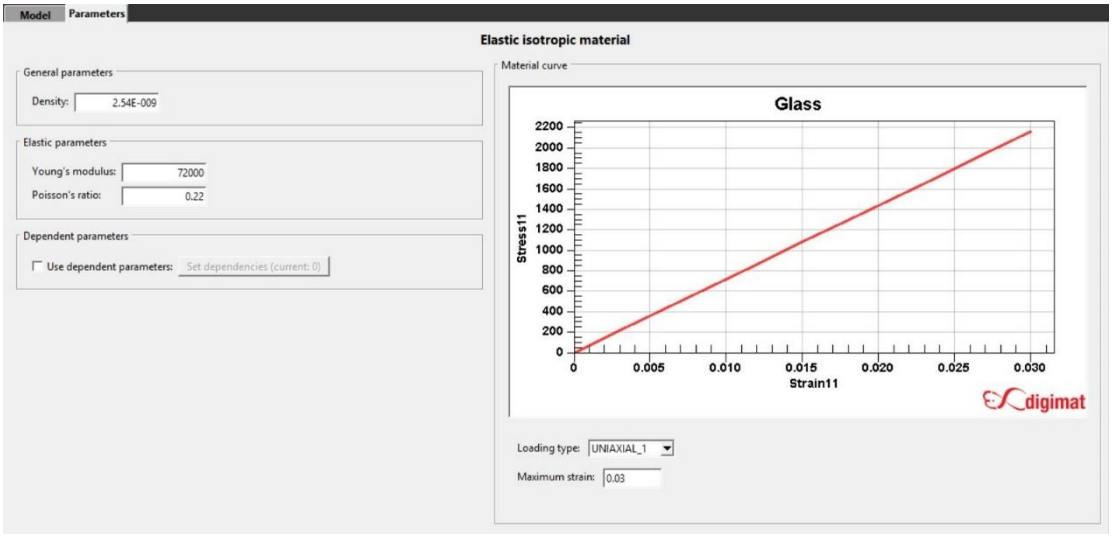

Figure 72. Elastic isotropic material curve of the Glass

The properties for these elastic isotropic material models were set for the glass, with a density of 2.54e-009 g/mm^3, an Elastic modulus of 72000 MPa and a Poisson's ratio of 0.22. The polyamide was defined with a density of 1.14e-0.09 g/mm^3, an Elastic modulus of 2780 MPa.

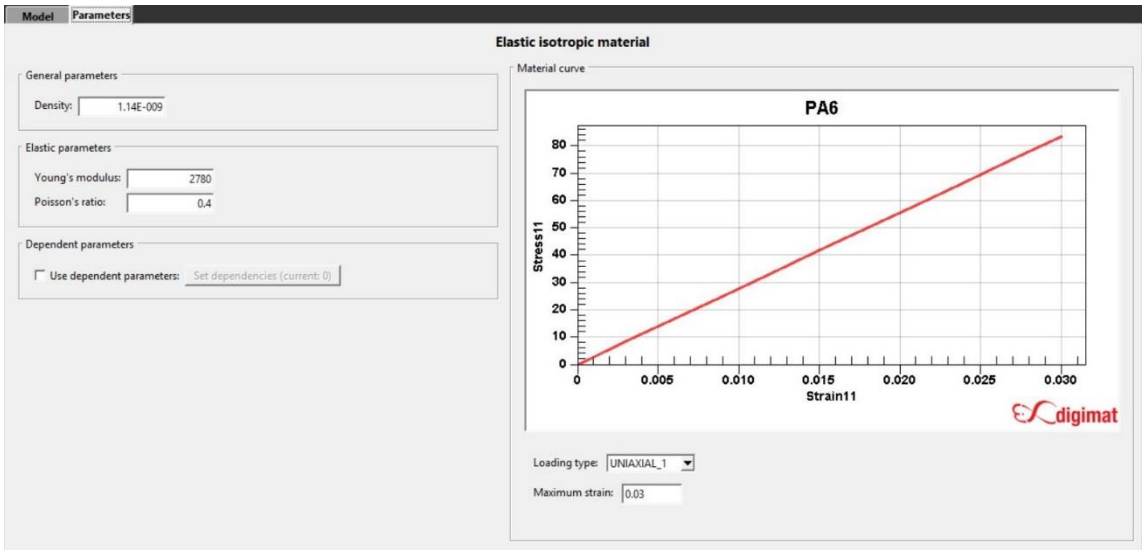

Figure 73. Elastic isotropic material curve of the PA6

The next step is the definition of the microstructure of the PA6-GF30. The PA6-GF30 is composed by a polymeric matrix of Polyamide 6, reinforced with 30% mass of glass fibers. These parameters were collected in the table showed below.

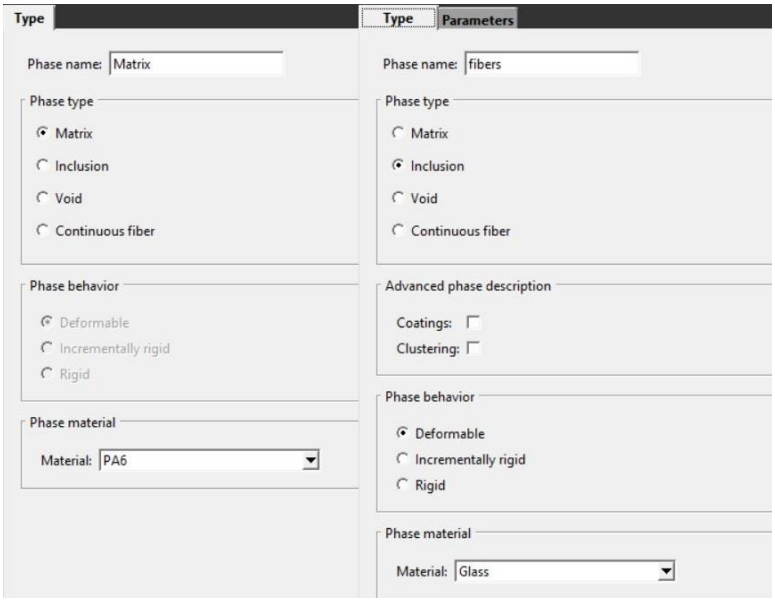

Figure 74. Matrix and fiber definition of the IM_PA6_GF30

The fiber phase required additional parameters definition. The mass fraction of fibers over the composite is 30%, as commented above. The aspect ratio of the fiber was set as fixed with a reliable value of 25. Common aspect ratios for SFRP composites are comprehend between 7 and 30 (Bernasconi, 2018) (Fu S-Y, 2009) (Hull D, 1996) (Thomason, 2001).

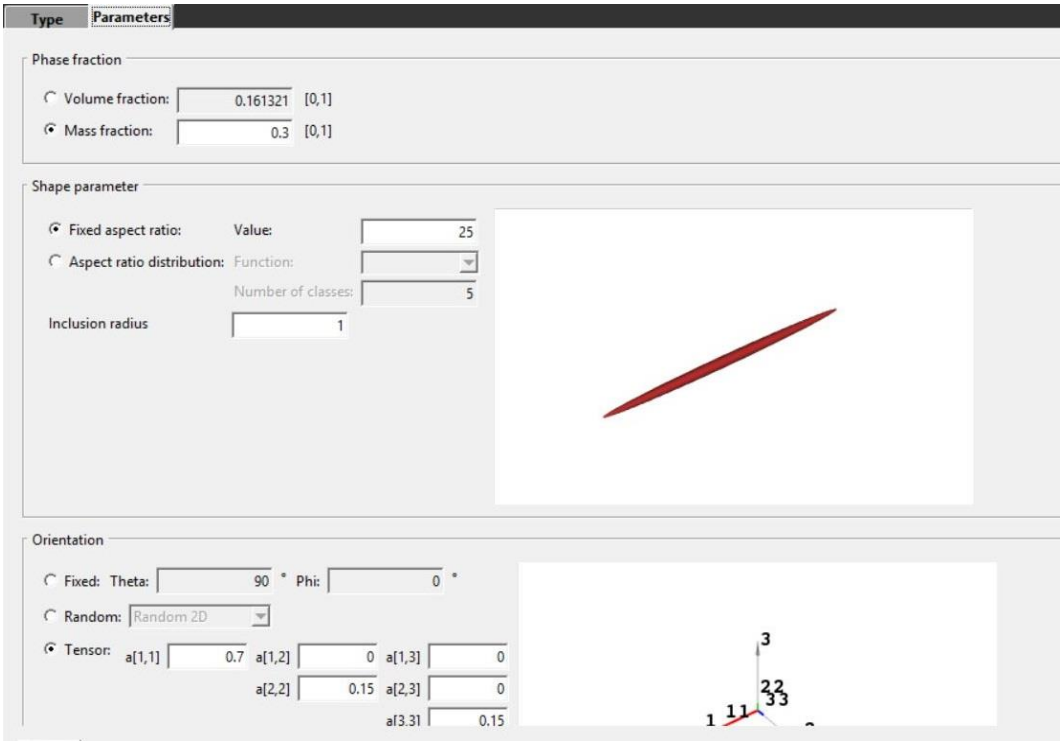

Figure 75. Parameters of the fibers of the IM_PA6_GF30

The orientation was set with the fiber tensor definition. A main direction in a11 was set, with a value of 0.7, while the a22 and a33 shared the remaining vector with a value of 0.15 each one (Fu S-Y, 2009) (Bernasconi, Short fibre composites, 2018).

After the definition of the microstructure, some comments about the mechanical loading conditions had to be made. These options were left as default to constitute the material model for the purposes stated at the beginning of the chapter.

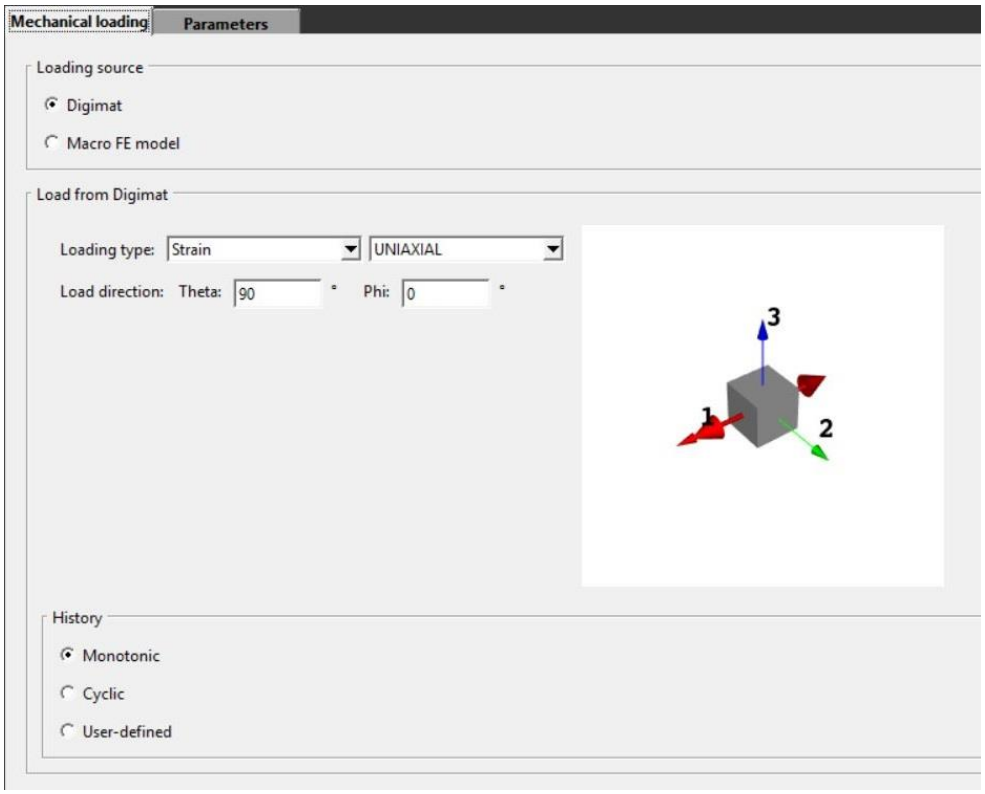

Figure 76. Mechanical loading definition of the IM_PA6_GF30

Once all these parameters were properly defined, the material model was ready to converge all this information and perform the homogenization. The homogenization process had a short duration, and once it converged, the resulting model was a **homogenized anisotropic SFRP composite. Proper assumptions meanwhile the micro-structure is being defined, will reproduce properly the real behaviour of the material when implementing it to the macro-structure model**.

The stress-strain relation in the 11 direction of the resulting homogenized model is plotted in the following figure.

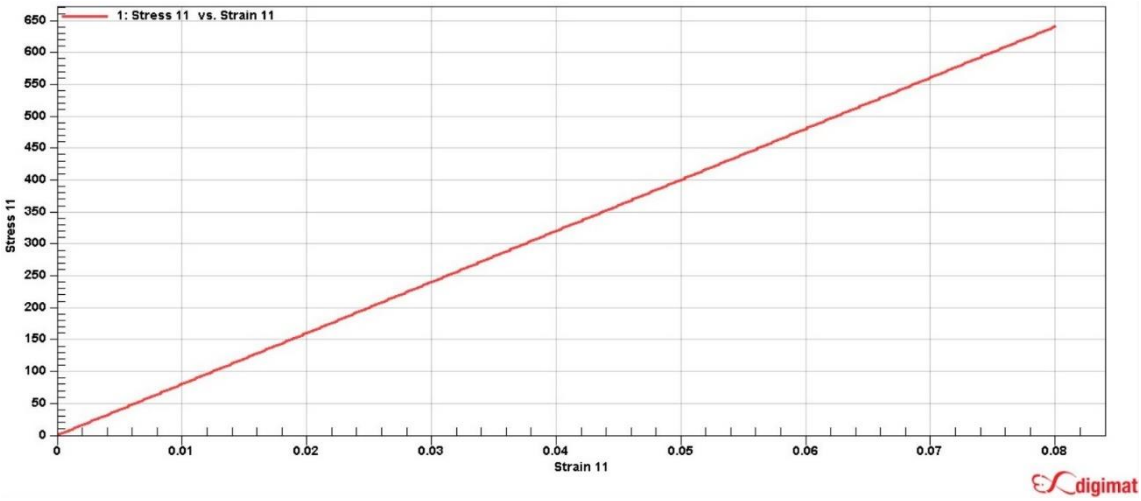

Figure 77. Homogenized model curve of the IM_PA6_GF30

The final results obtained, containing the compliance matrix, the stiffness matrix and all the engineering constants suitable for anisotropic elastic symmetry.

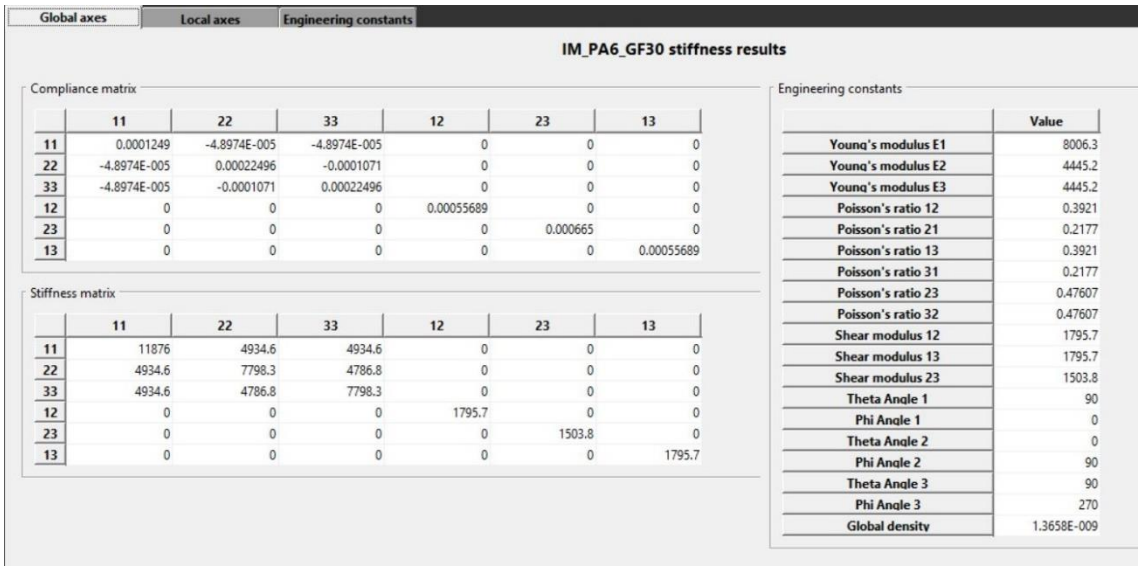

Global axes | Local axes | Engineering constants

IM_PA6_GF30 stiffness results

Compliance matrix

	11	22	33	12	23	13
11	0.0001249	-4.8974E-005	-4.8974E-005	0	0	0
22	-4.8974E-005	0.00022496	-0.0001071	0	0	0
33	-4.8974E-005	-0.0001071	0.00022496	0	0	0
12	0	0	0	0.00055689	0	0
23	0	0	0	0	0.000665	0
13	0	0	0	0	0	0.00055689

Stiffness matrix

	11	22	33	12	23	13
11	11876	4934.6	4934.6	0	0	0
22	4934.6	7798.3	4786.8	0	0	0
33	4934.6	4786.8	7798.3	0	0	0
12	0	0	0	1795.7	0	0
23	0	0	0	0	1503.8	0
13	0	0	0	0	0	1795.7

Engineering constants

	Value
Young's modulus E1	8006.3
Young's modulus E2	4445.2
Young's modulus E3	4445.2
Poisson's ratio 12	0.3921
Poisson's ratio 21	0.2177
Poisson's ratio 13	0.3921
Poisson's ratio 31	0.2177
Poisson's ratio 23	0.47607
Poisson's ratio 32	0.47607
Shear modulus 12	1795.7
Shear modulus 13	1795.7
Shear modulus 23	1503.8
Theta Angle 1	90
Phi Angle 1	0
Theta Angle 2	0
Phi Angle 2	90
Theta Angle 3	90
Phi Angle 3	270
Global density	1.3658E-009

Figure 78. Compliance and stiffness matrix and the engineering constants of the IM_PA6_GF30

This last information is the most important of the model, actually it is the information that defines the model itself, and how due the non-null engineering constants deliver anisotropic properties to the material model.

For the model it is know the Young's modulus for E1, 8006.3 MPa. In the Figure 5 was shown the values of tensile modulus and stress at break for the PA66-GF30. From the same source (CAMPUSplastics, 2018) can be obtained the mechanical properties for the PA6-GF30, and the values are almost the same. So, from a range of Young's modulus between 9500 and 6500 with an actual Young modulus of 8006 MPa, the Stress at break can be obtained from the range between the 180 and 120 MPa. **The IM_PA6_GF30 will have a stress at break at the E1 direction of 150.12 MPa**.

The information of the new model is saved in the Digimat-MX material database.

5.6 Bridging simulation and structural FEA

Until this point, all the information required for the final model has been gathered.
The model geometry, a preliminary isometric material model, the fiber orientation taken into account for the injection moulding manufacturing, and finally the micro-structure modelization of an equivalent homogeneous anisotropic material is obtained. The last step is to converge all these information within a unique model.

The software in charge for this duty is the Digimat-RP modulus. Digimat-RP enables to bridge the gap between processing simulation and structural FEA software (Ex-Stream, Digimat-RP IX, 2018). It gathers all the information regarding, geometry model, manufacturing technology, manufacturing critical behavioural aspects (FOD tensor) and a material model, to merge it into a single model and finally loaded and simulated with ABAQUS.

The final model will be constituted by the clutch pedal considering fibre orientation along the part with homogenized anisotropic material properties. A really accurate model for simulating SFRP composites parts manufactured with injection moulding technologies.

The Digimat-RP window shows the information in a way as it can be seen in the figure below.

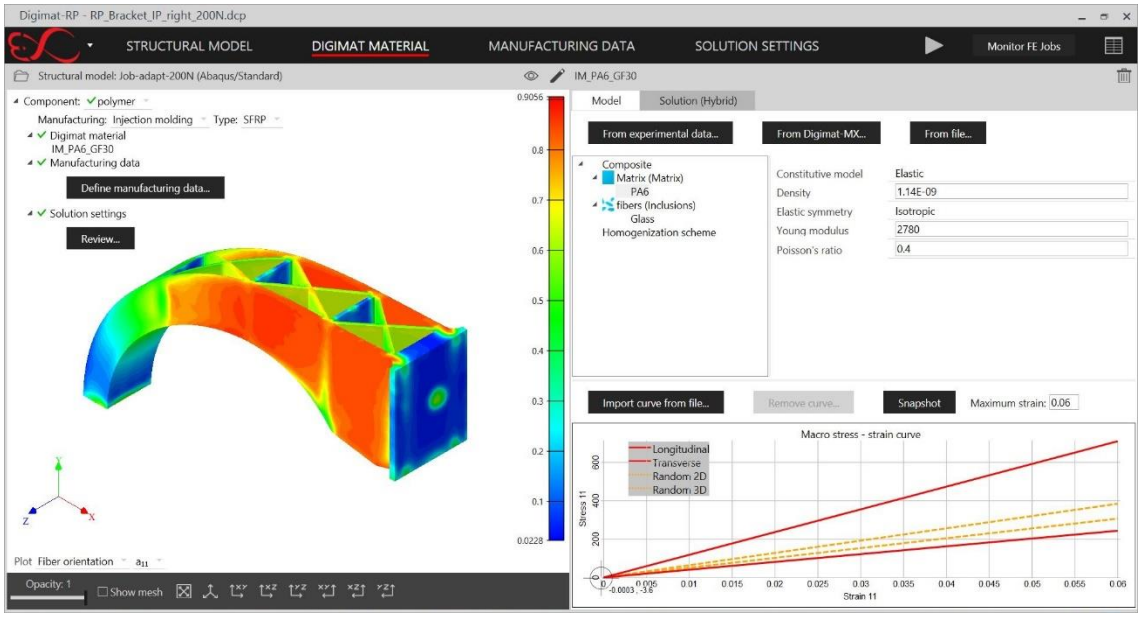

Figure 79. Digimat-RP window showing the FOD tensor component a11 of IM model

The 'Structural model' is the one created originally with ABAQUS with isotropic properties. The 'Digimat material' is imported from Digimat-MX database. The 'Manufacturing data' is those related with Injection moulding, like the fiber orientation tensor file resulting from Digimat-MAP after its importation from Moldflow. The 'Solutions settings' enables to review the numerical setting for the analysis requirements (Ex-Stream, Digimat-RP IX, 2018) at the same time it enables the coupling solution for running the FEA. The main set of variables to define are the FE analysis integration scheme and the Digimat solution procedure.

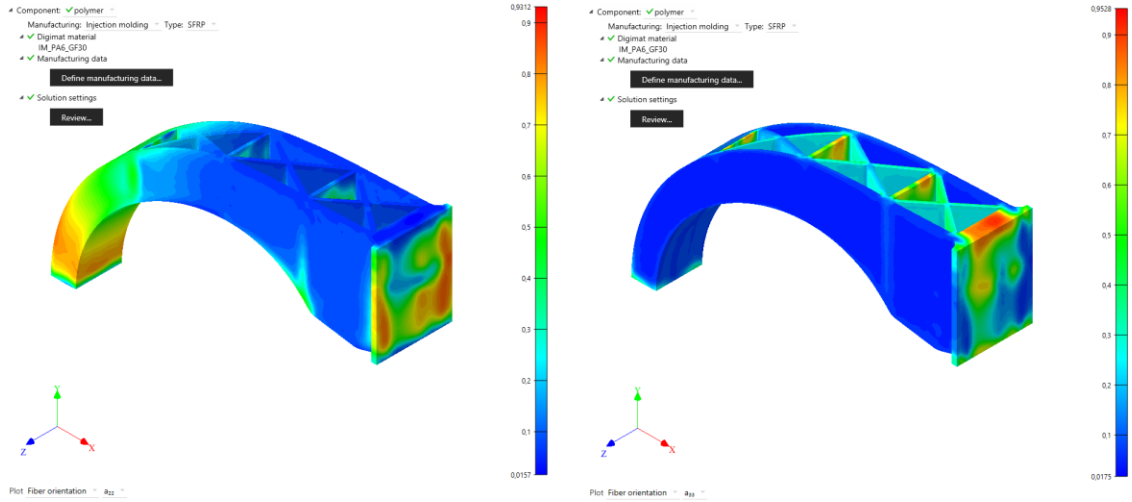

Figure 80. The FOD tensor components a22 and a33 of the IM model

In the previous images, from the fiber orientation tensor are extracted some components to see the direction of the fibers along the structure.

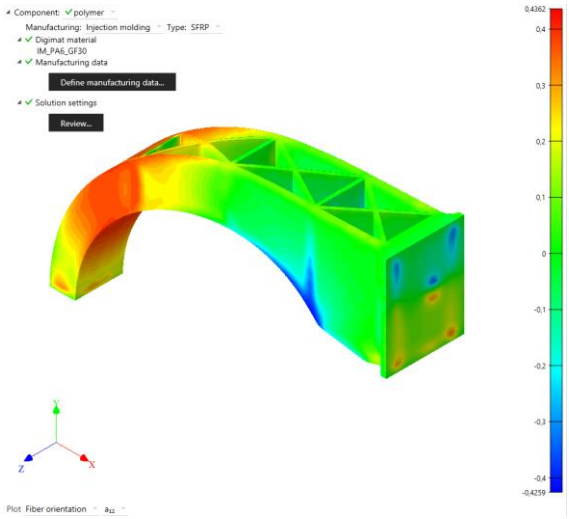

Figure 81. The FOD tensor component a12 of the IM model

As the FOD tensor follows the flow direction, the vector a11 has the greatest number of aligned fibers. From the injection point, the fibers travel through the arc shape until the end where the pedal is placed. The component a12 is more active at the middle stage of the arc. The component a22 is clearly absent at the middle part of the bracket where most of the fibers are oriented towards a11, and it acquires some relevance at the clamping area and close to the support as well. This is because there, the flow is stopped at the end of the mould, and several direction changes occur in the outflow. The direction at a33 mainly happens in the cross-sectional elements of the truss structure.

Due to the linear and static nature of the problem's loads, the integration scheme chosen is implicit. This solution scheme is more stable between calculation steps, even if each one takes more computational time.

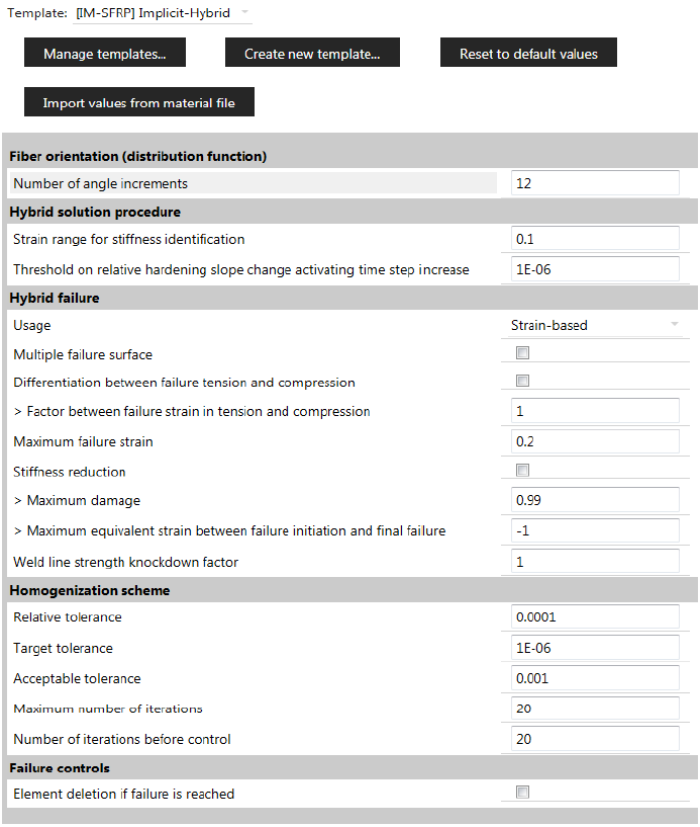

Figure 82.Solution procedure for Digimat-RP

In the other hand, the Digimat solution procedure chosen is Hybrid, to speed up the CPU usage and increase the robustness of coupled simulations. The option for element deletion when failure is reached must be disabled.

5.7 Structural FEA with FOD tensor and anisotropic material properties

Once the bridging between simulation and structural CAE has been completed, the results are shown in ABAQUS. As usual, the relevant information is kept within the displacement values and the stress field.

5.7.1 Displacement

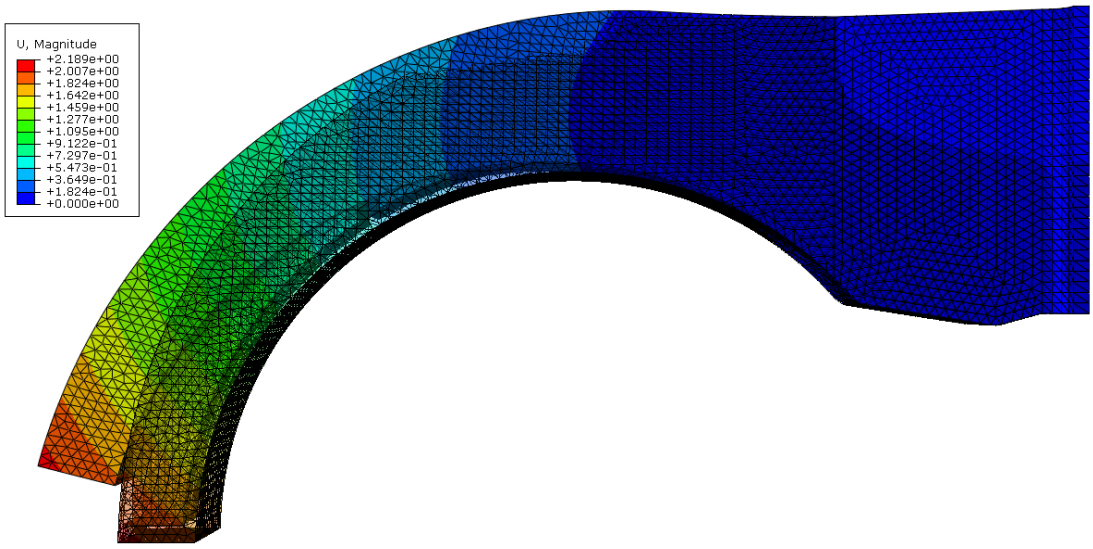

Figure 83. Displacement magnitude of the IM complete model analysis. Lateral view

The inclusion of the FOD tensor releases different values for the maximum displacement generated at the pedal surface of the bracket. This time, the higher magnitude is about the 2.189 mm. Higher than the model for isotropic material properties, and something expectable. Since the material is not isotropic, there are some regions that will behave weakly for the same load case. This accumulative effect along the whole structure will release a less stiff bracket and therefore the maximum displacement will be higher.

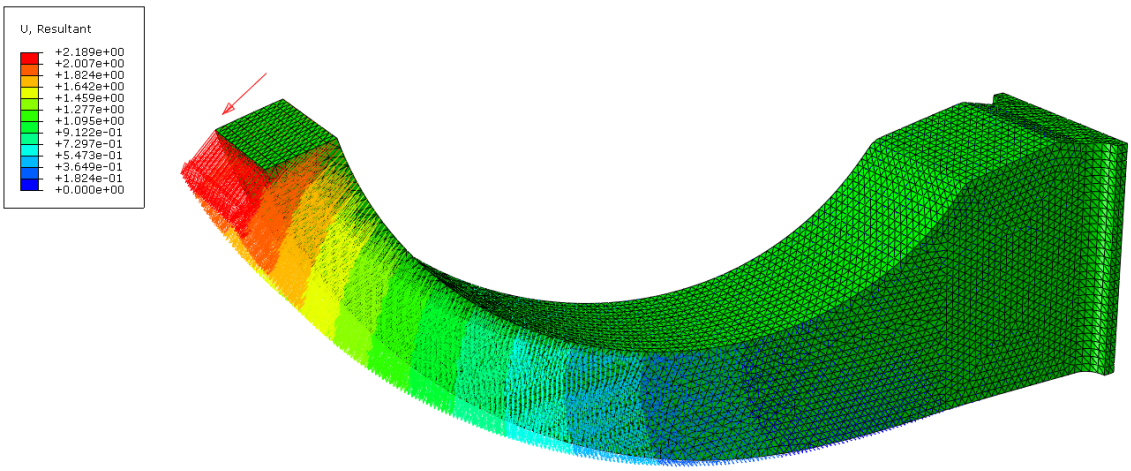

Figure 84. Displacement magnitude of the IM complete model analysis. General view

5.7.2 Von Mises Stress

Once more, Von Mises is the criteria for analysing the stress field generated.

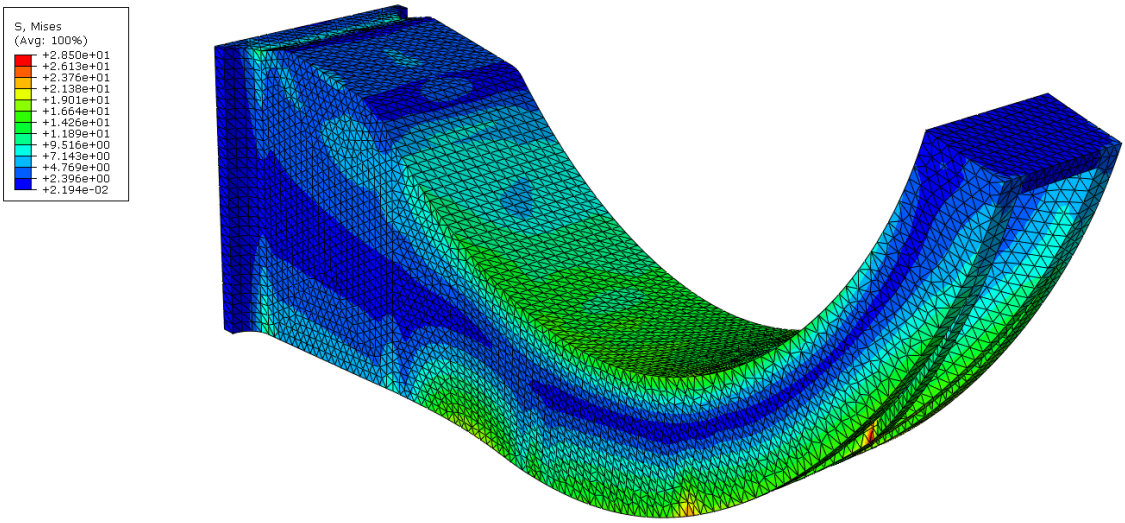

Figure 85. Von Mises stress of the IM complete model analysis. General view

This time, the maximum stress appearing in the cross intersection of the fourth row of crosses reaches a value of 28.5 MPa. Again, sharp edges are responsible of stress peaks even for loads of 200N. If the load increases linearly up to 800N, it would break at that critical point. With the addition of the FOD tensor, the stress field change and now some regions with different mechanical properties are shown are coloured differently. The appearing of stress islands in the mechanical part is an indication of non-isotropic properties.

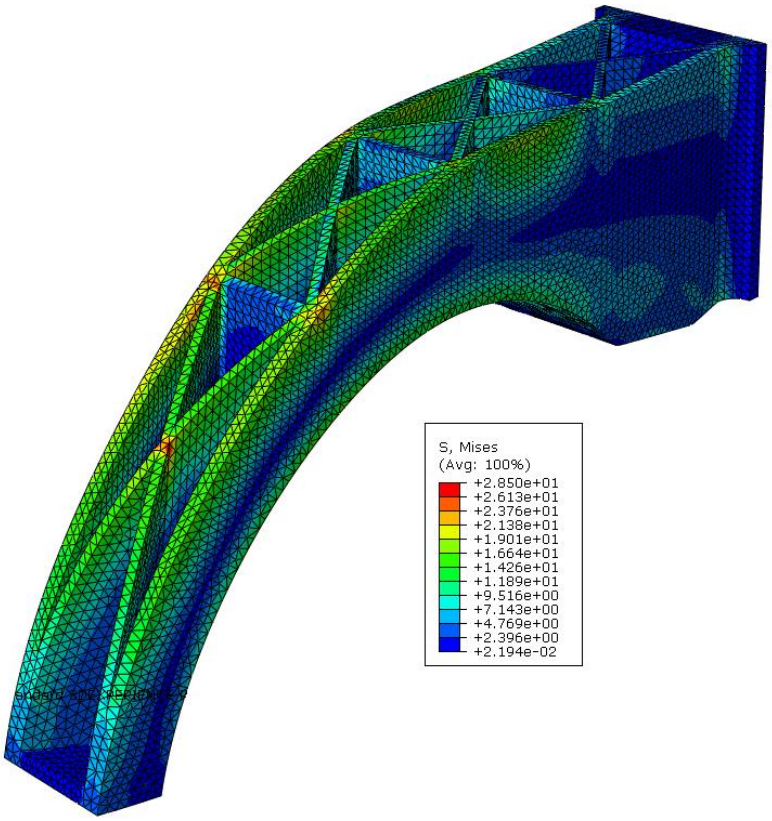

Figure 86. Von Mises stress of the IM complete model analysis. Isometric view

Even then, the results are very similar to the model with isometric properties. This confirms that the injection point has been correctly chosen since the material flow has released a good fiber orientation and not weakening the structural element.

6 Redesign for additive manufacturing

The new freedom capabilities of 3D printing allows to use of strong computational optimization tools like topology optimization with a feasible physical materialization.

With the integration of both, the mathematical algorithm and the technology, new ways of mechanical design arise for industrial purposes.

6.1 Topology optimization with ABAQUS

6.1.1 Initial CAD model

The geometry of the model used as an input for the topology optimization is changed. Because of the demoulding constraint, the model geometry for injection moulding has a specific shape. When another manufacturing technology is proposed this constraint is no longer imposed and the design rules change.

For topology optimization, the constrains imposed because of the manufacturing technique must be eliminated and let the algorithm work from an initial gross geometry. The decision of choosing the shape for the initial geometry will affect the final result, since the algorithm evolves along the part geometry with different patterns.

The initial geometry block chosen is a balance between a shape which may look like the original curved semi arc shape, but with no holes for the part demoulding. It could had been chosen a grosser block, but it was limited to reduce later additional computational effort.

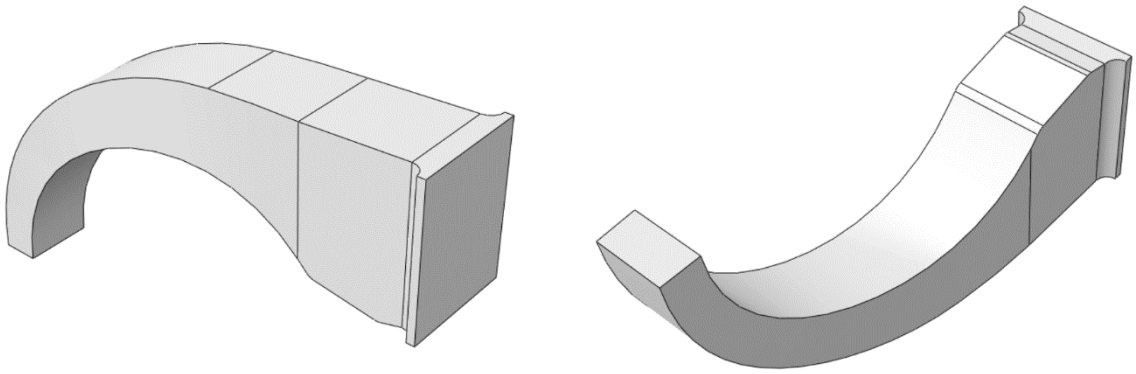

Figure 87. Input geometry part CAD model for topology optimization

Certainly there, two factors will strongly affect the results from the optimization process: The initial model geometry and its torsional shape.

6.1.2 ABAQUS Optimization module

The setup of this module includes the definition of an optimization task, the design responses, the objective function, the constraint definition and other options alike.

6.1.2.1 Optimization task

In this window, the optimization task is selected. An important decision is to choose the geometry for the task where the whole part has been selected except the fillets section around the clamping.

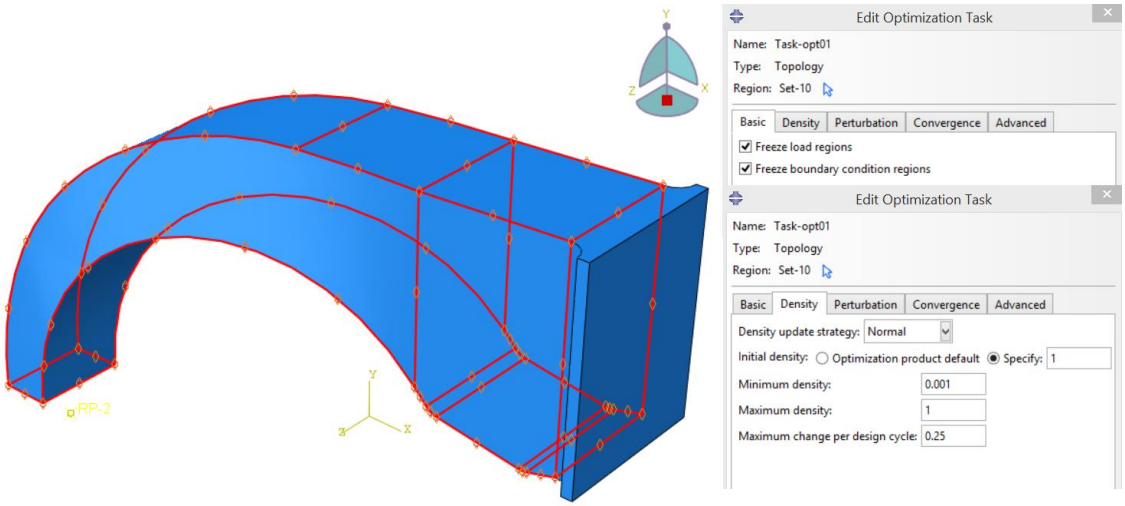

Figure 88. Optimization task definition for topology optimization

Due to the nature of the analysis, the option to freeze the load and boundary conditions regions has been chosen.
The initial density has been specified to 1 and the minimum density value changed to 0.001 with a maximum change per design cycle of 0.25. These parameters will make the algorithm stable between cycles while the optimization process is ongoing.
The remaining set of options have been left as default.

6.1.2.2 Design response

In this section, all the variables taking part of the analysis have to be defined. They could be as the total volume of the part, the strain energy or the eigenvalues of the structural element. After its definition, in later steps they will be used as constraints or objective functions, defining this way the optimization problem. For the analysis proposed, a displacement and volume variables have been defined.

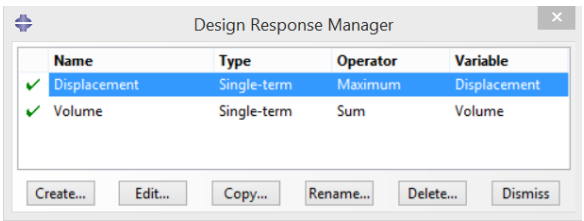

Figure 89. Design response manager for topology optimization

The displacement within the design response manager has been defined as a single-term type and specified in the node where the equivalent load is applied. Due to this node, and the pedal surfaced is fixed which a valid approximation to limit the maximum displacement appeared.
The displacement will be measures as an absolute value (in the direction of the equivalent load).

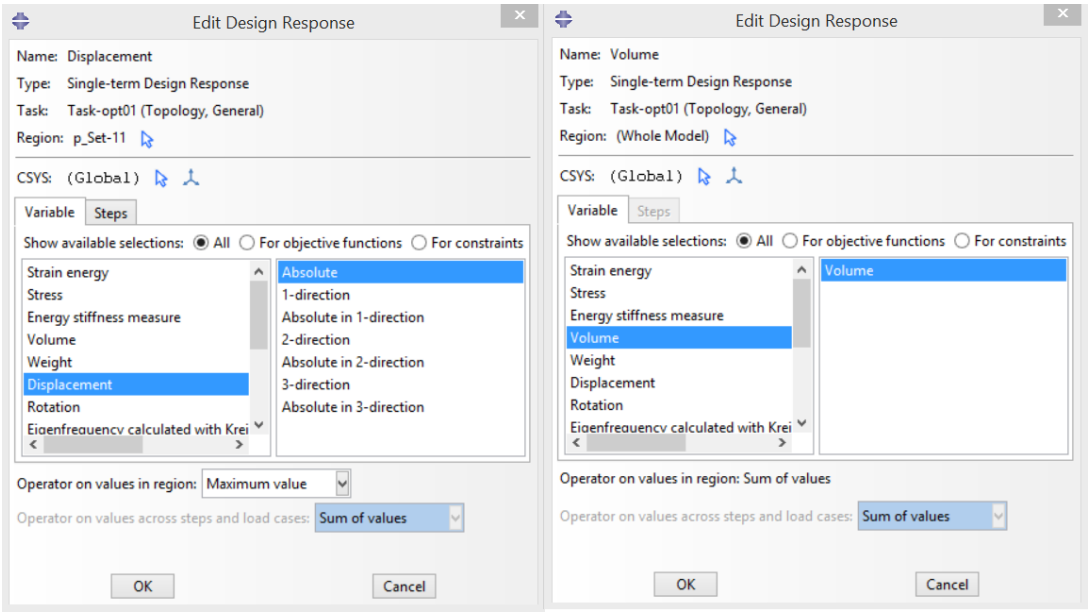

Figure 90. Design response definition for topology optimization

In the other hand, the volume has a design response which has been defined as a single-term type as well, but in this case it is applied in the whole model. This makes sense since the volume will decrease along all the geometry of the optimization task cycles.
For this case, all the secondary options are already chosen as a sum of values.

6.1.2.3 Objective function

The objective of the optimization problem is to reduce the total mass of the model. Since this case uses isotropic properties of the material, its density remains constant. Therefore, the optimization problem can be expressed as the reduction of the total volume of the model proposed. In this case, **the mass will be only function of the volume** (m=rho*V).

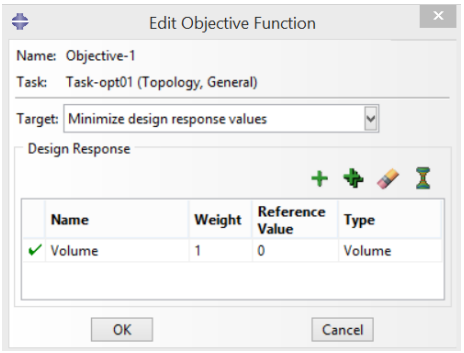

Figure 91. Objective function for topology optimization

As stated above, the target of the objective function is to minimize the design response values, adding the volume as the design response to be minimized.

6.1.2.4 Constraints

Therefore, once the optimization task geometry is bounded and the objective function stated, there is only one more thing to be set: the constraints of the optimization problem.

It has to be remembered that the original problem has only one design specification, the maximum displacement appearing in pedal during normal working conditions. Therefore, for the optimization problem will be defined as constraint the maximum displacement obtained from the initial CAE for injection moulding. This value for displacement was 1.85 mm.

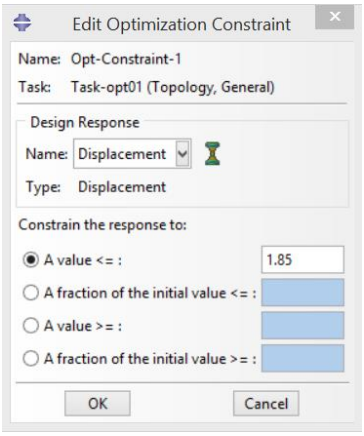

Figure 92. Optimization constraints definitions for topology optimization

Once all the modules are defined, the optimization task is ready to be run.

6.1.2.5 Optimization process

When the task is ready to be run, the evolution of the algorithm for the optimization can be monitored for each cycle.
In the optimization problem stated here, there is a compromise between the objective function (*the volume*) [red line] and the constraint (*the maximum displacement*) [blue line].
In each cycle, the value of the volume variable will tend to decrease whereas the maximum displacement increases. As the maximum displacement has a maximum value set in 1.85 mm, it will not overpass the constraint value.
So, in each cycle the algorithm tends to turn the part into a lighter one (less volume) at the expense of turning the part less stiff (more acceptable displacement).
The reason the part changes into a less stiff one is because of the loads (200N) are kept constant along the iterations in the optimization cycle while the displacement in the pedal increases.

$$K\ (stiffness) \leftrightarrow \frac{load\ (N)}{displacement\ (mm)}$$

That is why the displacement rising is limited to a constraint value, because otherwise the part would continuously become disproportionally flexible and therefore useless for loaded mechanical purposes.
The moment the algorithm cannot continue changing its variable values in the following steps at the same time it has satisfied all the design variables, the optimization task will reach an end.

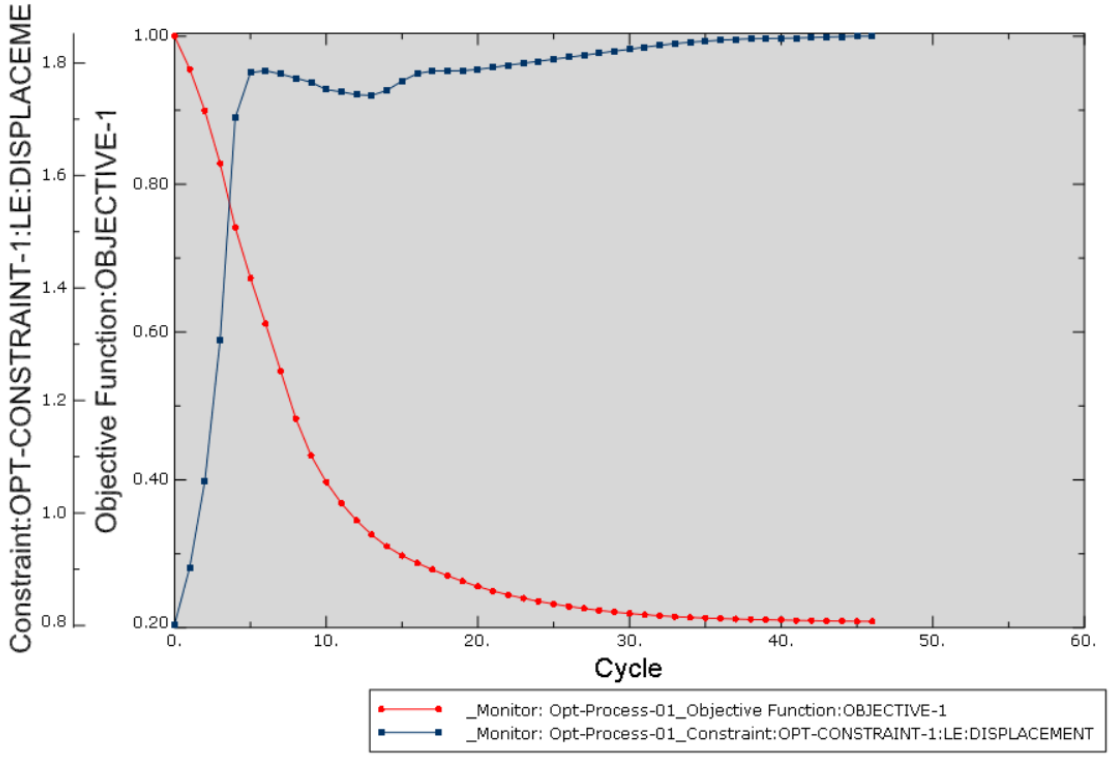

Figure 93. Monitoring the optimization task

The optimization task converged without any troubles at the cycle number 46. It took one hour and a half approximately to its completion.

6.1.3 Results

The final result after the optimization process leads to the following model

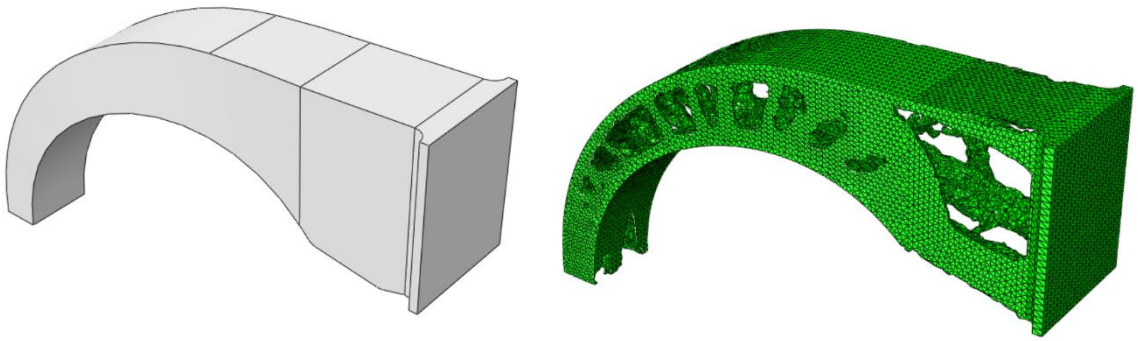

Figure 94. From the initial geometry to the optimized mesh

As it can be observed, the resulting model has a non-intuitive shape. Due the tri-dimensional nature of the part, the material redistributed along the part is not so obvious, and the final shape has to be analysed carefully.

In the next image the elements can be shown with higher relative density and the elements which are not being under heavy load solicitations. When the relative density of an element tends to zero (colder colours), the software removes it in the next optimization cycle.

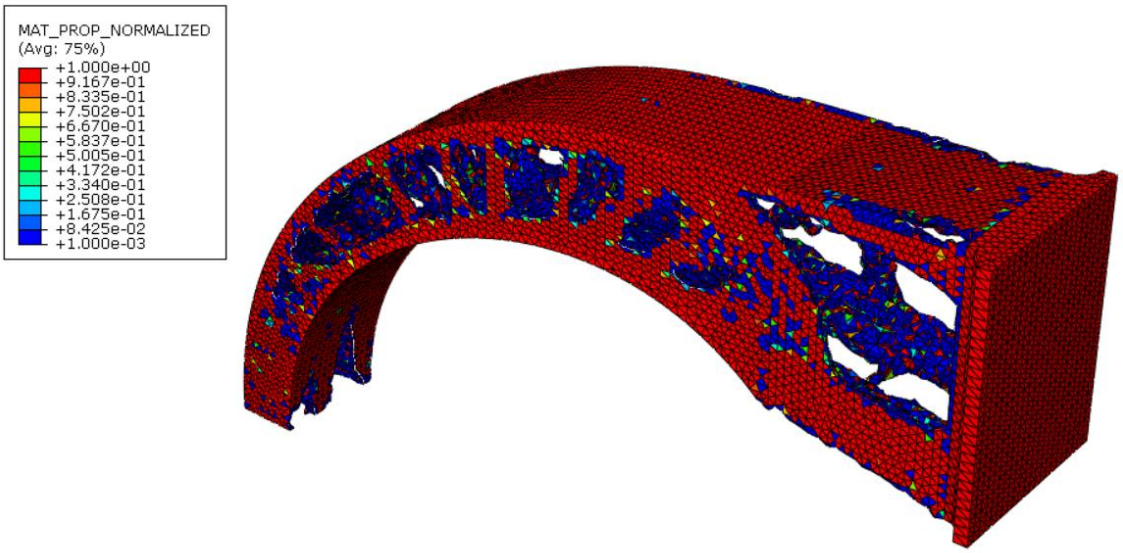

Figure 95. Relative density of the elements after the topology optimization. General view (I)

The first thing to make a comment about is the distribution of the heavier elements around the pedal. Most of them stay in the outer surfaces of the part, getting distributed in some recognizable patterns.

Both outer curved surfaces of the pedals, which will be compressed and tensioned, are completely kept. This makes sense since the arc formed will be the best structure to transmit loads from the pedal to the clamping, therefore the elements have a relative density equal to one. Actually the elements around these surfaces and it will not have bending or shear stresses; they will be affected only by tension or compression (**Membrane theory of shells**) (Rodríguez-Tembleque L., 2017) .

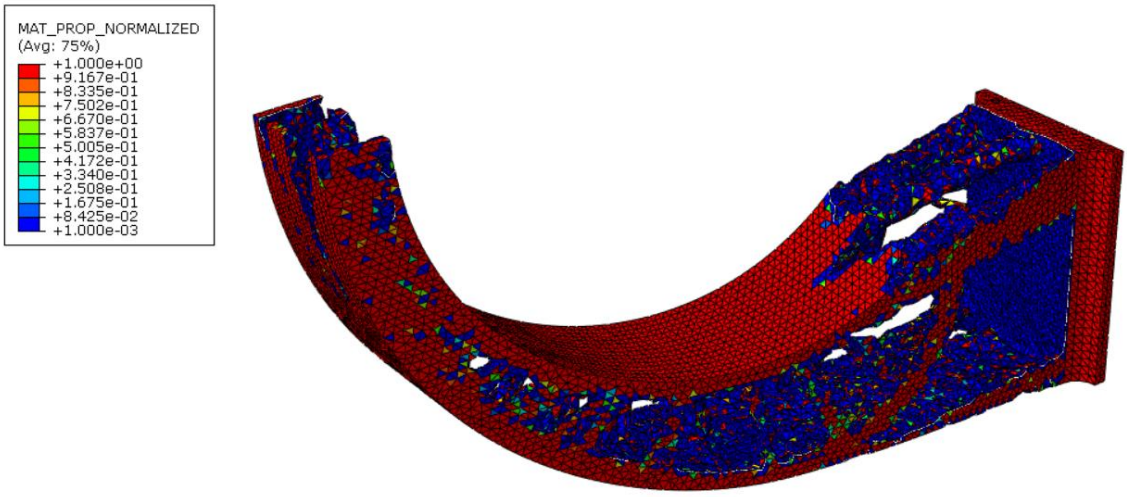

Figure 96. Relative density of the elements after the topology optimization. General view (II)

Another patterns found in the model are the lateral surfaces and its trends to create columns along the pedal, each of them perpendicular to the bottom an upper surfaces. This pattern creates geometries where the resulting structure hold better the loads, being this columns under compression or tension mainly.

Additionally, it can be observed how the resulting structure is hollowed. This has extreme impotency for the weight reduction, which will be very acute. It can be shown the among of material removed in the next picture, where it is displayed the part cut and its lateral cross section displayed.

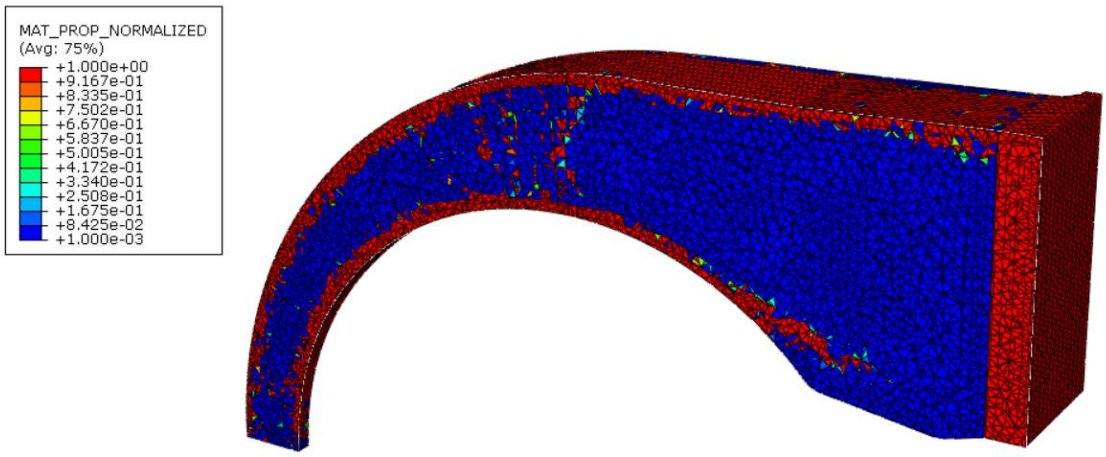

Figure 97. Relative density of the elements after the topology optimization. Lateral cross section view

Another structural factor to be discussed is the inner set of columns created in the middle of the lateral cross section over the bracket. They are non-negligible and add additional stiffness in the transversal plane of the structure along its reconstruction.

6.2 CAD Redesign

From the results obtained from the optimization, a new CAD model has to be created. This new model will keep the same shape, and some regions will be reinforced with extra geometrical thickness.
The arc shape and the different rows of columns have been conserved. The inner line of columns has been add too. These shapes are key for a stiff lightweight structure.
In addition, all the edges where different elements converge have been smoothed, in order to prevent tension concentration in this points.

Another important improvement has been the addition of extra reinforcement near the clamping. The geometry around these part has been increased to make it stiffer and stronger, because in that region the structural elements clamped to the base are under bending loads. The reinforcement of this are will increase the reliability of the part for the expected working conditions.

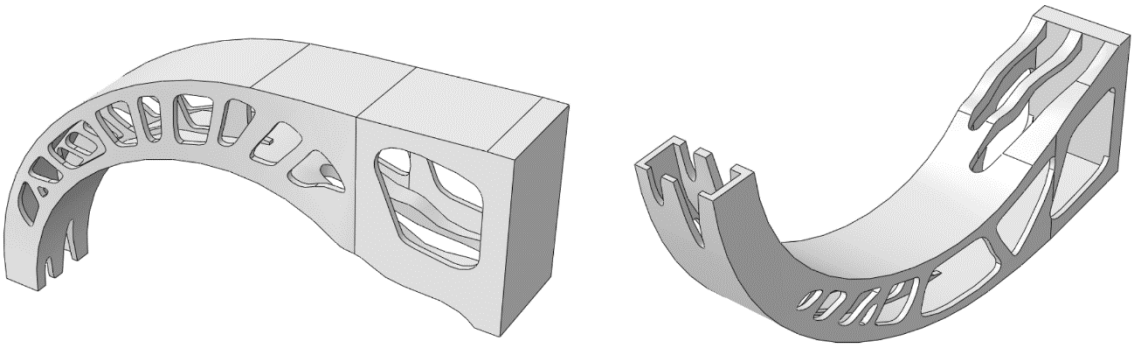

Figure 98. Optimized CAD model for additive manufacturing

Once the CAD model was completed, it was used as an input to perform a CAE analysis with isometric material properties with ABAQUS.

6.3 Structural FEA with isotropic material properties

As the process analysis made for the simulation of the part manufactured with injection moulding, the same paths must be followed to reach a final model that integrates properties which will give the model a behaviour closer to real anisotropic material properties of the reinforced plastics,

First, a CAE simulation with ABAQUS has to be completed successfully with ABAQUS using a material model of an isotropic and homogeneous material with similar gross mechanical properties to the final part.

6.3.1 Module property

For this preliminary analysis, the material behaviour is elastic, and its elastic law is isotropic with a Young's Modulus of 10000 MPa and a Poisson's ratio of 0.4 as it was done in the first model.

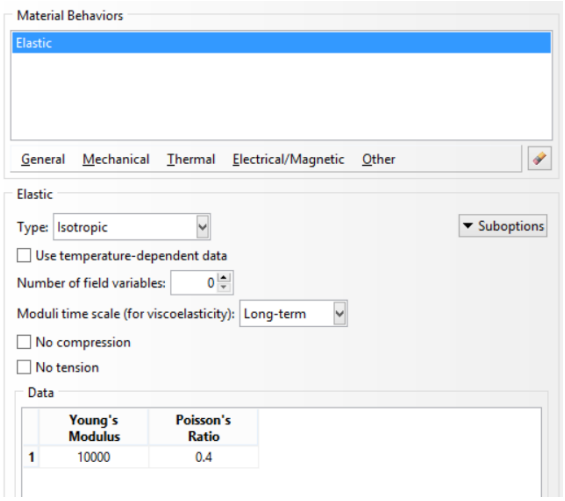

Figure 99. Material behaviour definition window for the AM model

The part section has been considered as a Solid and Homogeneous. To this configuration the material properties commented above have been added.

6.3.2 Step module

The type of analysis has to be defined in this module. In order to do it, a step requires its creation, being defined as static with a linear perturbation.
As did for the Injection Moulding analysis, the nature of the analysis will be an implicit analysis in where ABAQUS will have to calculate the stiffness matrix of the model to solve a linear elastic problem.

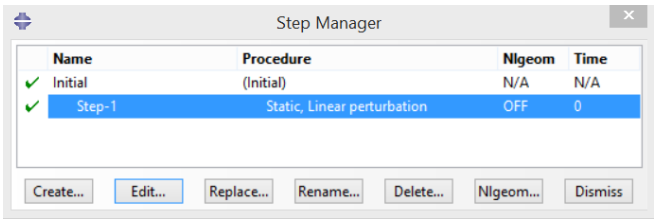

Figure 100. Step manager window for the AM model

6.3.3 Interaction module

The force exerted by the car driver to the clutch pedal while clutching the engine, as it is known, has been considered as an equivalent load applied in a single spatial point. This has to be correctly translated into a way ABAQUS is able to release similar analysis behaviours. The way to do it properly with an acceptable simplicity and compliant results is creating a reference point in the space where the load is applied. This reference point has been aligned in the lateral cross sectional plane were the bracket ends, and slipped slightly away to the side of the clamping.

Afterwards when the reference point is placed properly, it is attached to the pedal surface as if both would be part of the same body. If the RP is displaced, the pedal surface geometry will do it in the same direction and magnitude.

The coupling type selected is kinematic, and all the degrees of freedom have been constrained. With this configuration the desired effect can be achieved.

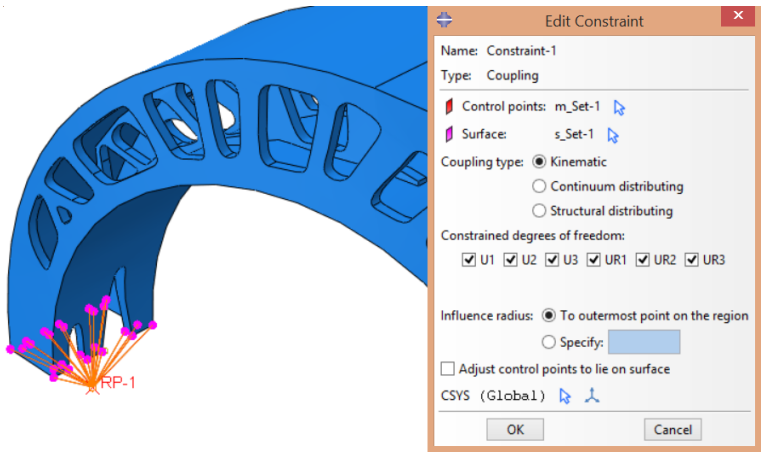

Figure 101. Coupling definition for the AM model

6.3.4 Load and Boundary conditions

The equivalent load of 200N is applied in the reference point created at the bottom of the pedal. The load has an inclination of 45º as in the horizontal and vertical axis. Of course, the type of load selected has been a concentrated force.

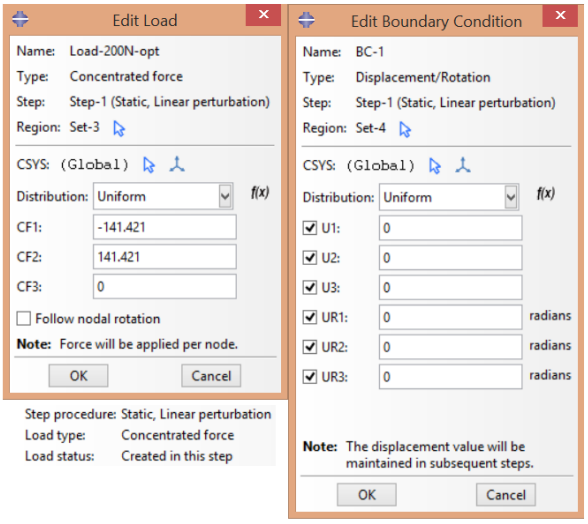

The boundary conditions have been defined constraining the displacement and rotation of the lateral surface where the clamping is placed. The displacement in each axis and its rotation have been not allowed.

The model would appear with this new features, and clearly it can be appreciated where the loads and the boundary conditions are applied.

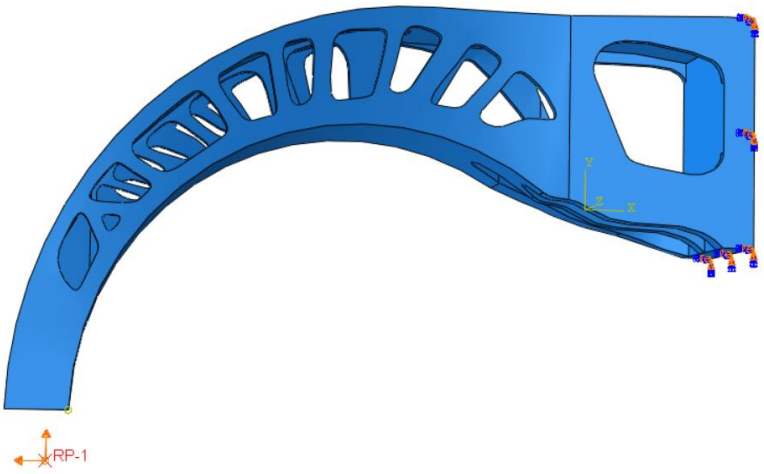

Figure 102. Load and boundary conditions definition for the AM model

6.3.5 Mesh definition

The mesh definition is probably the step which requires more attention by the engineer. This will affect significantly the output of the analysis, and depending a proper mesh setup, the results could not be compliant nor adequately shown.

The finer the mesh, the finer the results will be, and the evolution in the displacement field and specially the stress field will be better captured in the analysis output.

The mesh definition consist of the global seeds definition, the element type and its internal controls.

The approximate global size for the mesh has been chosen 2 mm. This will provide a mesh fine enough to obtain good results with no disproportional computational time.
The curvature control and the minimum size control has been left by default.

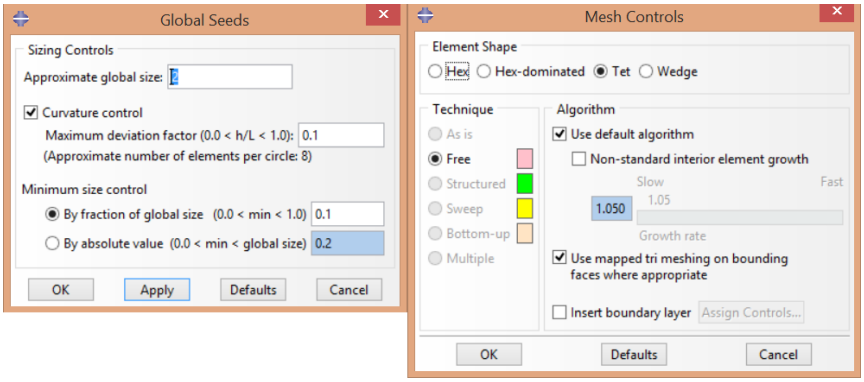

Figure 103. Global seeds and mesh control definition for the AM model

Within the mesh controls, the element shape chosen was tetrahedral, with the technique *'free'*, and the algorithm options set by default.

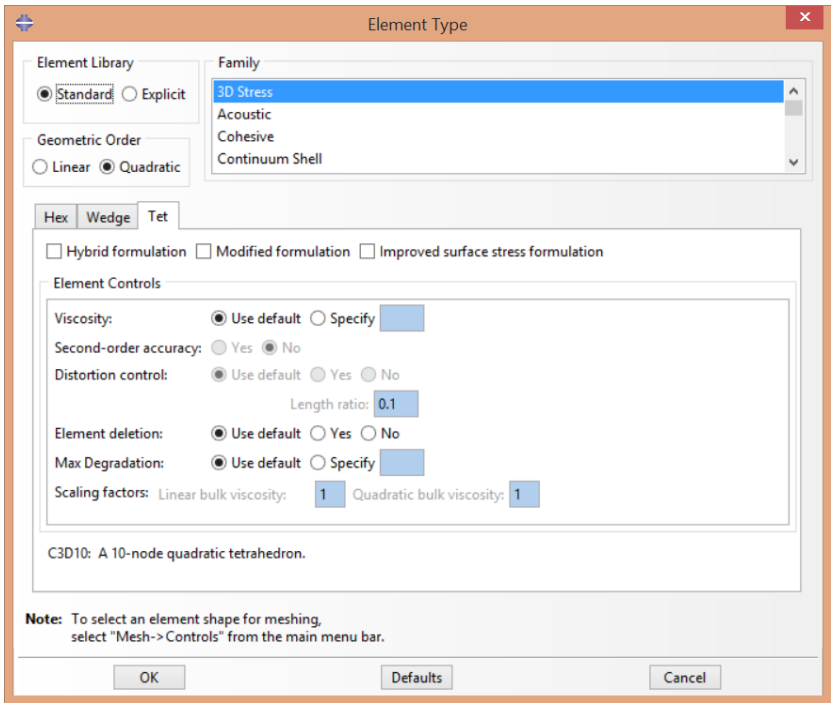

Figure 104. Element type definition for the AM model

The resulting mesh can be shown in the next image:

Figure 105. Structural optimized mesh for additive manufacturing

6.3.6 Mesh verification

Before carrying out the CAE analysis, the mesh had to pass a reliability check.
Due to the high complexity of the part and its tedious CAD completion, the resulting geometry required special attention for the creation of its mesh.

Small geometry edges or thicknesses along the part could make a way more difficult its mesh conversion. Therefore the mesh verification was carried out in order to detect the number of elements in which under a certain tolerance values of element size could be critical. If an element size is small enough compared to its elements neighbours, the moment the stress field is computed, the element could show significant higher values of stress than its adjacent neighbours.

These values are far to be the real, being a numerical issue, consequence of an improper mesh creation. In the mesh, elements size transition between nodes has to be smooth enough in order to prevent this numerical issues.

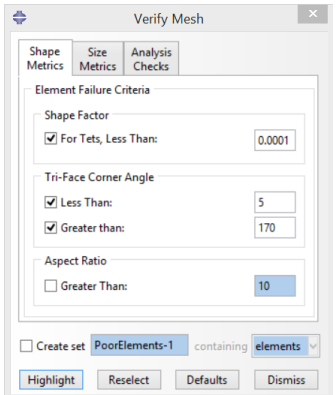

Figure 106. Verifying mesh for complex meshes

ABAQUS has a mesh verification tool in where starting from the mesh created, it runs a check of the element size depending the desired tolerance value. If some element size are smaller than the defined one, it will appear as critical elements to care for. One available option to make these elements warning no longer appear is to fuse adjacent elements. This will reduce the total number of elements in the analysis (less computational time) and the numerical issues during the analysis run. This is extremely useful since for complex parts dealing with implicit analysis with computationally intensive steps, the calculation of the stiffness matrix will be faster.

Inside the '*verify mesh window*', it has been selected as an element failure criteria the shape factor less than 0.0001 and the tri-faced corner face which must be between 5 and 170.

```
Part: Pedale_FIAT_punto_topology_05
 Tet elements:  67600
   Min angle on Tri Faces < 5:  138 (0.204142%)
   Average min angle on tri faces:  38.88,  Worst min angle on tri faces:  0.0218
   Max angle on Tri faces > 170:  8 (0.0118343%)
   Average max angle on tri faces:  88.27,  Worst max angle on tri faces:  176.38
   Shape factor < 0.0001:  40 (0.0591716%)
   Average shape factor:  0.670393,  Worst shape factor:  2.15e-008
  Number of elements :  67600,  Analysis errors:  0 (0%),  Analysis warnings:  212 (0.313609%)
```

Figure 107. Output from the mesh verifier

The total number of tetrahedral elements in the mesh was 67600. From this quantity, 138 elements where detected with a minimum angle on tri faces lower than 5º, 8 elements where over the maximum angle of 170º and 40 elements had a shape factor lower than 0.0001.

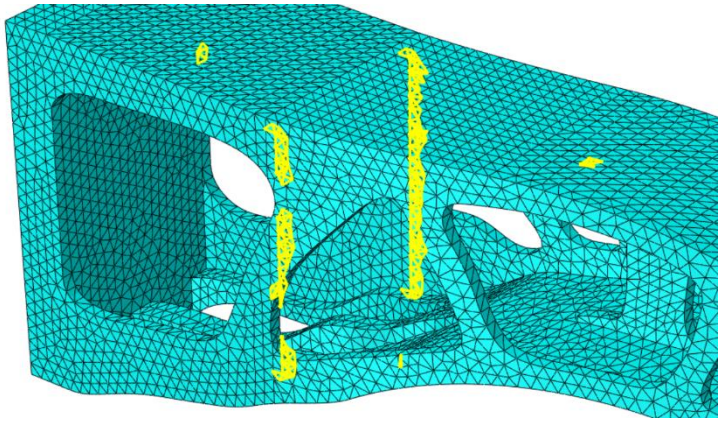

Figure 108. Elements with potential warnings

Discussing this information, a total of 212 elements with potential warnings appeared, a 0.31% from the total number of elements and none elements appeared with analysis errors.

The highlighted elements shown in the image appeared around the intersection of the part base with the bracket structure. The way of the model was made in CAD delimits this two sections, appearing elements in both sides.
These warnings need to be offset to reduce any chance of numerical issues appearance in later steps.

Anyway, it can be concluded that the quality of the mesh elements was good enough.

Afterwards the mesh, the loads, the boundary conditions and the material selection are defined, everything is ready to be run.

6.3.7 Analysis results

After the analysis run, the discussion about the results can start.

6.3.7.1 Displacement

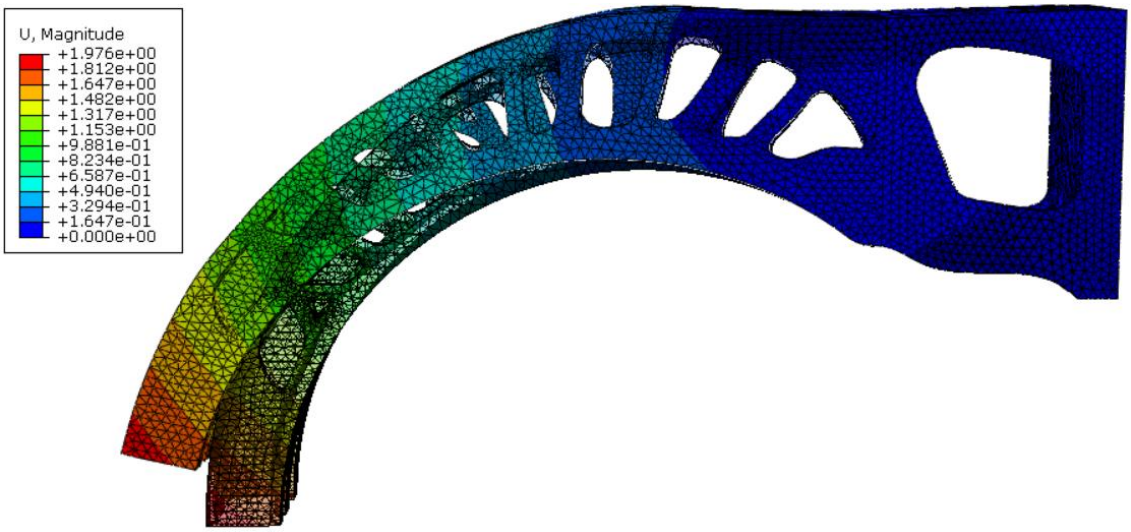

Figure 109. Displacement magnitude for the optimized iso model. Lateral view

The final displacement results from the analysis was a resultant displacement in the tip of the bracket pedal of 1.976 mm. This value is slightly upper to the value of displacement for the model for Injection Moulding with isotropic properties.

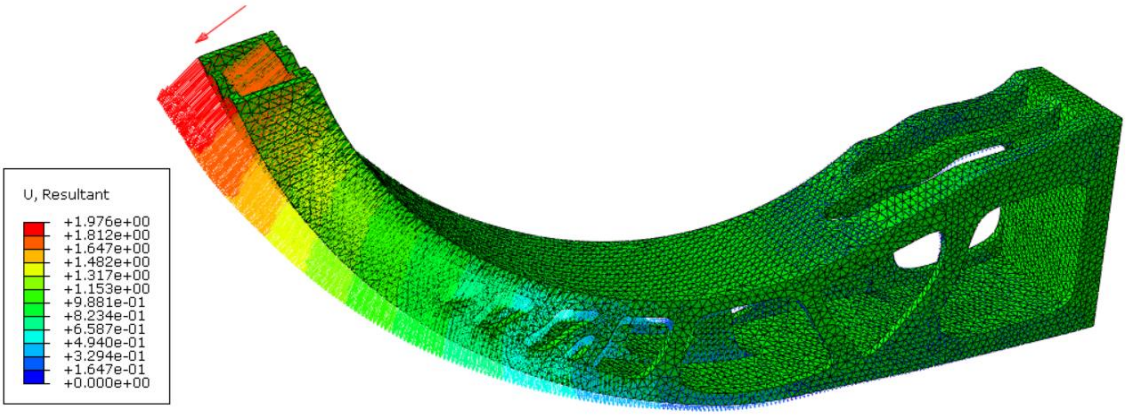

Figure 110. Displacement magnitude for the optimized iso model. General view

Nevertheless, the maximum displacement has slightly increased due the significant weight reduction in the part respecting its injection moulding equivalent. **The reduction achieved in one design iteration has been of the 40% volume reduction (39.69%)**.

6.3.7.2 Von Mises Stress

The criteria of Von Mises has been used for the stress analysis in the structure.

Some plot options have changed to show the results in a determined way. The deformation scale factor has been set to approximately 11 times the real behaviour.

Has been changed as well the computation of the scalars before averaging to the 100% in order to obtain more accurate results in the elements shown.

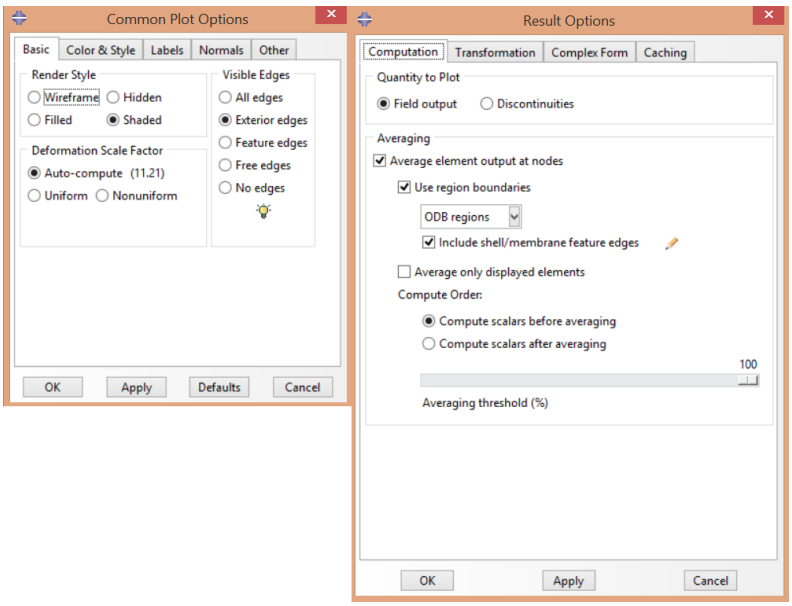

Figure 111. Results plot options

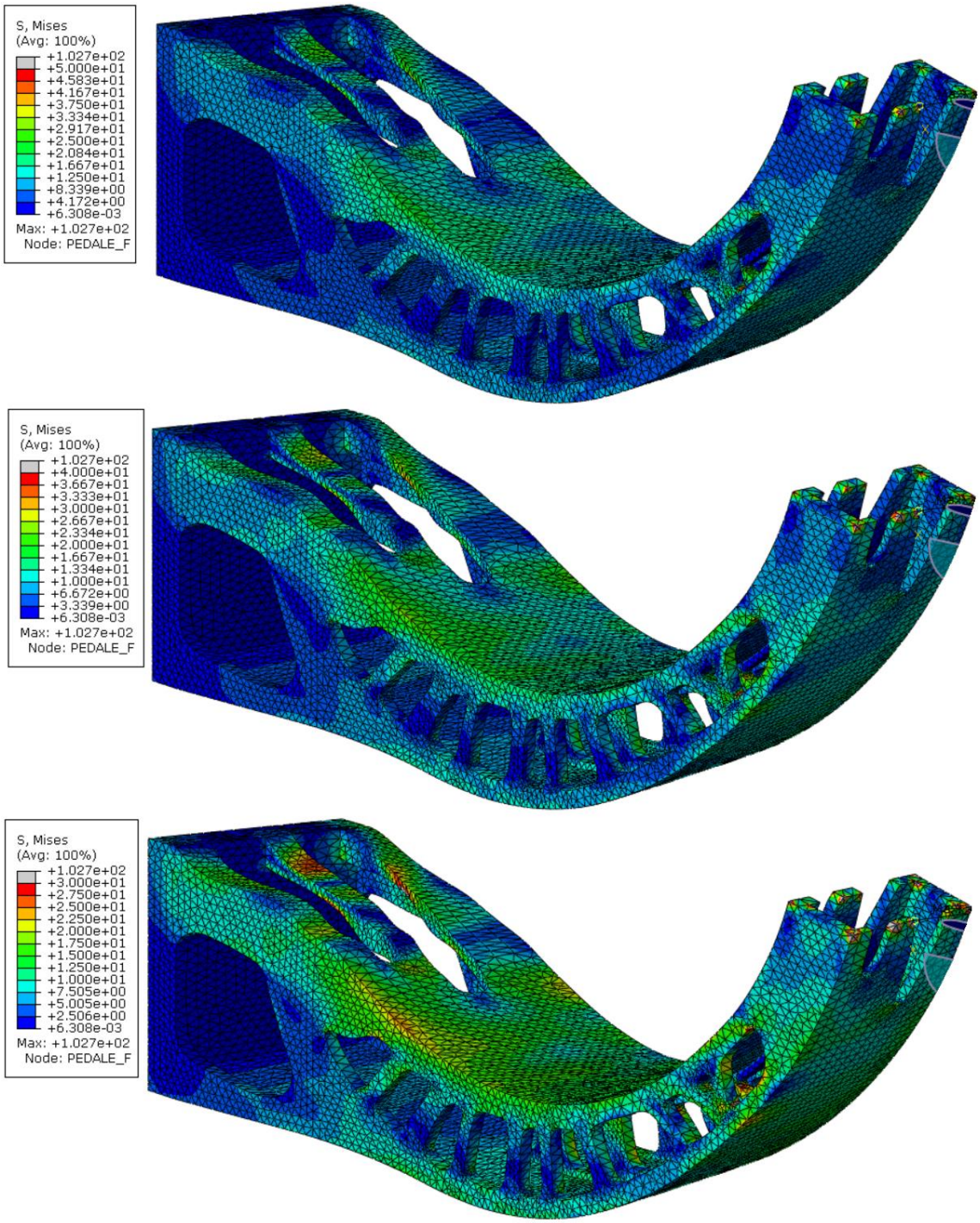

Figure 112. Von Mises stress with 100% averaged stress. The upper image shows the model with a limited maximum stress value of 50 MPa. The middle one for a value of 40 MPa. The last image is limited for a stress value of 30 MPa

The results show the stress distribution for the Von Mises stresses. In the triple image shown above, it can be appreciated the maximum stress value appearing in the results are 102.7 MPa. Even if this value apparently shows a high stress number in the new designed bracket, the FE model requires a deeper interpretation.

In all kind of structural CAEs, the interpretation of the data is fundamental but it is even more critical when the models have complex shapes, like this case.

It is common to find along the structure numerical artefacts due adjacent elements with abrupt stress changes jumping through them. With the mesh verification performed before, these kind of artefacts are actually reduced significantly.

Another important interpretation that must be done is regarding the adjacent elements to the boundary conditions or the regions where the loads are applied. These elements usually show over-increased stresses because it is usual not to create smooth transitions between the nodes or edges where the boundary conditions are placed and the first row of elements. For the case, this does not happened in the clamping side because the model was slightly intentionally modified in this region, exactly to avoid this issue. This has been avoided adding long and smooth geometries where the clamp is placed.

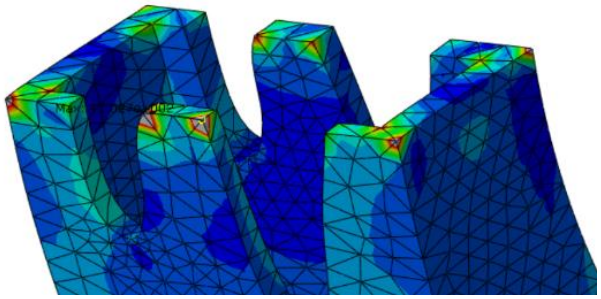

Figure 113. Detailed capture of the elements close to the load application area

Nevertheless, in the side where the equivalent load is applied, this courtesy at the time cad was created was not taken into account. It can be shown in the following picture how the corners and edges where elements with acute angles emerge in the same node exhibit several stress increases. A mesh refinement around this area or in case, a CAD model modification of the load application area, would release into better results with lower stress peaks in the surrounding elements.
It has to be said that in the real part, these 'legs' would be joined to the pedal surface, so the area created in the CAD is a partition of the real part and therefore this stresses would not appear in the real clutch pedal.

Apart from the bracket tip, in the results appear other regions with high significant stresses. These regions are around the holes created in the model. This is something expected because the moment was chosen the proportion of material had to be removed after the topological optimization, some regions would lead to an additional stress.

It can be seen that limiting the maximum stress to 50 MPa, apart from the tip, there are no elements overpassing this value.
The maximum levels of admissible stress in the material appears when the limit is decreased to 40 MPa. Here, it can be appreciate how regions close to the clamping start to be heavily loaded, and some elements around some holes are overcame.

If we decrease the level of tolerance of the stress even more, for 30 MPa it can be seen how in many points of the structure the maximum allowed value of stress is overpassed, failing the bracket at the same moment in different regions of the structure.

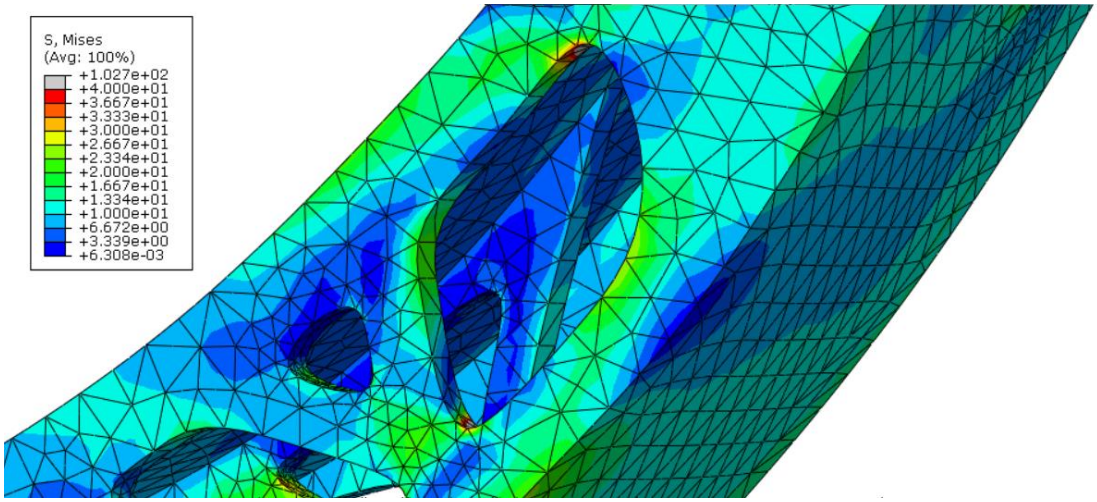

Figure 114. Detailed capture of the elements around the first lateral holes of the bracket

In the last picture, it can be appreciated with more level of detail the stress field around the holes where the structure overpass its maximum allowed stress when limiting its value to 40 MPa. The red elements are high loaded while the grey ones have exceeded its resistance capacity.

So it can be said, that for 40 MPa would appear the maximum real stress along the structure when it is loaded with a 200N force for an isotropic material model.

6.4 Extruder toolpath definition

6.4.1 Printer and material

The toolpath needed for the printing machine is a fundamental information for the printer to guide the extruder nozzle along its path to print successfully the part.

For the occasion, the software in charge to do this will be the Ultimaker Cura. This program allows multiple options during the machine setup with a large number of parameters. The obtained toolpath can be exported into the 3D printer directly or the information can be saved as gcode for other purposes.

Once the CAD model is imported into the software, the 3D printing machine which will be used has to be chosen from the available list of printers. The Prusa i3 is a famous commercial model of 3D printers because of its quality/price ratio. It is usually used for household users a.k.a '*makers*'. For research or prototyping purposes, it is a good 3D printer with good dimensional tolerances achievable.

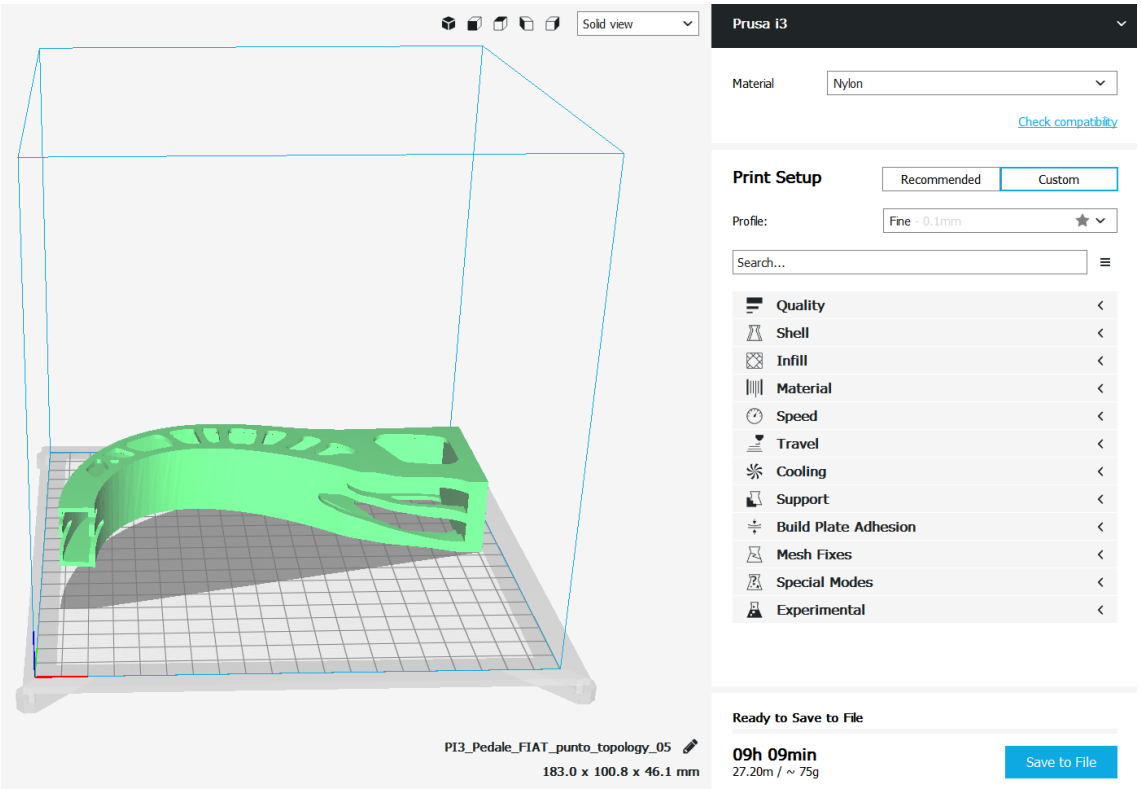

Figure 115. Ultimaker cura workstation window

The Prusa i3 is suitable for using Nylon as printing material, which suits the purpose of this project. Once the material and the printer are chosen, a set of manufacturing parameters have to be defined before launching the printer.

Prototyping experience with 3D printers streamlines the proper values choice. For this case, it is going to print a part with significant infill density in order to reduce excessive air inclusions between layers.

First of all, a fine profile of 0.1 mm for the extruder filament has been chosen.

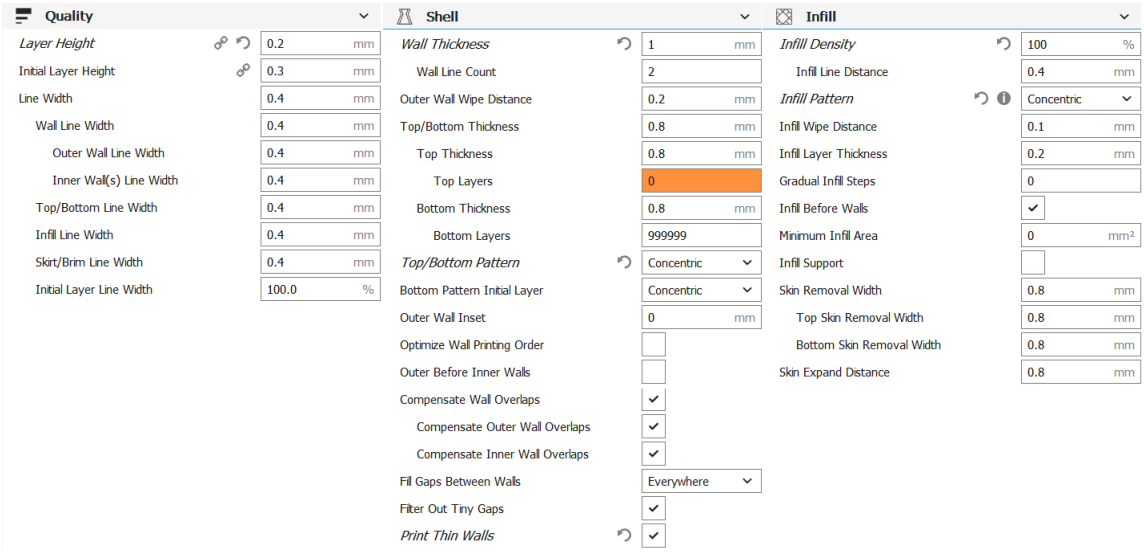

Figure 116. Print setup quality, shell and infill parameters

6.4.2 Quality

About the quality of the layers, a 0.2mm layer height has been chosen with an initial layer height of 0.3 mm. A line width of 0.4 mm will provide a sufficient base line to maintain each line stuck to each other.

6.4.3 Shell

Into the shell options, a wall thickness of 1 mm has been chosen, with a top/bottom thicknesses of 0.8 mm. A key factor to be chosen here is the top/bottom pattern and the bottom pattern initial layer. In this case, the chosen one is the *concentric* option.
Additionally, the overlapping wall compensation has been activated and the option filling gaps between walls has been chosen.

6.4.4 Infill

The infill requires special attention from the designer. If the part wanted to print is going to be used for mechanical loaded applications, the infill density must be as big as possible. In other words, if the desired is to print the part with an infill equal to a solid part, this will require to be setup as 100% in the window box.

The infill pattern is probably the most important parameter to insert in this step. This will completely decide the mechanical behaviour of the printed part. The infill pattern parameter will tell to the extruder which path has to follow while filling each layer. Since there are some interesting options like creating three dimensional cubes up along the printed layers, the *concentric* option has been chosen.

This alternative has been selected as the winner over others because the printed lines will follow the shape of the external curves and the inner holes of the bracket. This way, this will avoid unnecessary abrupt printing direction changes and most importantly, the material will be printed with the desirable path to facilitate the load be carried from the pedal to the clamping side with the fibers tending to the aligned to the extruded lines direction.

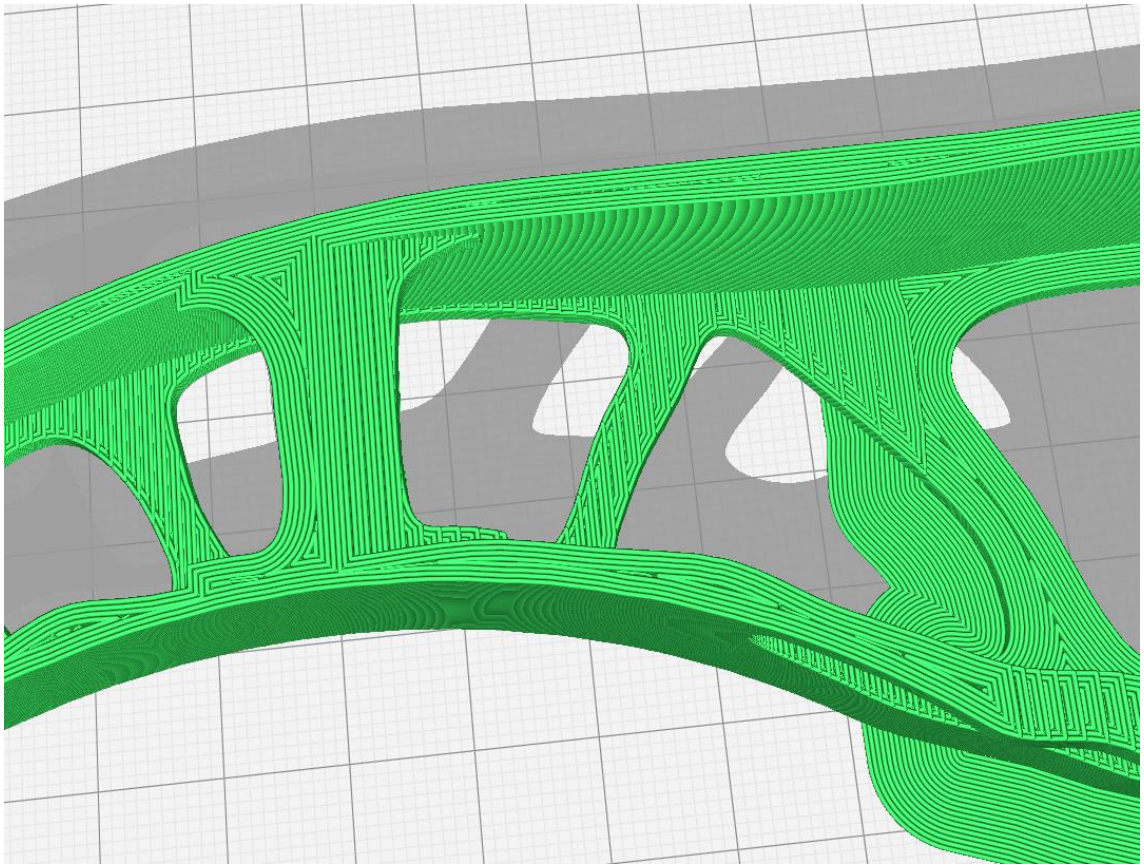

Figure 117. Concentric infill pattern

6.4.5 Material

The default printing temperature chosen is 245 ºC. This is the temperature of the composite the moment before it is coming out from the extruder nozzle. The build plate temperature chosen was 60ºC.
The chosen diameter for the nozzle is 1.75 mm. Depending the printer model, this could be different. In any case, the nozzle can be changed if the application requires so.
The retraction distance and speed has been defined as 8mm and 25 mm/s respectively.

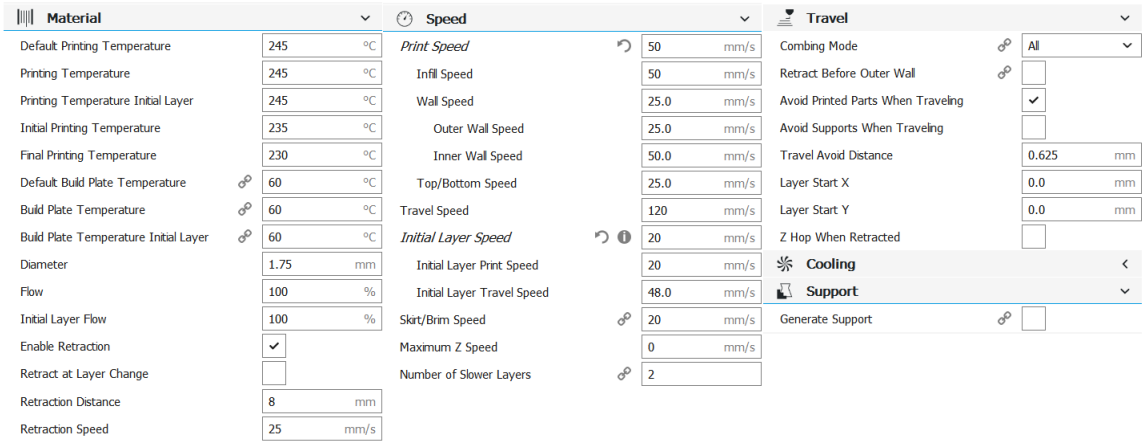

Figure 118. Print setup material, speed and travel parameters

6.4.6 Speed

The printing speed has been changed to 50 mm/s. The wall speed has been decreased into a value of 25 mm/s and the travel speed has been increased up into 120 mm/s.

6.4.7 Travel

The option to avoid printed parts while travelling has been activated in order to avoid crashes between the extruder and the part.

6.4.8 Support

Support definition in additive manufacturing is one of the key factors that require special attention during its creation. If they are not properly defined, the upper printed layers will finally collapse during printing due its own weight and because the lower layers wouldn't be cooled down enough to be sufficiently strong to hold the structure.

Even so, the support generator has been disabled. The reason is because this is necessary for the next simulation step. **The file required as an input for the incoming Digimat module must not include supports within its data, otherwise the simulation will not be performed correctly**.

6.4.9 Results extraction

Once all the manufacturing parameters are defined, **the total printing time of the part is 9h and 9 min without support addition**. If parameters like printing speed are changed into lower ones, the total time will be significantly higher but the part reliability will be increased.

The results can be saved as .*gcode, as if it were a CNC toolpath file.
This file will be imported in the next software package, the Digimat-AM.

Ultimaker Cura results data processing			
Results extracted from Ultimaker Cura	**File format**	**Does it need manual modification?**	**Data file goes as an input for**
Toolpath file	*.gcode	NO	Digimat-AM

Table 6. Ultimaker Cura results data processing

6.5 The simulation of additive manufacturing

6.5.1 Introduction to Digimat-AM

The Digimat AM module is a process simulation software dedicated to the additive manufacturing of polymers and short fiber reinforced polymers composites. It allows to predict warpage and residual stresses while building up the parts during its manufacturing process. The material used and the printing strategy can be chosen (Ex-Stream, Digimat-AM XII, 2018).

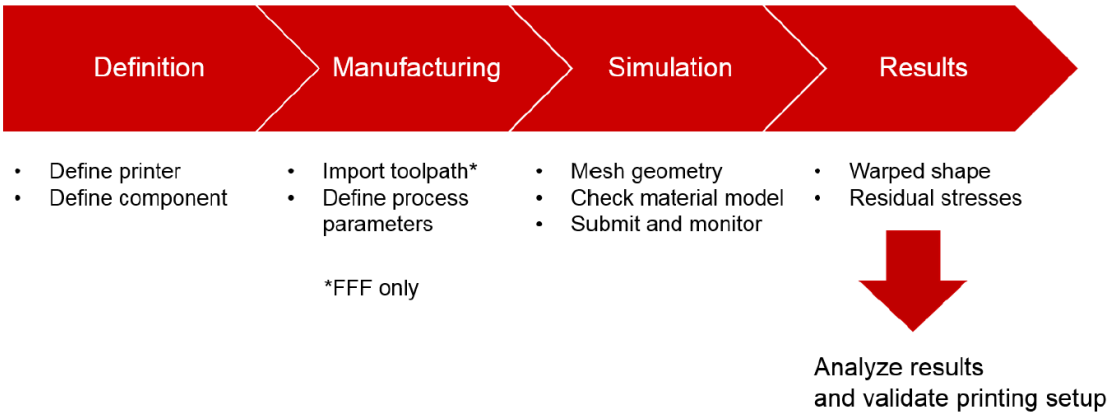

Figure 119. Digimat-AM process diagram

In further complex simulations, the printing setup can be optimized using the warpage compensation to apply it correctly and therefore the desired designed geometry.

6.5.2 Process definition

The software starts with the definition of the printing project, defining some manufacturing parameters and setting up the simulations to finally post-process the results of the analysis.

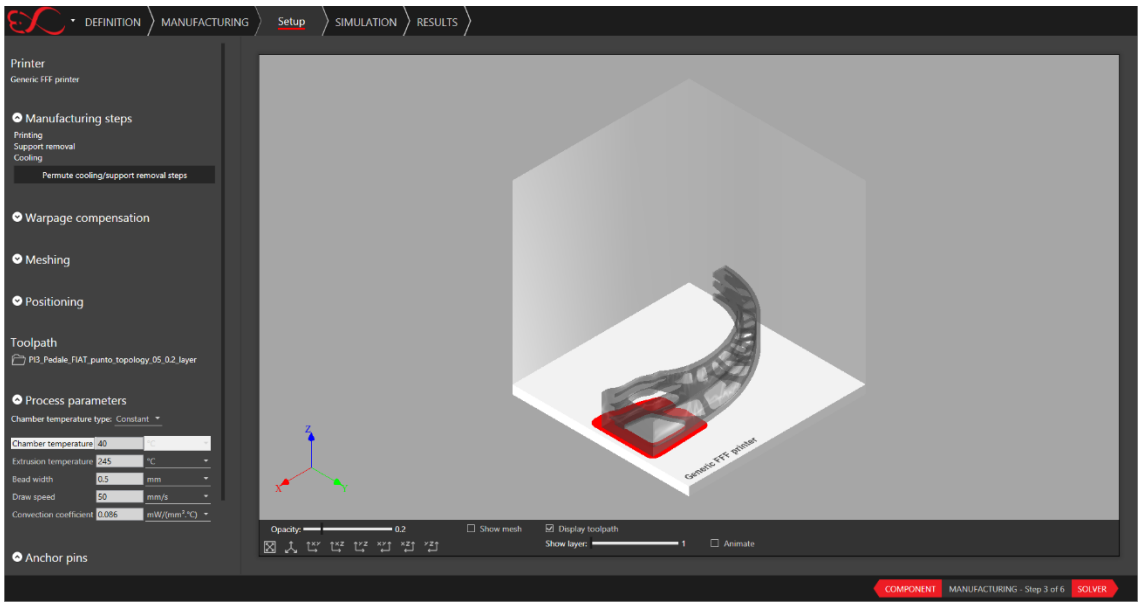

Figure 120. Manufacturing setup for Digimat-AM

The STL from the new cad model is required as the input, moreover, this, plus the toolpath from Ultimaker Cura is what is needed to use in Digimat-AM.

The material is fiber glass, and it will be setup as a generic printer for Fused Filament Fabrication (FFF), as the option available for the analysis.

The manufacturing steps followed by Digimat-AM are printing, support removal and cooling.

If cooling is performed after the support removal, the part will suffer warpage deformation plus body weight deformation.

The toolpath used is the one created with Ultimaker Cura. The total number of layers is 116. It can be highlighted in red each of the layers along the part.

For the process parameters, a constant temperature type has been chosen. Complex analysis would be an interesting option to change and check the results in the final simulation respect the option with constant chamber temperature.

For the analysis shown here, the chamber temperature has been changed to 40ºC.
The extrusion temperature has been set to 245ºC, the same value used during the toolpath definition.
A bead width of 0.5 mm has been chosen.

The convection coefficient has been set into 0.086 mW/(mm^2*ºC) as recommended for the printing setup and the material used.

For Digimat-AM, it is required a mesh definition.

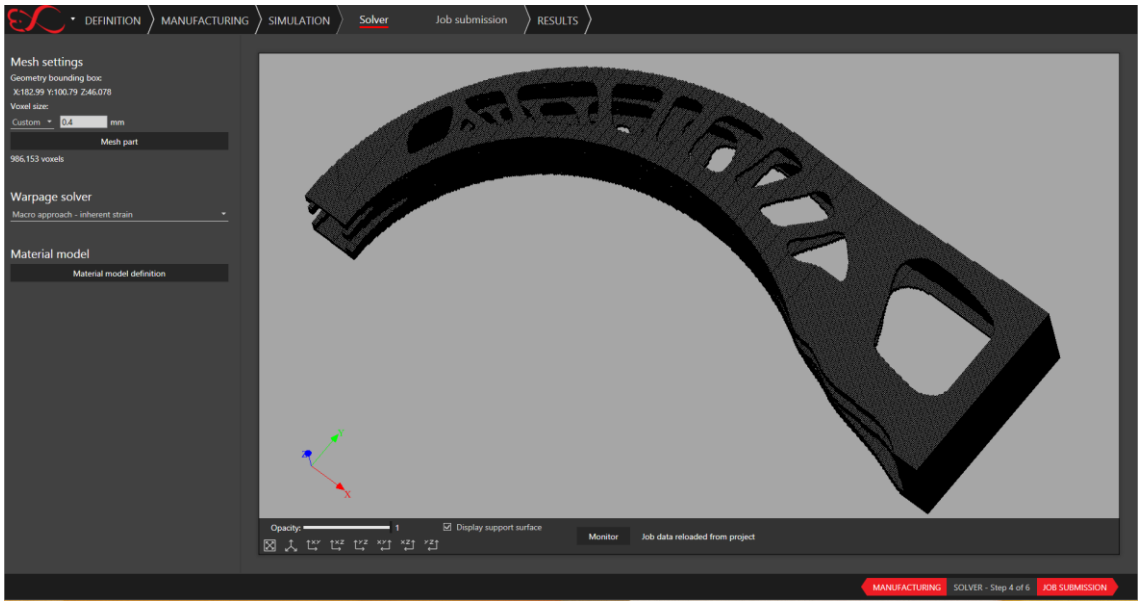

Figure 121. Mesh setting for Digimat-AM. Solid Elements

In order to create a finer mesh than the one obtained in the previous analysis, the voxel size chosen to 0.4 mm. This will increase significantly the computational time, but will prevent any mathematical errors during mapping both meshes. The elements used are 'bricks' type.

Once the mesh is created, it can be seen the number of elements increases to 986153 voxels.

Within warpage solver options, the macro approach has been chosen as the inherent strain.
These inherent strain values described by strain tensors represent the warpage behaviour of the material. In other words, the way the material contracts and generates distortion once it has been deposited under some given process conditions. When inherent strain values are known for a given combination of material properties and process parameters, a simple mechanical layer-by-layer structural simulation can then be run to simulate the manufacturing process.

Inherent strain values are applied on each layer as they are added, until the full part is built up completely.

The material model chosen is a composite material for a PA6 reinforced with 30% glass fibers for thermal analysis. The unit system has been considered in MPa.
The warpage available source is pre-process by Digimat-AM, computing inherent strain values for given material properties and process parameters.
The mechanical parameters introduced are defined as previously done.

The microstructure is defined for a reinforced plastic. The fiber aspect ratio and fiber orientation used ware the ones defined in the Injection Moulding material model. In FFF, fiber orientation tensor is aligned with the bead direction.

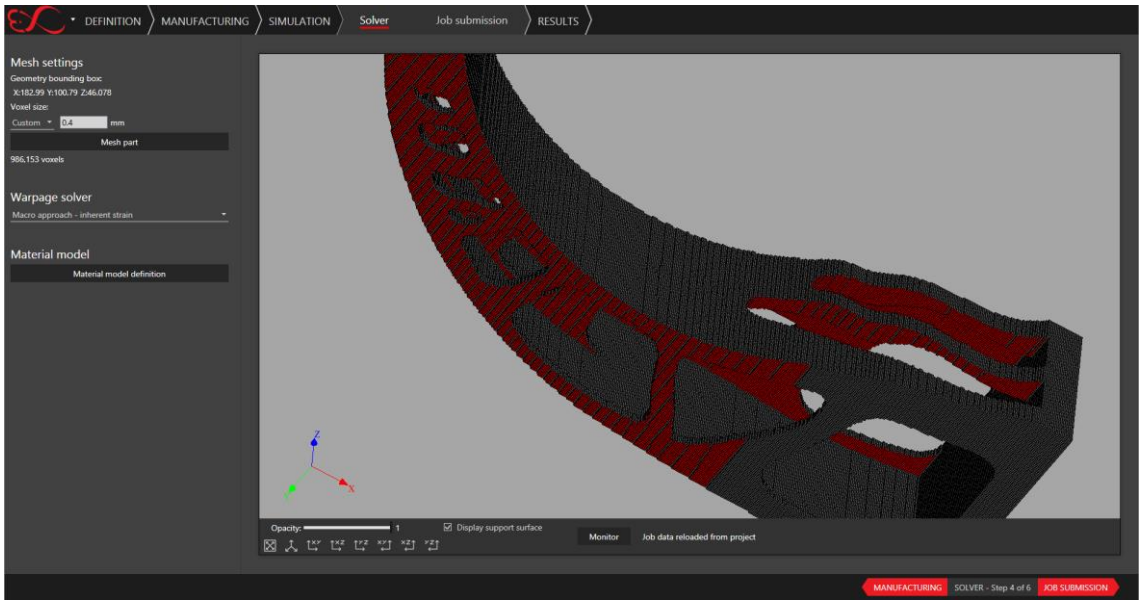

Figure 122. Mesh setting for Digimat-AM. Boundary conditions

It can be appreciated in red, how in the cantilever surfaces are applied boundary constraints that will act as an equivalent supported structured with no cantilever areas. This is the way Digimat-AM deals with the cantilever areas instead computing printing supports given by the commercial 3D printer software like Ultimaker Cura.

6.5.3 Results

6.5.3.1 Warpage deflection

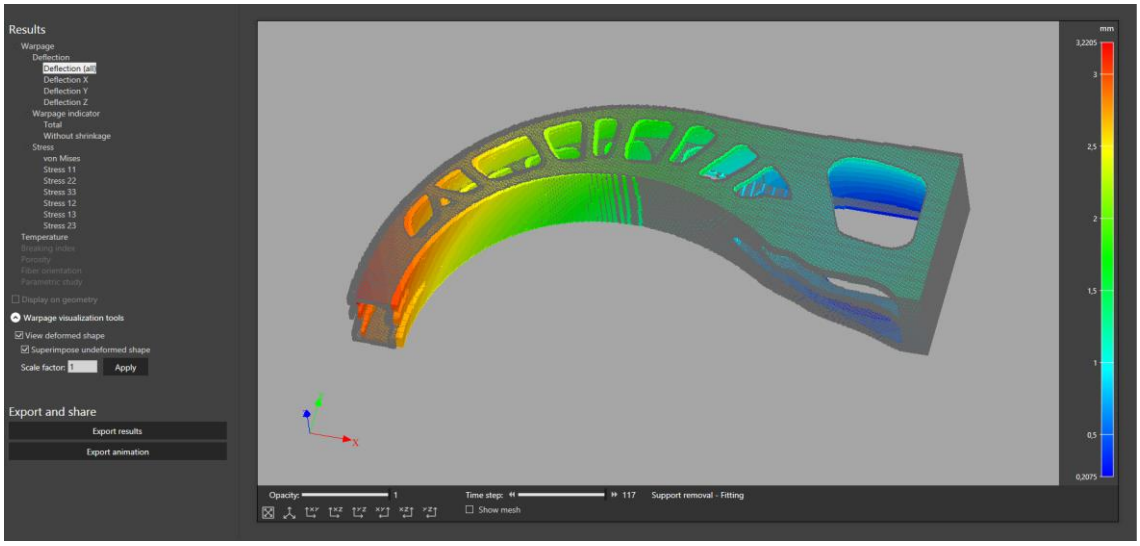

Figure 123. Warpage deflection results after the support removal and the cooling down. General view

The magnitude of warpage deflection from the FFF can be appreciate in the previous image. After the bracket has been successfully printed, the software removes internally the boundary conditions from the part and cools down the bracket before it displays the results.

With a material thermal model, during the temperature cool down, the part is under heavy warpage deformations until the mean bracket's temperature reaches a steady temperature value of the printing chamber. At that moment, the part has been cooled down. The accumulated warpage deflection of the bracket is shown, and the maximum value of deformation reached is 3.205 mm.

This maximum deflection appears in the tip of the bracket. The meaning of the warpage deflection is that the actual dimensional geometry of the part after its printing, support removal and cooling process will be the coloured shape.
This gives important information about the actual geometry once manufactured. Therefore, the absolute real displacement in working conditions will be the sum of the warpage plus the displacement caused by the load application.

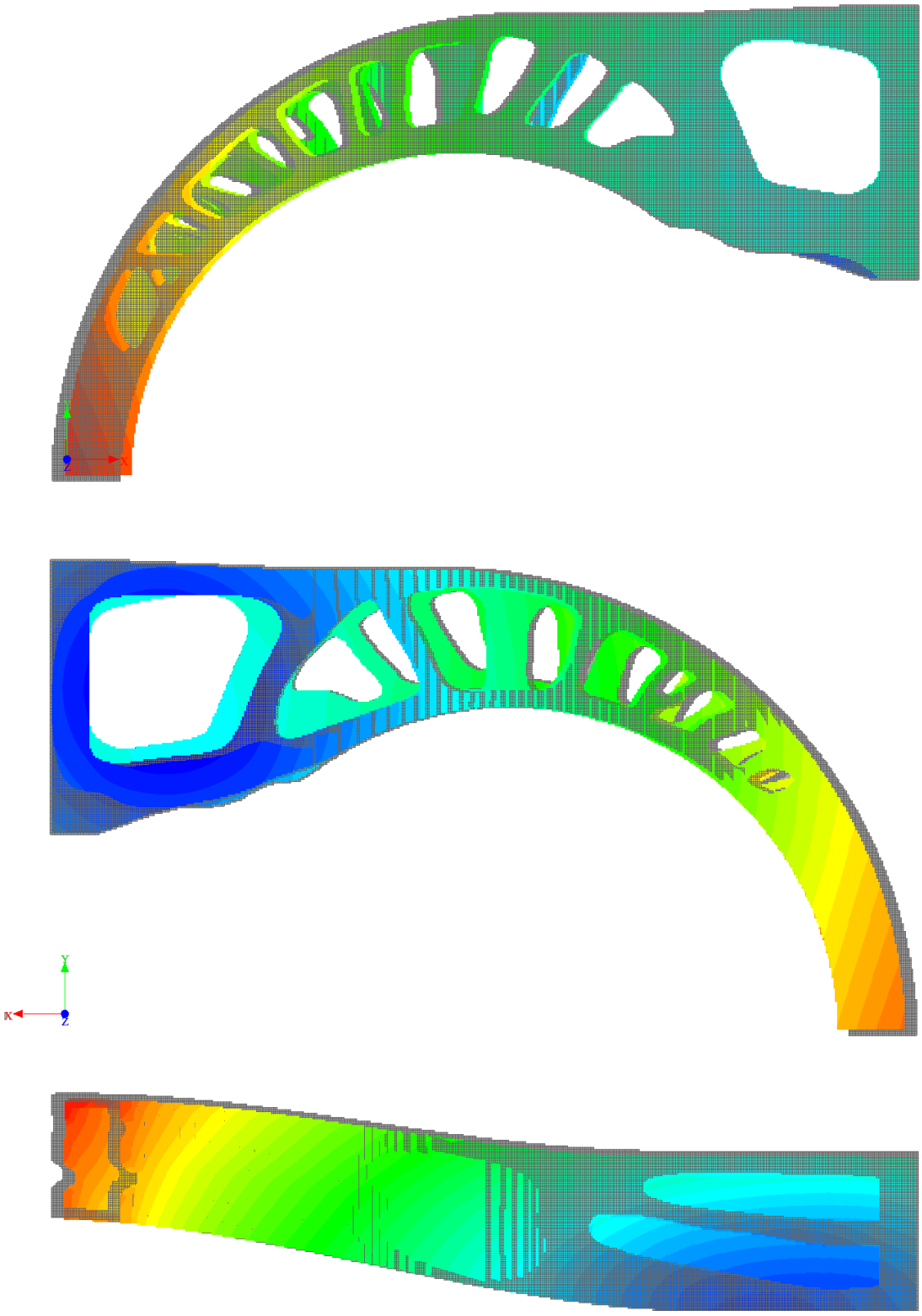

Figure 124. Warpage deflection results. The upper picture shown a later view. The middle one the dark side of the part. The last image shows the lower view of the model

In this large picture the warpage deflection can be seen in the different views. As it can be appreciated, the tip nose geometry is contracted in both x and y axis decreasing its dimension.

The arc shape of the bracket changes due this contraction, something to take into account the moment the pedal is wanted to be used under working conditions.

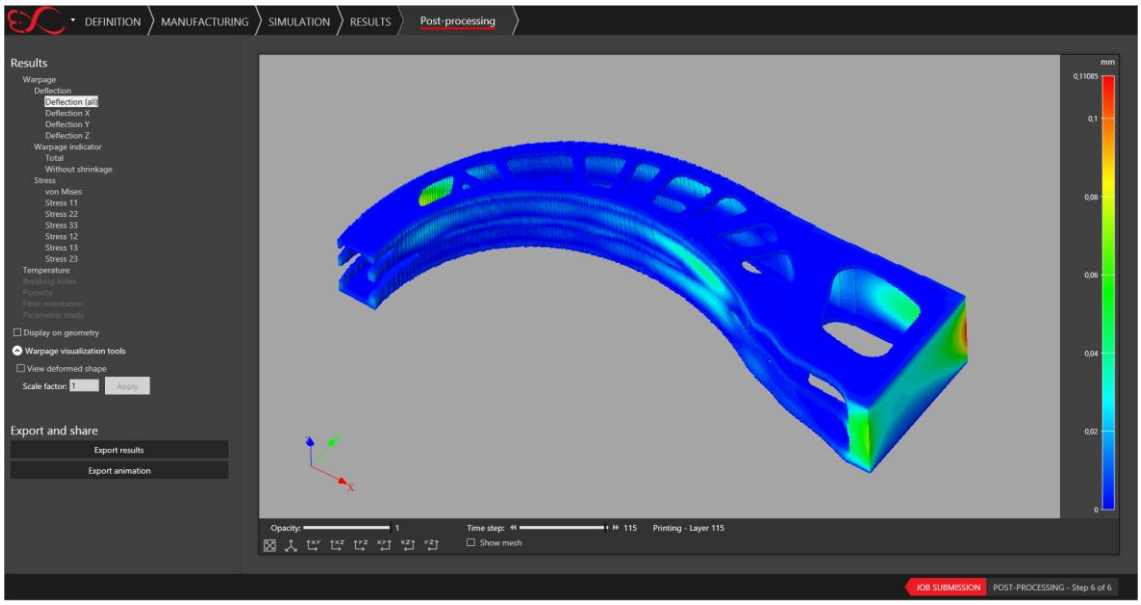

Figure 125. Warpage deflection results during the printing of the last layer. General view

Additionally, Digimat-AM can show the value of warpage deflection during the printing process for each printing layer. This is an interesting option to see how the warpage evolve during the additive manufacturing process. In the previous picture the region affected by warpage deflection can be seen during printing the layer number 115 (the last one). Additional warpage deformation will be an indicator of residual internal stresses after the part is cooled down.

6.5.3.2 Stress

The resulting stress outcome are shown in the figure ahead.

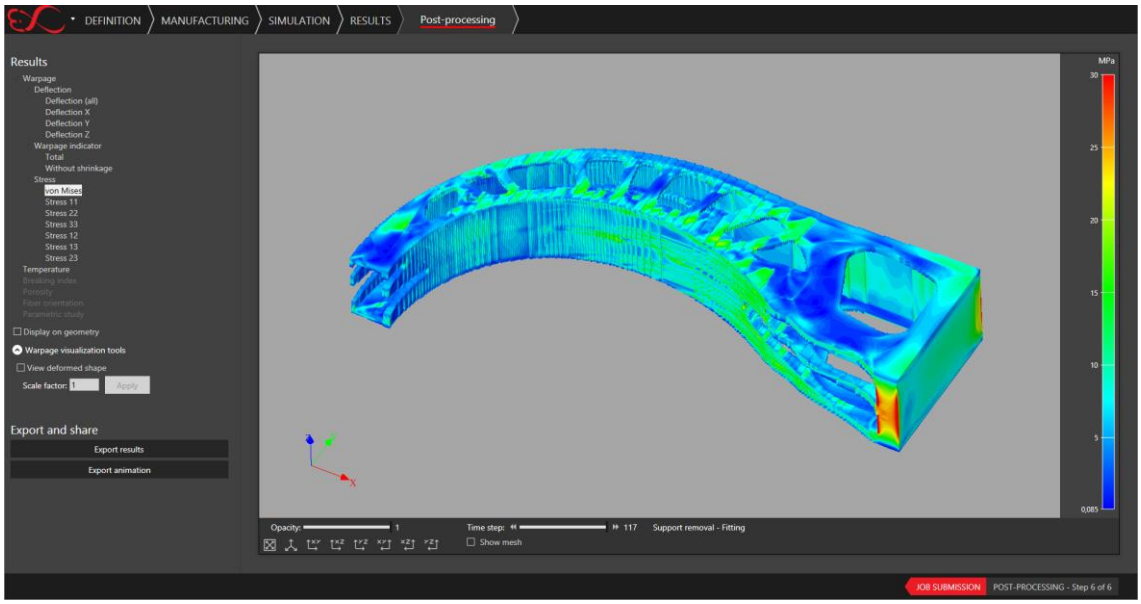

Figure 126. Von Mises stress results after the support removal and the cooling down. General view

The image shows the stresses appeared after the support removal and the part cooling down. An interpretation of the data is required. The regions in where more warpage occurred, after cooling down, some additional residual stresses had appeared.
Internal stresses are present during printing but increase significantly after the cool down. This is something to take into account and to use it in the final structural model which can deliver results more accurate.
The maximum value of internal stress appears to be near 30 MPa. This value only appears close to the clamping and probably is due to high warpage occurred in that area, which is acting as the clamping of a cantilever beam under bending stresses. The effect of additional warpage in this area with the addition of the effect of the cantilever once the supports are removed, will mean high internal stresses in the neighbourhood elements.

In fact, how this high internal stresses are not present in the rest of the structure can be appreciated. Lower values between 5 and 15 MPa appear along the bracket.

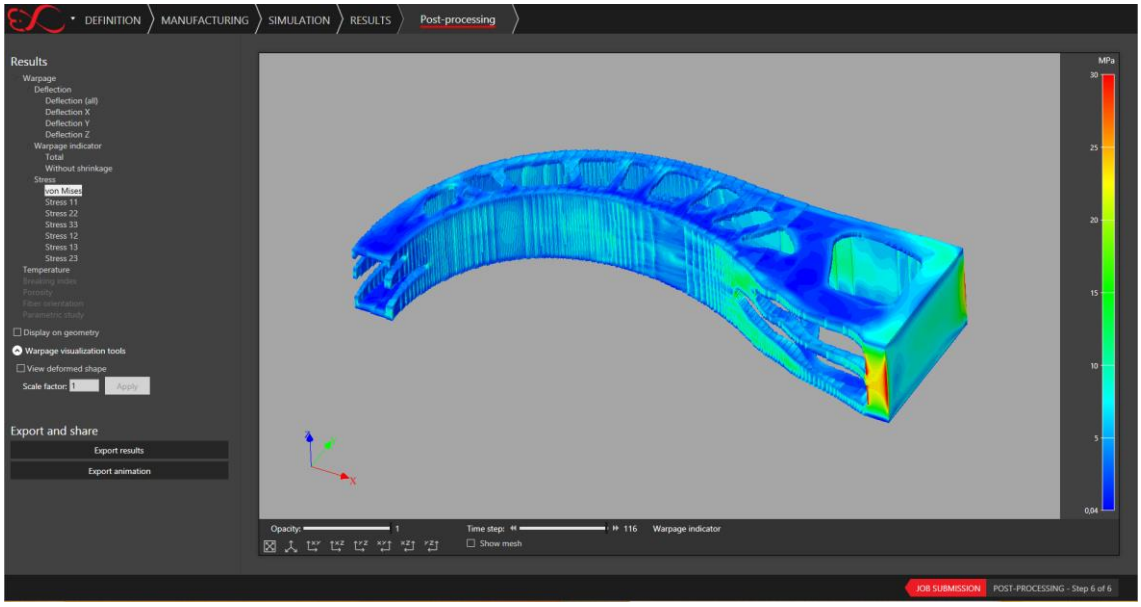

Figure 127. Von Mises stress results during the printing of the last layer. General view

As discussed before, the effect of cooling down is highly important and increases the values of the final warpage and the residual stresses.
This can be confirmed checking the stress values in the image where the supports have not been removed yet and the cooling process has not started either. Even in this situation, there are high values close to the clamping, the average stress value in the overall structure is lower, rounding the value of 5 MPa.

With this fact, the final value of warpage and internal stresses in the printed part can confirm the importance of cooling.

6.5.3.3 Warpage indicator

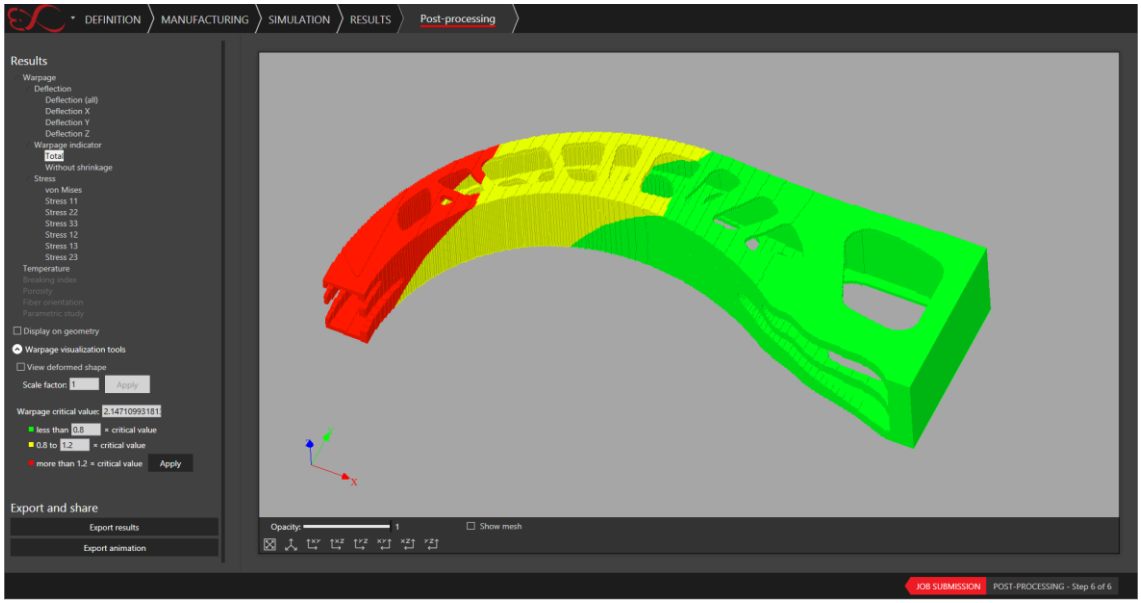

Figure 128. Warpage indicator. General view

The last image shows a warpage indicator along the bracket. This is shown in a clear way in which the regions of the structure are present with higher relative values and defined in colours. As stated before, the warpage is acute at the tip of the bracket, in where the tip suffers an important contraction along its x and y axis, becoming this region more critical. As the geometry gets closer to the clamping section, the warpage criticality decreases.

6.5.3.4 Data extraction

The results from Digimat-AM can be exported in different formats.
First, the internal stresses can be extracted in a format which can be integrated with ABAQUS/CAE and can be displayed in the model.

For Digimat-MAP, the mesh used in Digimat-AM will be required (constitute of solid elements).

Digimat-AM results data processing			
Results extracted from Digimat-AM	**File format**	**Does it need manual modification?**	**Data file goes as an input for**
Digimat-AM Mesh file	*.dat	NO	Digimat-MAP
Initial stresses	*.xml	NO	Digimat-MAP

Table 7. Digimat-AM results data processing

6.6 Material model for additive manufacturing

As discussed later on, Digimat-RP 2018.0 does not support the inclusion of reinforced polymers for Fused Filament Fabrication technologies in its merging module. Therefore, a solution that provides the most accurate model to that case must be found. Instead, for FFF technologies, Digimat-RP only takes unfilled polymers models from the database. So, an “equivalent unfilled

material" has to be created with Digimat-MF which makes distinction between the mechanical properties along different material orientations.

Once this has been introduced, the procedural step by step sequence definition is shown ahead.

Despite the thermal plastic model required for the AM simulation in the Digimat-AM module, for the structural CAE application there is a need to model a linear material behaviour of an equivalent reinforced plastic for fused filament fabrication.

Due to the fact that Digimat 2018.0 is the first version of the software that includes additional possibilities for FFF simulations, there are not many options to create material models for being manufactured by FFF. Therefore, only materials models with elastic isotropic properties or elastic transversally isotropic can be created. Hopefully, additional options for material modelling in FFF will be launched in later versions of the software.

Luckily, an elastic transversally isotropic material will give the necessary behaviour of the material for different load applications. It is not a complete anisotropy, but will fulfil the purpose of this project.

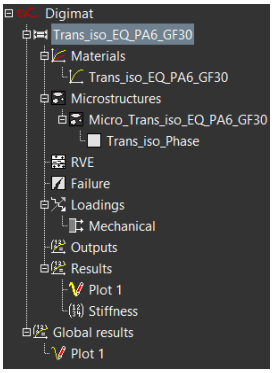

Figure 129. The Trans_iso_EQ_PA6_GF30 model

Once this has been clarified, it is time to start building the material model.

The model has been named as Trans_iso_EQ_PA6_GF30 which is constituted by an equivalent single phase material, in which mechanical properties as the Compliance matrix, the Stiffness matrix and the engineering constants are extracted from the homogenization results from the IM_PA6_GF30 model.

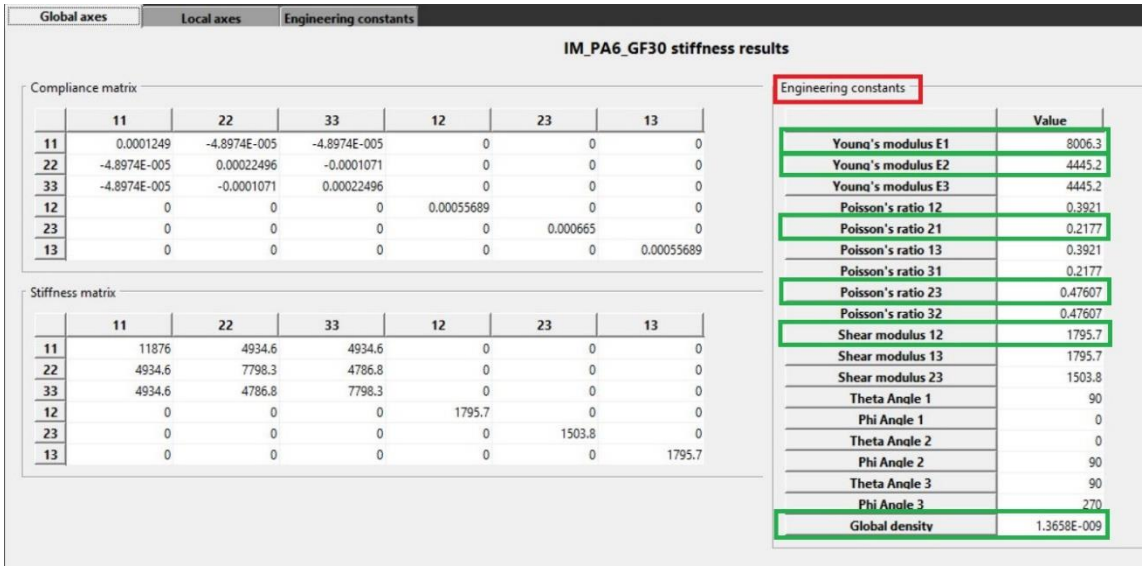

Figure 130. Engineering constants extraction to fill up a transversally isotropic material model. 5 engineering constants are required

From the set of parameters of the engineering constants table, it is mandatory to extract the required for the transversely isotropic model. Paying attention carefully to the reference system, from where the needed ones have been extracted.

Unlike the previous procedure to model the material for injection moulding now, the model will be defined using directly as inputs these constants.

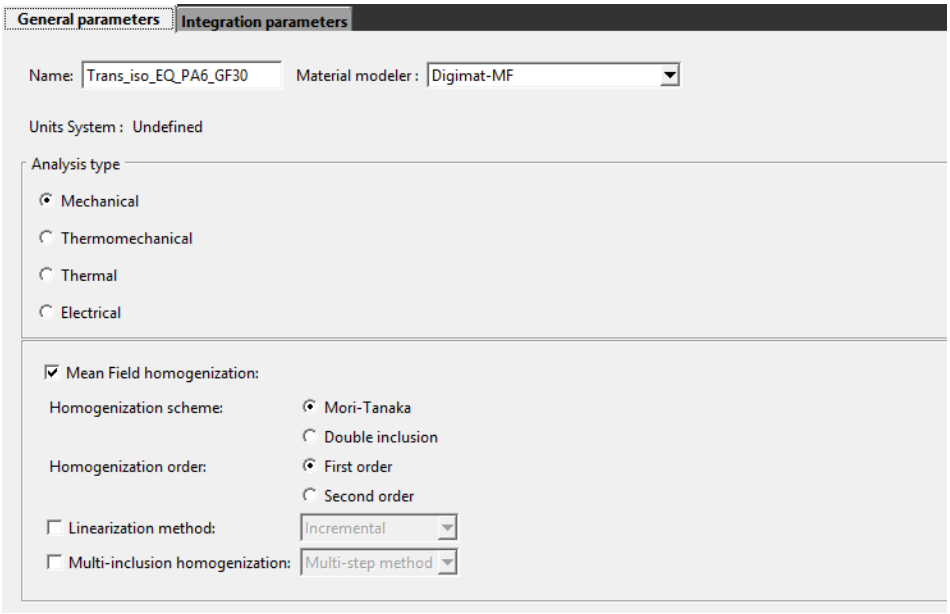

Figure 131. General and integration parameters definition for the Trans_iso_EQ_PA6_GF30 model

General parameters have to be input first. The analysis type has to be specified as mechanical, and as chosen in the previous model, the homogenization scheme is the Mori-Tanaka one. The integration parameters are left as default.

The material model, as stated before, will be set as elastic with transversally isotropic symmetry. This required immediately the input of the necessary engineering constants to define the non-

complete isotropy. In the next window, the constants are input and the material curve is automatically generated.

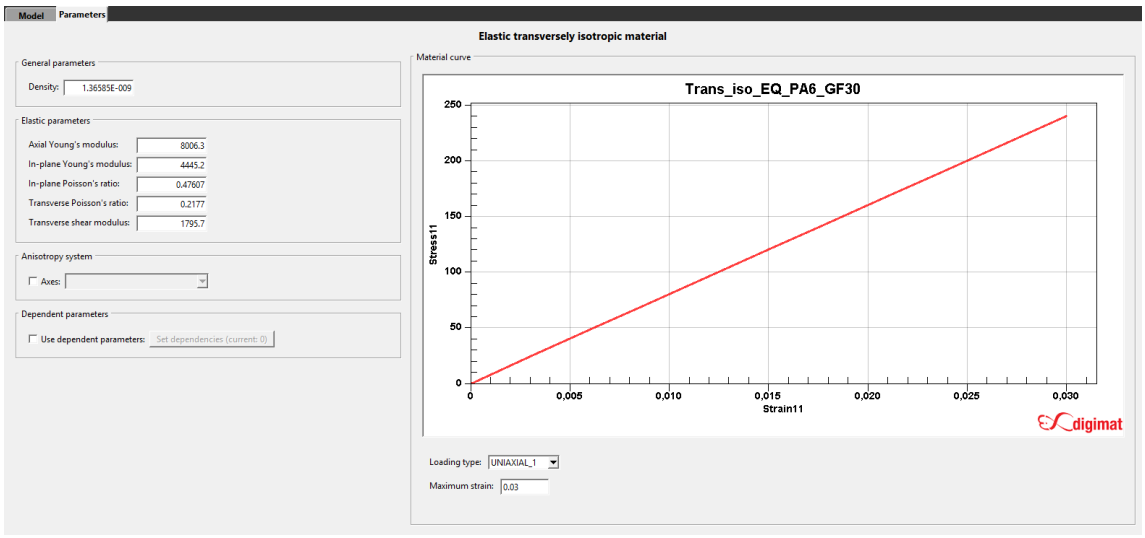

Figure 132. Elastic transversally isotropic material curve of the Trans_iso_EQ_PA6_GF30

Remember: for an isotropic material the number of elastic parameters needed is 2 while for a transversally isotropic material, the number of elastic constants is increased up to 5. They are the axial Young's modulus, the in-plane Young's modulus, the in-plane Poisson's ratio, the transverse Poisson's ratio and the transverse shear modulus.
The next step is about the microstructure definition.
In order to be used for additive manufacturing, the type selected is lattice (or filament).
Taking into account the parameters used during the toolpath definition in Utimaker Cura, the filament cross-section shape has been defined with a ratio between extrusion width and layer height of 2. The relative bonded width and height has set has 0.33 for both cases.

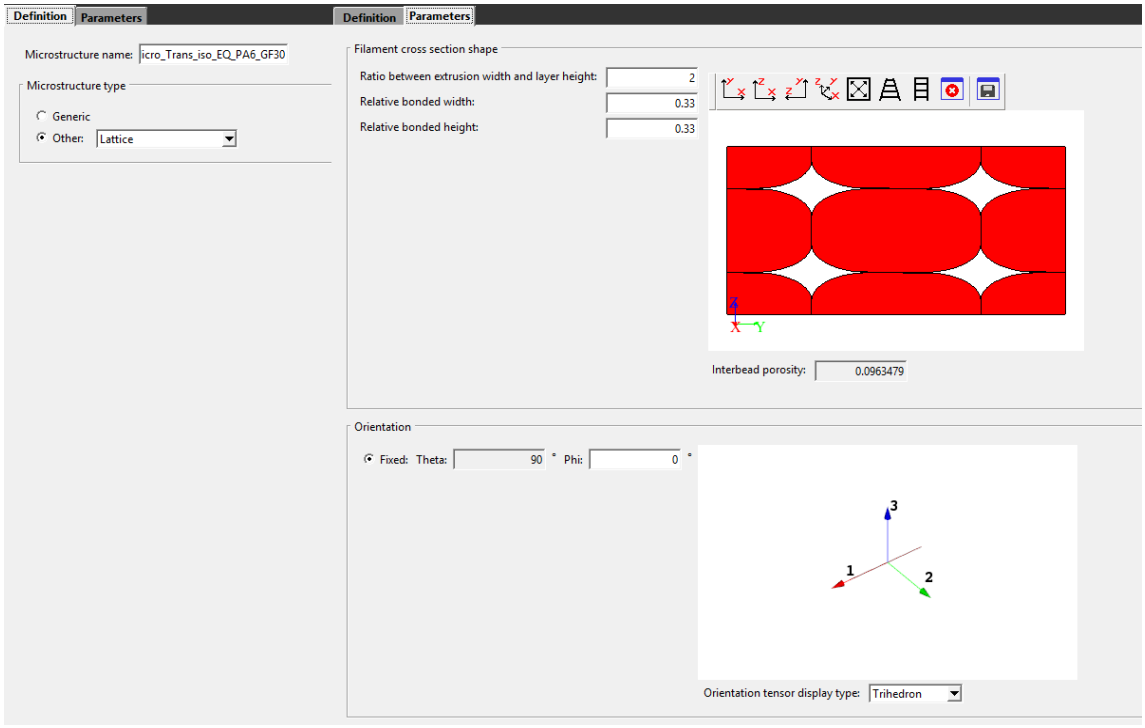

Figure 133. Definition of the parameters of the microstructure for the Trans_iso_EQ_PA6_GF30 model

With this parameters setup, the interbead porosity is automatically calculated, obtaining a value of 0.0963479.
The orientation has left as default too.

The last thing to be done for the material definition is to say the phase type of the material. As it is being treated, the material, as a single phase one, to be chosen is the matrix type.

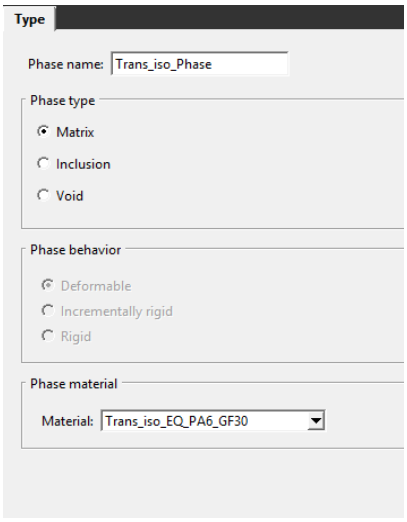

Figure 134. Type definition for the Trans_iso_EQ_PA6_GF30 model

Later on, the information of the new model is saved in the Digimat-MX, the material database of Digimat.

6.7 Merging initial stresses with the mesh file

In order to get ready, the data of the initial stresses for being used in ABAQUS/CAE, a mapping process has to be performed.
Digimat-MAP can load .xml files with information regarding the fiber orientation or the residual initial stresses. This file can be fused with the mesh used in the structural CAE software.

As in the previous part made for injection moulding, the mesh from Digimat-AM must be uploaded as a ‘Donor mesh’ and the ABAQUS mesh will be used as an input for the ‘Receiving mesh’ window.

The next step to be done, is to upload the initial stresses file. This will we integrated in the Digimat-AM mesh and afterwards will appear uploaded inside the ‘Donor mesh’.

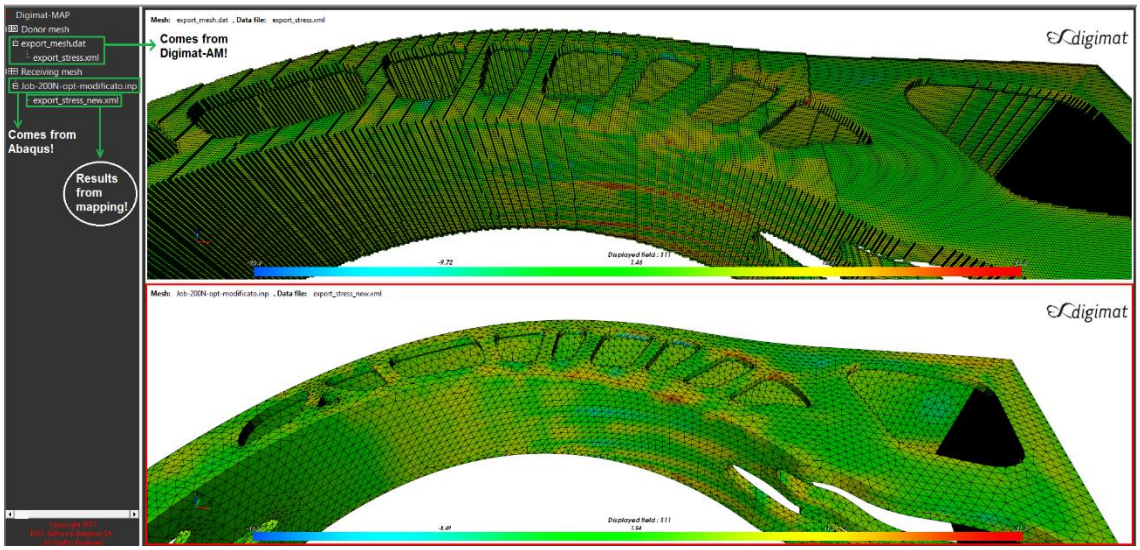

Figure 135. Mapping meshes for the AM model

Therefore, the problem is set to run the mapping process. Due to the fact that to both meshes do not match its reference system, some things have to be modified before running the mapping. It is needed to rotate the reference system of one of the meshes, and afterwards the analysis will be ready to be run.

The resulting file will appear annexed to the receiving mesh as a new initial stresses file. This file can be saved in a general file format or specify it for a certain CAE software. To the case presented, it is extremely useful that the file is available to be extracted for ABAQUS/CAE file. The information within this file is translated to the syntaxes which ABAQUS reads information about initial stresses and how to integrate them into the model.

Digimat-MAP results data processing			
Results extracted from Digimat-MAP	**File format**	**Does it need manual modification?**	**Data file goes as an input for**
Initial streeses file	*.xml, *.dof or *.str	*.dot NO *.str YES	Digimat-RP or ABAQUS CAE

Table 8. Digimat-MAP results data processing

6.8 Bridging simulation and structural FEA

In order to create a model which fuses all the information gathered in a unique model, Digimat RP has to be used one more time.

The model geometry, the preliminary isometric analysis result, the toolpath, the initial stresses due the additive manufacturing process and finally the micro-structure modelization of an equivalent transversally isotropic material is obtained. All that information can be fused in a single model.

Digimat-RP 2018 only allows to use one file as manufacturing data to integrate in the ABAQUS model. In the same way, the manufacturing parameter used for the final model in the injection moulding analysis was the fiber orientation tensor.

This time, the .dof file will be used as the toolpath followed by the nozzle extruder during the additive manufacturing. To integrate the initial stresses into the model would require an additional analysis performed in Digimat-RP.

For further analysis, the output file from the isometric material analysis in ABAQUS/CAE could be modified, and try to add to the code the initial stresses file (.str this time) before it is uploaded into Digimat-RP. In this way, a final model could be obtained which has the initial stresses suffered during the 3D printing process with the proper material micro-structure.

The information regarding the model and its computational solution that will be followed is shown ahead:

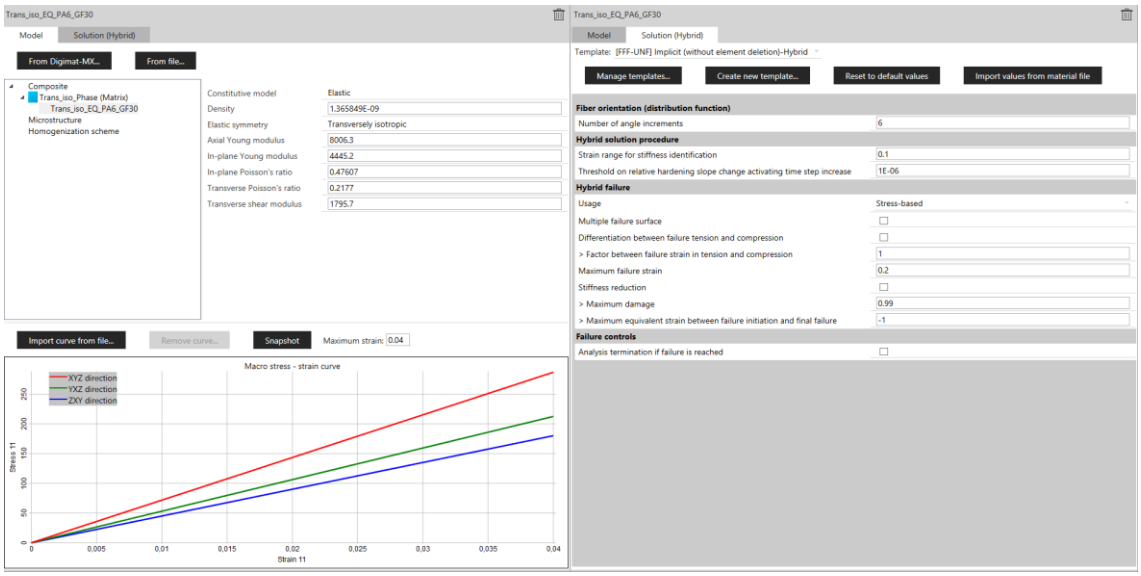

Figure 136. Digimat-RP window for the AM transversally isotropic model

The model used for this analysis, has been uploaded from Digimat-MX. The material model 'Trans_iso_EQ_PA6_GF30' as said before, is a transversally isotropic polyamide 6 reinforced with 30% volume of glass fiber, with a homogenization performed.

The details regarding its elastic properties, the engineering constants, its microstructure and the homogenization scheme followed can be found in the previous chapter.

About the computational solution used, as in the previous analysis for injection moulding, since the analysis performed is implicit, a hybrid solution with no element deletion will be used. Once it failure control option disabled, the solution configuration is ready.

The structural model used is the Job-200N for the optimized part. As Digimat-RP cannot use reinforced polymers to be printed with fused filament fabrication (FFF), with Digimat-MX a material model for an unfilled polymer was created to be manufactured with FFF but with equivalent mechanical properties as transversally isotropic considered.

Once the toolpath is uploaded in the CAD model, a pre-visualization of the filament orientation tensor appears. Different vectors of the toolpath tensor can be chosen to see the evolution of the orientation of the filament along the part. This will definitely characterize the strength of the printed part.

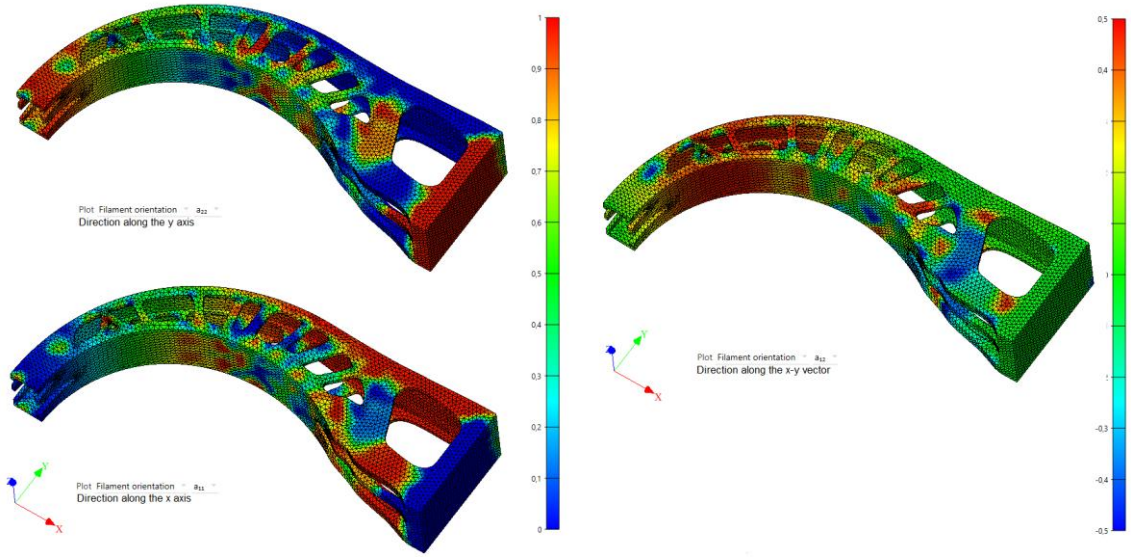

Figure 137. The toolpath tensor components a11, a22 and a12 for the AM model

The remaining vector components of the filament orientation tensor are null. This is because of the working plane of the printing machine. After all, the AM printer used is working as a 2.5 axis CNC machine, printing the filament along the x-y plane additively in layers. This superposition of layers with the heterogeneous properties of the material will definitively determine the final behaviour of the part.

At this point, everything is already setup to run the final analysis. After Digimat-RP makes the fusion of all the files, ABAQUS CAE is opened to run there the analysis.

6.9 Structural FEA with toolpath and transversal isotropic material properties

The structural CAE opened is ABAQUS, as in the previous works. Inside the multiple options to display, the results with relevant interest are those related mainly with the displacement, and secondly with the stresses generated in the model.

6.9.1 Displacement

One more time, the displacement is shown. As it was supposed, the behaviour of the bracket was the expected, appearing the maximum displacement in the area where the pedal surface is placed.

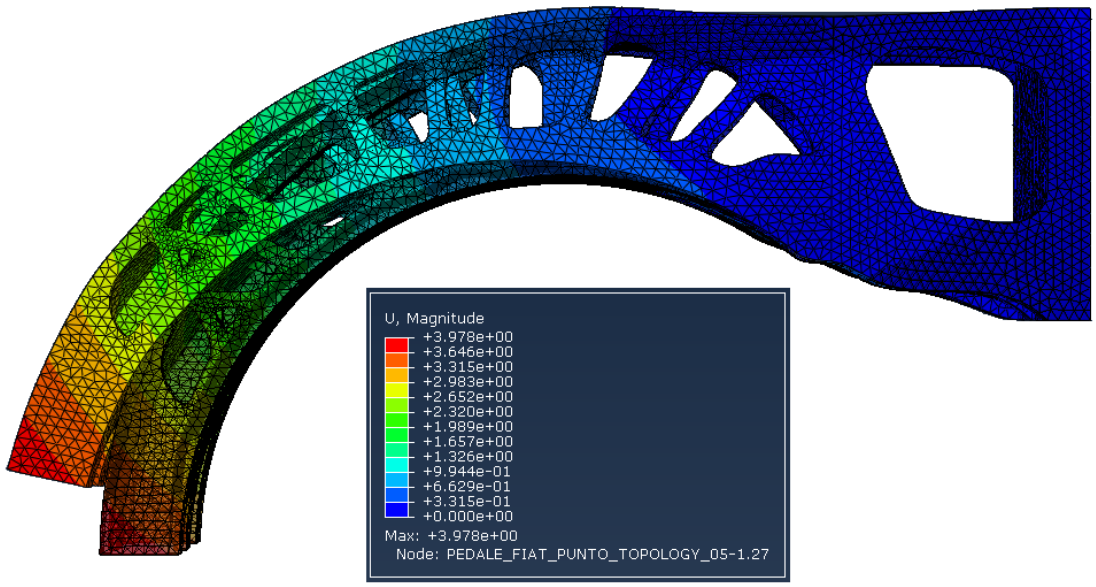

Figure 138. Displacement magnitude result for the AM trans. iso model. Lateral view

The displacement field shows a maximum displacement of 3.978 mm. In the first figure appears the contrast between the non-deformed structure against the deformed one. An amplification of the effect is done to make it more visual and clear.

The deformation patter follows the same as it was in the other analysis, just that this time the magnitude of the deformation is higher. This was something expected because this time the materials have non-isotropic properties and this is strongly influenced by the orientation of the filament defined in the toolpath. This means that in regions where the material had stronger properties before, due the isotropy, now the same region could behave in a weaker way depending the load application.

The accumulative effect of weaker inertias against the load transition along the bracket releases an increased value of maximum displacement in the tip of the bracket.

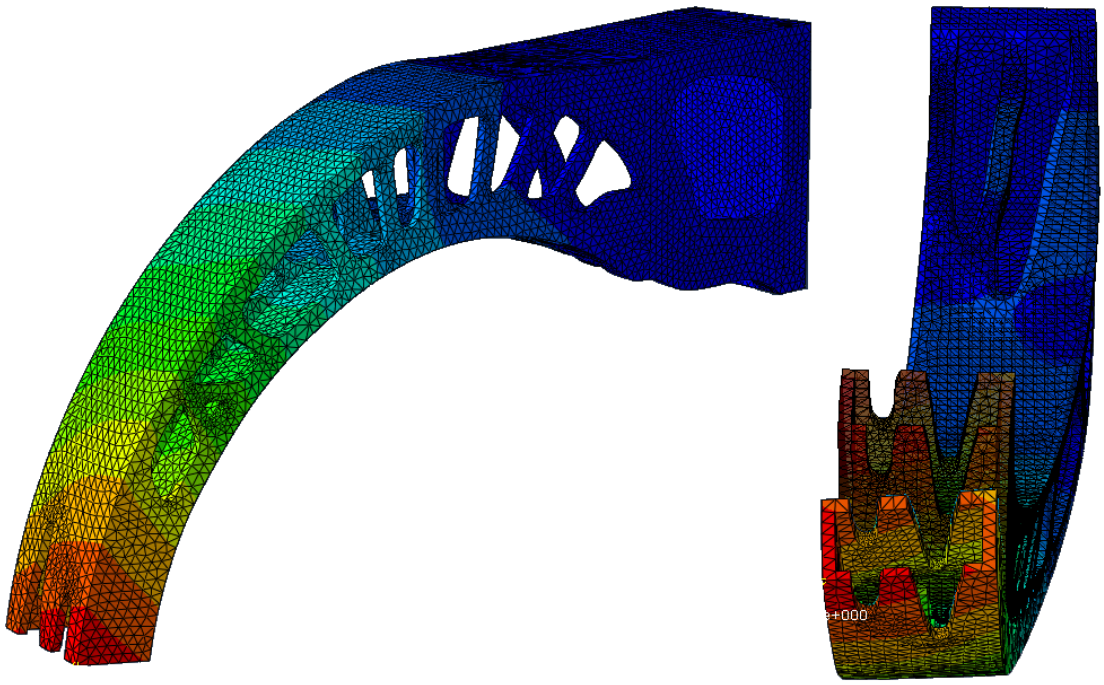

Figure 139. Displacement magnitude result for the AM trans. iso model. Isometric and inverted frontal view

In the second image the effect of the rotation in the geometry of the structure can be seen from a frontal view. As previously mentioned, the inclusion of a tri-dimensional pattern in the geometry of the part makes the result from the analysis more complex.

It can appreciated how the rotation appears when the load is applied and how the bracket is slightly under torsion at the same time is mainly bended.

6.9.2 Von Mises Stress

As already known, the stress results always need some extra interpretation. The first thing one can see when the stress field show up, is its maximum value of 115 MPa. Quite high. However, this stress peak is not actually real.

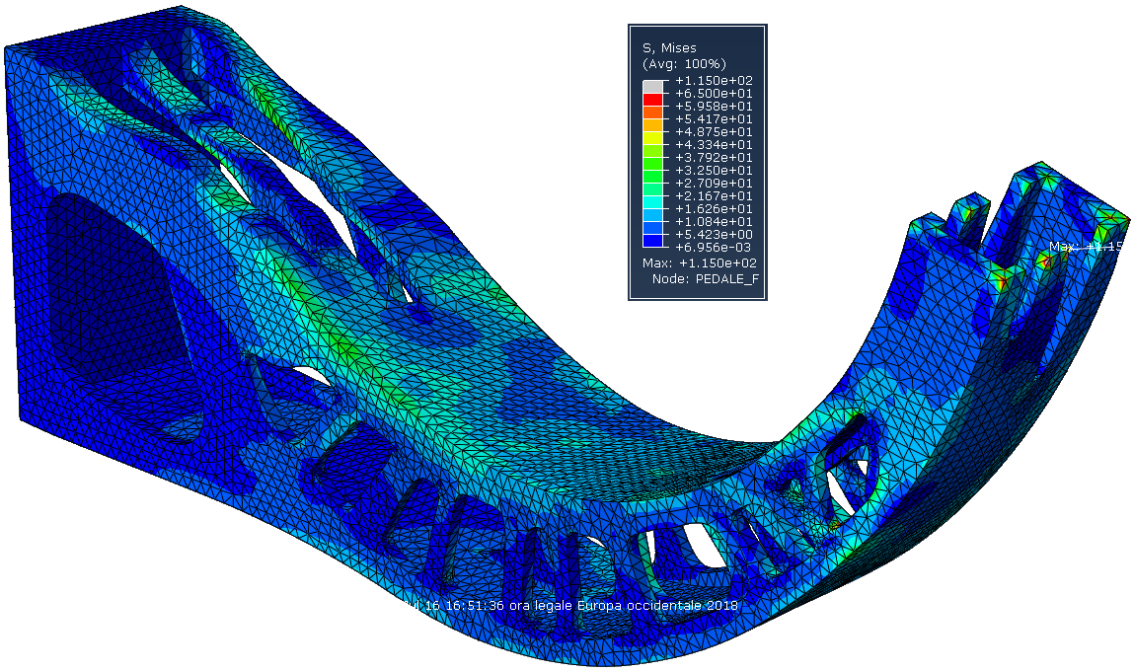

Figure 140. Von Mises stress results with maximum stress limited to 65 MPa for the IM trans. iso model. Isometric view

Once one starts to investigate where these values come from, one can notice that the 'tip legs' are under heavy stresses. As said before, it is not because in the real part will appear these stresses in the same area, it is just because there is a numerical issue due the model is not properly modelled there. As the corners in that area are quite acute and the areas formed are small, only a few elements are in charge to calculate the stress produced in these areas, therefore a stress peak appears. The other factor is because the load is applied directly there, and the tension is increased quickly because some areas are really small to bear the load without troubles.

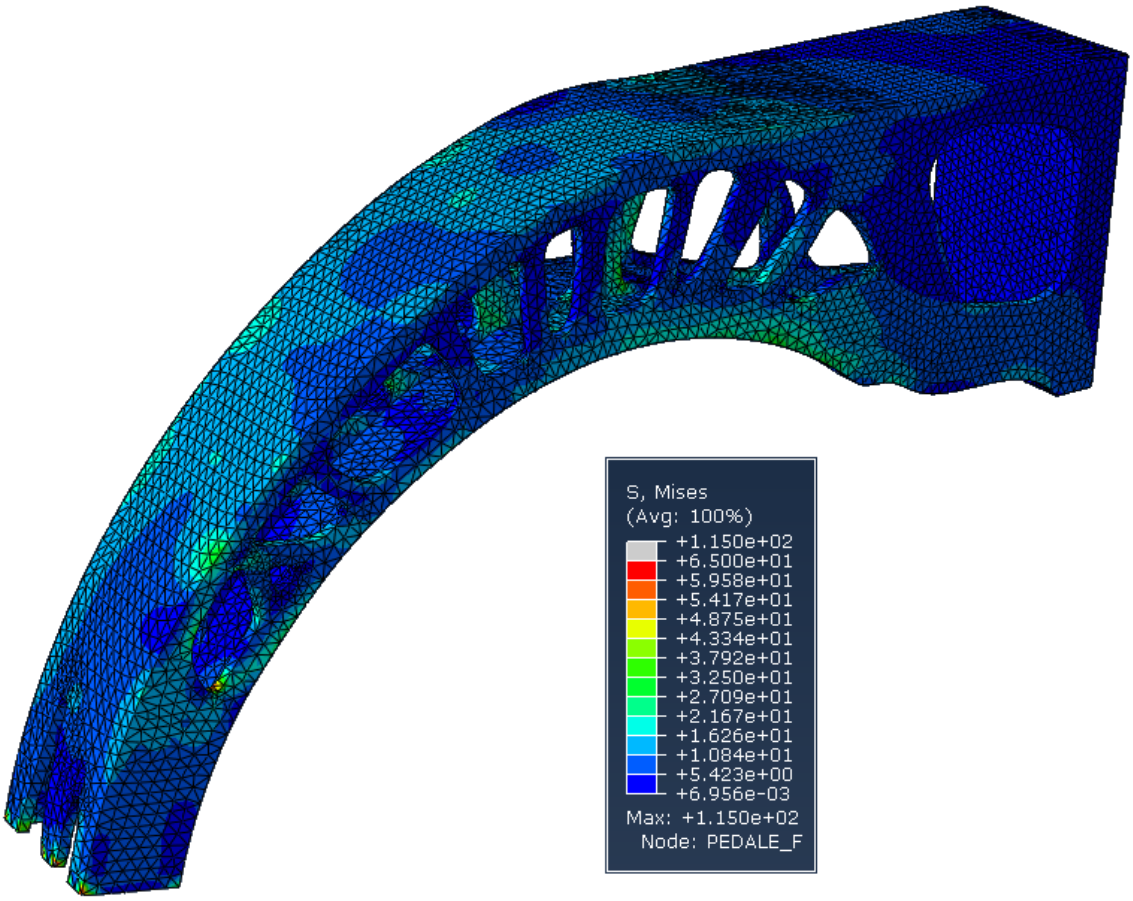

Figure 141. Von Mises stress results with maximum stress limited to 65 MPa for the IM trans. iso model. General view

Once this is discussed, High values of stress can be disregarded because as mentioned before, they are not real. If the maximum value of stress is limited to 65 MPa, How the stress fields get intensified can be seen.

The average stress value along the different stress islands which appear in the structure rounds the 15-30 MPa, a value much more closer to the expected behaviour. Most of the elements stay far away from the 65 MPa. There is only one small region in where these stresses are present: one of the first holes close to the tip. Even if the material can stand 65 MPa, it is a concentrated stress which is way larger than the rest of the elements (more than 30 MPa of difference). An improved solution would release in further iterations a geometry CAD modification. In this modification the angle of the hole would become smother and additional geometry could be added in the nearby region. With this simple change, the stress peak could be removed and the design improved.

If it goes further and the maximum value is constrained even more, the results change drastically. Being 30 MPa the maximum admissible stress value, several elements are overwhelmed. A lot of grey areas arises along the bracket, and most of them are close to sharpening edges.

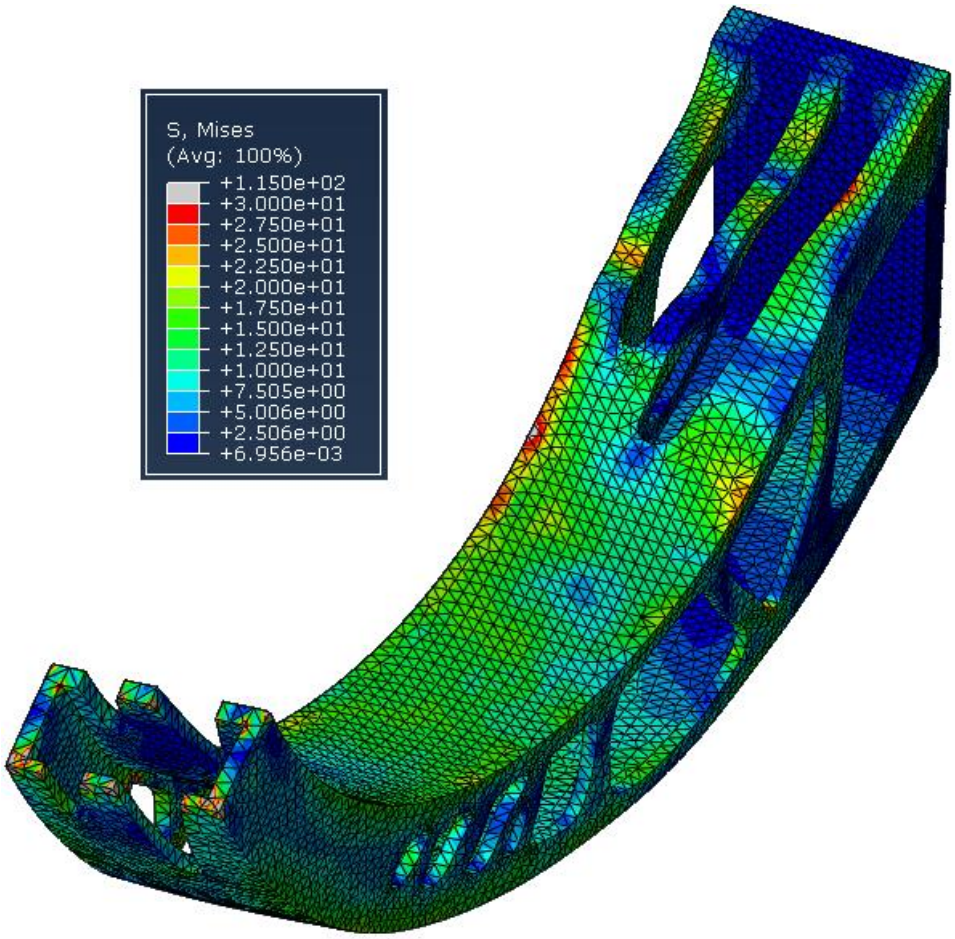

Figure 142. Von Mises stress results with maximum stress limited to 30 MPa for the IM trans. iso model. General view (I)

In the outer lateral arcs, some elements near the base of the columns are overpassed by the stresses. A row of elements in the corner of the compressed main arc are under solicitations above the 30 MPa.
Besides, elements close to the base of the inner columns are showing values over the 30 MPa. In the case these stresses would not be admissible, the solution proposed is the same as before: additional design iterations.
Modifying the CAD model and adding additional geometry to reinforce the regions where needed is a good solution which add no significant weight to the part but will prevent the bracket to get broken in these areas.
In further iterations, once the areas with higher levels of stress have been identified, the designer must modify them adding the necessary geometry.

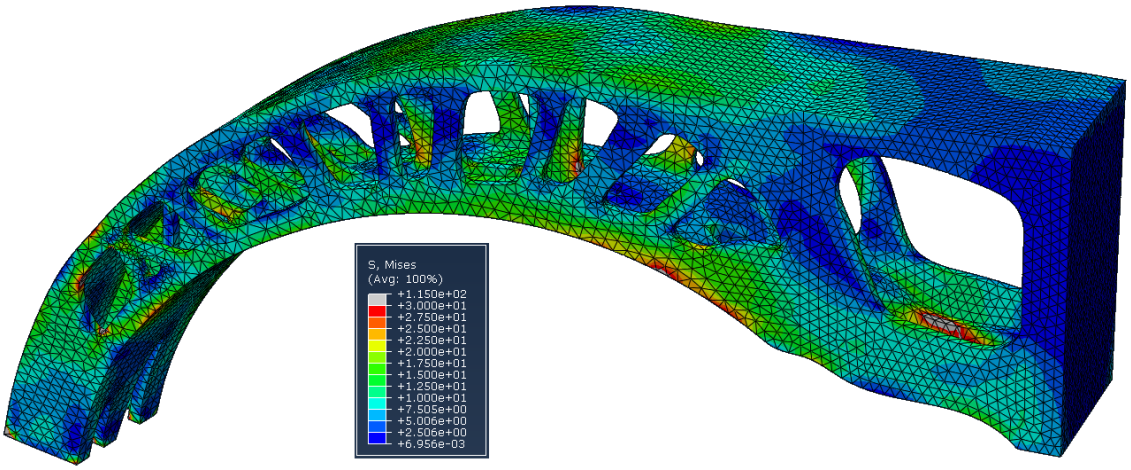

Figure 143. Von Mises stress results with maximum stress limited to 30 MPa for the IM trans. iso model. General view (II)

Apart from the regions in which the 30 MPa are overpassed, and as it can be seen in the last picture some regions are under stressed, and the idea of some material removal should be considered by the engineer in subsequent iterations.

One more thing to say is that a limiting value of 45 Mpa would release a part with the vast majority of the elements under the threshold. This value is something that the material can hold with no major issues.

7 Model comparison

During the study performed in this work, different models has been created to simulate the structural behaviour of a clutch pedal made of PA6-GF30 manufactured with injection moulding (IM) and additive manufacturing (AM).

Each fabrication technology gathers two models, one with coarse material modelling and the other with finer models.

At the end, for each model an analysis has been performed separately-
In this chapter the information of all the models has been gathered and will be discussed later.

The models' name has been coded with the following procedure:

- **IM_ISO**: IM model with isotropic and homogeneous material properties
- **IM_FOD**: IM model with FOD tensor and anisotropic but homogenised material properties
- **AM_ISO**: AM model with isotropic and homogeneous material properties
- **AM_T_ISO**: AM model with toolpath tensor and transversally isotropic material properties plus additional information about warpage and residual stresses.

Clutch pedal model comparison				
Model code	**IM_ISO**	**IM_FOD**	**AM_ISO**	**AM_T_ISO**
Model image		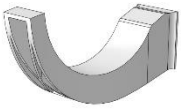		
Material model	Elastic	Elastic	Elastic	Elastic
Material behaviour	Isotropic and Homogeneous	Homogenized anisotropic	Isotropic and Homogeneous	Transversally isotropic
Manufacturing data	None	FOD tensor	None	Toolpath tensor
Max. Displacement	1.848 mm	2.189 mm	1.976 mm	3.978 mm
Peak Stress Average Stress	27 MPa 18.33 MPa	28.5 MPa 19.01 MPa	40 MPa 23.34 MPa	65 MPa 27.09 MPa
Young mod. (E1)	10000 MPa	8006 MPa	10000 MPa	8006 MPa
Stress at break	-	150.12 MPa	-	150.12 MPa
Density	-	1.3658 g/cm^3	-	1.3658 g/cm^3
Part volume	105.43 cm^3	105.43 cm^3	63.69 cm^3	63.69 cm^3
Volume reduction	-	-	39.59 %	39.59 %
Bodyweight	-	144 g	-	86.987 g
Accessory data	-	-	-	AM simulation warpage and residual stresses

Table 9. Clutch pedal model comparison

Non isotropic material properties deliver accurate models less conservative, and therefore with worse strength properties.

Integration of manufacturing data like FOD tensors and toolpath tensors are key to improve the reliability of the data which the models show.

The model IM_FOD represents better the behaviour of the pedal design for IM. In the same way, the model AM_T_ISO represents better the behaviour of the pedal design for AM.

Comparing the maximum displacement obtained in the AM_T_ISO against the IM_FOD, an additional displacement magnitude of 81.72% has been obtained. As the load applied is the same in both models, it can be concluded that the AM_T_ISO is less stiff than its equivalent IM_FOD.

Comparing the peak stress value obtained in the AM_T_ISO vs. the IM_FOD, an additional peak stress of 128.07 % is shown.
The average stress value is increased in a 42.5% compared to the IM_FOD model.

This significant increase of peak stress value can be reduced in the AM_T_ISO model following some tips. As discussed in the previous chapter, with additional design iterations, the CAD model could be modified adding more geometry in the critical regions. Additionally, adding fillets and rounding sharp edges into the model will help to attenuate the effect. These techniques would release into a better design in which the final stress peak value would be lower.

Another tip would be to improve the FEM model. Firstly, removing the stress concentrations in the area where the load is directly applied. These stress values are not real, and only increase the maximum value of stress unnecessarily. Secondly, in the regions where the stress increases, finer meshes will give reliable models.

However, the increment in average stress is not too high. This means that the structural design of the bracket is good enough to transmit the load properly from the pedal to the clamping where the clutch linkage is placed.

In the other hand, the part volume for the IM_FOD was 105.43 cm^3 and for the AM_T_ISO was 63.69 cm^3. This means a total volume reduction of 39.59%. As the density of the material has been considered constant, **the redesign process has achieved a mass reduction of the 40% of the part bodyweight in only one iteration**.

For the AM_T_ISO, additional information has been obtained. The warpage effect and the residual internal stresses after the printing process give information about the initial state of the pedal. This alters the displacement and stress values during working conditions.

Knowing the stress at break, for the IM_FOD model and for working conditions, the structural element of the clutch pedal will be at its 18.92% of resistance capacity for the most critical areas, and at its 12.66% of resistance capacity for the average regions.

For the AM_T_ISO model, at the working conditions, the structural element of the clutch pedal will be at its 43.29% of resistance capacity for the most critical areas, and at its 18.04% of resistance capacity for the averages regions.

8 Conclusions and further works

Additive manufacturing as a new technology for making mechanical parts opens news possibilities within the area of SFRP composites.

This technology loosen the constraints imposed by traditional manufacturing techniques during the design phases. Moreover, the new available design freedom match perfectly with topological optimization software which improves and enhances mechanical designs. Furthermore, the results from the mathematical algorithms can have now a physical materialization, opening a new paradigm in engineering design.

Additionally, the combination of these techniques with cutting-edge FEA simulations in which material micro-models as manufacturing processes can be accurately simulated, delivers a set of powerful CAE tools for evaluation purposes.

Additive manufacturing of SFRP composites can deliver lighter parts in which design specifications can be still accomplished. Topology optimization sets the dichotomy between having lighter parts and having stronger parts. In mechanical parts with low criticalities, these alternatives can be really interesting in order to get a cost saving due the mass reduction during design. It is especially amusing in the aero-spatial or the automotive industries where mass reduction downgrade additional costs regarding fuel saving.

These accurate tools make the strength of materials to be pushed into its limits getting parts using less material while achieving its design goals. Following with this idea with iterative design cycles, the gap between the addition of extra materials with conservative methods and the use of exact amount of material can be shortened.

Even then, the inclusion of this new manufacturing technology for the SFRP composite science, brings new challenges to face.

The AM process is still far from being mastered and final parts quality need a substantial improve. In order to do so, controlling parameters of the printing chamber as chamber temperature, nozzle printing temperature or the cooling system will allow to improve the final quality of the part.
The printing process must be mastered in order to reduce as maximum air inclusions within the printed part.

Furthermore AM is not totally design constraint free. It is true that it removes several limitations of the traditional methods but it introduces another ones that have to be faced. One of them is to think in advance the correct utilization and removal of supports during the printing and post-printing phases. Actually, not all geometries can be manufactured with AM. Complex hollowed shapes like the one presented in this work will bring several issues for remove properly the supports after the part is completed. This is something that the designer will have to bear in mind during the design phases.

Additional challenges to increase the adhesion between layers are ahead. The control of the temperature where the material is deposited in each layer will reinforce the material adhesion.

It has been exposed how the filament orientation can be controlled during the printing process with the definition of a toolpath. The fibers tend to get aligned to the path followed by the extruder nozzle, which is really important in order to control the local strength of the printed part. Controlling this can make long-lasting and stronger parts in parallel directions to the load application as if they would had been manufactured in injection moulding.

The definition of the toolpath to get fibers aligned in the desired direction is critical. Similarly, this was done for the FOD tensor during injection moulding simulations, for AM the toolpath will determine the filament orientation and therefore the fiber orientation as well.

A powerful topology optimization software is critical to obtain better design results. Stable and powerful optimization tools are usually integrated with other powerful software which are more expansive than most of the commercial CAE software. This requires an investment if an improvement of this way of making engineering design is desired.

The cost of manufacturing with AM are significantly lower than with injection moulding. Using AM, do not require to use an injection moulding machine and a part mould. Besides, IM is an expensive technology which feasibility is possible thanks to scale economies. Taking profit from AM will save this great investment. A good commercial FFF AM machine for unfilled polymers or SFRP composites is a cheaper investment than the machine for IM.

Using a different initial material distribution as the input for the topology optimization would release different solutions. It has to be explored different alternatives starting from different geometries. In this way, the algorithm will be working in different directions and ending up with a diverse element connectivity and therefore, a particular element reorganization.

To conclude, new Digimat versions of AM and RP will allow to integrate the toolpath within a single model, as well as initial stresses and warpage. Displaying in the same model all the results will give a better approach of the actual behaviour of the part. The inclusion of the initial stresses into the model will decrease the maximum strength of the part, being able to bear less stress coming from external loads.

9 Bibliography

Atair. (2016, December). *giesserei-praxis.de*. Retrieved from Motorradrahmen aus dem 3D-Drucker: https://bit.ly/2DxRnbf

Autodesk. (2018). *autodesk.com*. Retrieved from Plastic injection and compression mold simulation: https://autode.sk/2qnnUsG

AZO Materials. (2001). *azom.com.* Retrieved from E-Glass Fiber: https://bit.ly/2R1oVCD

Baggaley, K. (2018, Feb). *nbcnews.com*. Retrieved from Soon you may be able to 3D print clothing in your own home: https://nbcnews.to/2HvUIY1

Bassi, M. (2016). *Non linear analysis and validation of through process modeling of injection moulded specimens of glass fiber reinforced polyamide PA6.*

Bates, P. (2018). *industries.ul.com.* Retrieved from The Evolving World of Polymer-Based Additive Manufacturing: https://bit.ly/2DN3sdw

BBC. (2012, July). 3D-printed sugar network to help grow artificial liver.

Bernasconi, A. (2018). Composite materials I. In *Lightweight design of mechanical structures.*

Bernasconi, A. (2018). FE based optimum design. In A. Bernasconi, *Lightweight design of mechanical structures* (pp. 1-28).

Bernasconi, A. (2018). Short fibre composites. In A. Bernasconi, *Lightweight design of mechanical structures* (pp. 52-55).

Braha D, M. O. (1997). The Design Process: Properties, Paradigms and Structure. *IEEE Transaction on Systems, Man, and Cybernetics* (pp. 146-166). IEEE.

Bralla, J. G. (1998). *Design for Manufacturability Handbook.* McGraw-Hill Education, 2th edition.

Brenken B, B. E. (2018). Fused filament fabrication of fiber-reinforced polymers: A review. *Additive Manufacturing, vol. 21*, 1-16.

CAMPUSplastics. (2018). *RADILON A RV300 from RadiciGroup*. Retrieved from campusplastics.com: https://bit.ly/2KhGyeI

Chua C K, L. K. (2010). *Rapid Prototyping: Principles and Applications.* World Scientific.

Colosimo, B. (2017). Design topology optimization. In B. Colosimo, *Additive manufacturing* (pp. 8-26). Milan.

CustomPartNet. (2007). *Injection Molding*. Retrieved from custompart.net: https://bit.ly/2zgtEcX

Dassault Systemes. (2018). *3ds.com*. Retrieved from TOSCA, efficient optimization based on FEA and CFD simulations: https://bit.ly/2QYfnIE

D'Aveni, R. (2015, May). The 3-D Printing Revolution. *Harvard Business Review*, pp. 48-48.

Dhondt, G. (2014, March). *web.mit.edu*. Retrieved from Ten-node tetrahedral element (C3D10 and F3D10): https://bit.ly/2wnsMn2

Dym, C. L. (2008). *Engineering Design Third Edition: A Project Based Introduction.* Wiley, 3th edition.

Ensinger. (2018). *ensingerplastics.com*. Retrieved from TECAMID 66 GF30 black: https://bit.ly/2OMdwVr

ESA. (2018, July). What's your idea to 3D print on the moon - to make it feel like home? *ESA*.

Ex-Stream. (2018). Digimat-AM XII. In MSC_Software, *Digimat User's Manual 2018* (pp. 1171-1207).

Ex-Stream. (2018). Digimat-MAP VII. In MSC_Sofware, *Digimat User's Manual 2018* (pp. 737-785).

Ex-Stream. (2018). Digimat-MF IV. In MSC_Sofware, *Digimat User's Manual 2018* (pp. 163-446).

Ex-Stream. (2018). Digimat-RP IX. In MSC_Software, *Digimat User's Manual 2018* (pp. 1011-1078).

Frketic J, D. T. (2017). Automated manufacturing and processing of fiber-reinforced polymer (FRP) composites. *Additive Manufacturing, vol. 14*, 69-86.

Fu S-Y, L. B.-W. (2009). *Science and engineering of short fibre reinforced polymer composites.* Oxford, Cambridge, New Delhi: Woodhead Publishing Limited.

Gardiner, G. (2016, March). *compositesworld.com.* Retrieved from Additive manufacturing comes to composites fabrication: https://bit.ly/2qsE9o0

Gibson I, R. D. (2014). *Additive Manufacturing Technologies: 3D Printing, Rapid Prototyping, and Direct Digital Manufacturing.* Springer New York.

Gibson, R. F. (2011). *Principles of Composite Material Mechanics.* CRC Press, 3th edition.

Goh G D, D. V. (2018). Characterization of mechanical properties and fracture mode of additively manufactured carbon fiber and glass fiber reinforced thermoplastics. *Materials and Design*, 79-89.

Haden E. Quinlan, T. H. (2017). Industrial and Consumer Uses of Additive. A Discussion of Capabilities, Trajectories, and Challenges. *Journal of Industrial Ecology*, S15-S20.

HellermannTyton. (2011, April). *Properties of polyamide PA66.* Retrieved from wurth-international.com: https://bit.ly/2Q998V7

Hine. (1996). *Polymer Composites, vol 17.* John Wiley & Sons Ic.

Hoffman, T. (2018, June). *pcmag.com*. Retrieved from 3D printing: What you need to know: https://bit.ly/2jMZOHF

Hofstätter T, P. D. (2017). Applications of Fiber-Reinforced Polymers in Additive Manufacturing. *1st Cirp Conference on Composite Materials Parts Manufacturing* (pp. 312-316). Elsevier.

Hull D, C. T. (1996). *An introduction to composite materials.* Cambridge Solid Sate Science Series.

Incropera, F. P. (2012). *Fundamentals of Heat and Mass Transfer.* John Wiley & Sons.

Integrated Publishing. (2007). *tpub.com*. Retrieved from Introduction automotive clutches: https://bit.ly/2TrtZlq

Ivey M, M. G. (2017). Characterizing short-fiber-reinforced composites produced using additive manufacturing. *Advanced Manufacturing: Polymer & Composites Science*, 81-91.

Korger M, B. J. (2011). Possible Applications of 3D Printing Technology on Textile Substrates. *IOP Conference Series: Materials Science and Engineering* (pp. Volume 141, number 1). IOP Publishing Ltd.

Langefeld, B. (2013, November). Ctrl.P - How new business models evolve. *Roland Berger*.

LaSelle. (2018). *jabil.com*. Retrieved from Meeting Mass customization Demands with 3D Printing: https://bit.ly/2OS392g

Locker, A. (2016). *all3dp.com*. Retrieved from This is How to Make a Custom 3D Printed T-Shirt: https://bit.ly/2R1t35q

Luxon Engineering. (2018). *luxonengineering.com*. Retrieved from Optimization Techniques as Applied to Computer Aided Analysis: https://bit.ly/2S0BxtL

Maldonado, T. (1993). *El diseño industrial reconsiderado.* Gustavo Gili.

Materialise. (2017, February). *3dmpmag.com*. Retrieved from Optimized Design Yields Complex Bracket: https://bit.ly/2DNKzrg

MIT. (2017). *ocw.mit.edu.* Retrieved from Optimization Problems and Algorithms: https://bit.ly/2A6H1fo

Ning F, C. W. (2015). Additive manufacturing of carbon fiber reinforced thermoplastic composites using fused deposition modelling. *Composites Part B vol. 80*, 369-378.

Pahl G, B. W.-H. (2007). *Engineering Design. A systematic approach.* Springer, 3th edition.

Paoletti, I. (2017). Mass Customization with Additive Manufacturing. *Procedia Engineering vol. 180*, 1150-1159.

Parandoush P, L. D. (2017). A review on additive manufacturing of polymer-fiber composites. *Composite Structures, vol. 182*, 36-53.

Pentagon Plastics Ltd. (2014). *pentagonplastics.co.uk.* Retrieved from PA6 - Nylon 6: https://bit.ly/2DQIbA2

Quinlan H E, H. T. (2017). Industrial and Consumer Uses of Additive Manufacturing: A Discussion of Capabilities, Trajectories, and Challenges. *Industrial Ecology*, vol. 21, S1.

Renishaw. (2016). *renishaw.com.* Retrieved from Industrial applications of Renishaw metal additive manufacturing technology: https://bit.ly/2DLTJV2

Renishaw. (2016). *renishaw.com.* Retrieved from Metal 3D printing for healthcare: https://bit.ly/2E7mPL4

Resins Online. (2013, June). *resins-online.com*. Retrieved from 3D printed clothing becoming a reality: https://bit.ly/2S3TIPw

Rodríguez-Tembleque L., R. A. (2017). Teoría de la Membrana I. In L. Rodríguez-Tembleque, *Ingeniería Estructural II* (pp. 1-35). Sevilla.

Roland Berger. (2016). *Additive Manufacturing, next generation. Study.* Roland Berger.

Siemens. (2018, April). *siemens.com*. Retrieved from The factory of the future: https://sie.ag/2K8h0R1

SPI Lasers. (2018). *spilasers.com*. Retrieved from Additive Manufacturing Materials: https://bit.ly/2A3U7Kc

Tang Y. (2015). A survey of the design methods for additive manufacturing to improve functional performance. *Rapid Prototyping*.

Tang Y., D. G. (2017). Lattice Structure Design and Optimization With Additive Manufacturing Constraints. *IEEE Transactions on Automation Science and Engineering*.

Thomason, J. (2001). Micromechanical parameters from macromechanical measurements on glass reinforced polyamide 6.6. *Composites Science and Technology vol. 61*, 2007-20016.

Ullman, D. G. (2015). *The Mechanical Design Process.* McGraw-Hill Education, 5th edition.

Wong, V. (2014, January). *bloomberg.com*. Retrieved from A Guide to All the Food That's Fit to 3D Print (So Far): https://bloom.bg/2jFkCga

Zeijderveld, J. V. (2018, April). *sculpteo.com*. Retrieved from Mass Customization In 3D printing: The Best Projects!: https://bit.ly/2PC1pPS

Zelinski, P. (2017, March). *additivemanufacturing.mdeia.* Retrieved from GE Team Secretly Printed a Helicopter Engine, Replacing 900 Parts with 16: https://bit.ly/2TpR2gu

Zhong W, L. F. (2001). Short fiber reinforced composites for fused deposition modelling. *Material Science and Engineering A301*, 125-130.

II. ANNEXES

Annexes index

1. Design evolution